MECHANISM OF *CASK*-LINKED OPHTHALMOLOGICAL DISORDERS

Chen Liang

Dissertation submitted to the faculty of the Virginia Polytechnic Institute and State University in partial fulfillment of the requirements for the degree of

Doctor of Philosophy

In

Biological Sciences

Konark Mukherjee (Chair)

Michael A. Fox

Gregorio Valdez

Robert G. Gourdie

August 7, 2018

Roanoke, Virginia

Keywords: CASK, Optic nerve hypoplasia, Subcortical visual pathway

MECHANISM OF *CASK*-LINKED OPHTHALMOLOGICAL DISORDERS

Chen Liang

Abstract

Calcium/calmodulin-dependent serine protein kinase (CASK) is a membrane-associated guanylate kinase (MAGUK) family protein, which is encoded by a gene of identical name present on the X chromosome. CASK may participate in presynaptic scaffolding, gene expression regulation, and cell junction formation. CASK is essential for survival in mammals. Heterozygous mutations in the *CASK* gene (in females) produce X-linked intellectual disability (XLID) and mental retardation and microcephaly with pontine and cerebellar hypoplasia (MICPCH, OMIM# 300749). *CASK* mutations are also frequently associated with optic nerve hypoplasia (ONH) which is the most common cause of childhood blindness in developed countries. Some patients with mutations in *CASK* have been also diagnosed with optic nerve atrophy (ONA) and glaucoma. We have used floxed *CASK* ($CASK^{floxed}$), *CASK* heterozygous knockout ($CASK^{(+/-)}$), *CASK* neuronal knockout ($CASK^{NKO}$) and tamoxifen inducible *CASK* knockout ($CASK^{iKO}$) mouse models to investigate the mechanism and pathology of *CASK*-linked ONH. Our observations indicate that ONH occurs with 100% penetrance in $CASK^{(+/-)}$ mice, which also displayed microcephaly and disproportionate cerebellar hypoplasia. Further, we found that *CASK*-linked ONH is a complex developmental neuropathology with some degenerative components. Cellular pathologies include loss of retinal ganglion cells (RGC), astrogliosis, axonopathy, and synaptopathy. The onset of ONH is late in development, observed only around the early postnatal stage in mice reaching the plateau phase by three weeks of birth. The developmental nature of the disorder is confirmed by deleting

CASK after maturity since *CASK*^{iKO} mice did not produce any obvious optic nerve pathology. Strikingly the *CASK*^{floxed} mice expressing ~49% level of CASK did not manifest ONH despite displaying a slightly smaller brain and cerebellar hypoplasia indicating that ONH may not simply be an extension of microcephaly. We discovered that deleting *CASK* in neurons produced lethality before the onset of adulthood. The *CASK*^{NKO} mice exhibited delayed myelination of the optic nerve. Overall this work suggests that CASK is critical for neuronal maturation and *CASK*-linked ONH is a pervasive developmental disorder of the subcortical visual pathway. Finally, in a side project, I also described a new methodology of targeting neurons using receptor-mediated endocytosis which would help target retinal neurons for therapeutic purposes in the future.

MECHANISM OF *CASK*-LINKED OPHTHALMOLOGICAL DISORDERS

Chen Liang

General Audience Abstract

7 in 10,000 children suffer from childhood blindness, for whom all the visual information from the outside world is completely blocked. Although classified as a rare disease, optic nerve hypoplasia (ONH), or the underdevelopment of optic nerve, is the leading cause of childhood blindness in developed countries, accounting for 15% of childhood blindness. Only a handful of genes have been shown to associate with ONH. The *CASK* gene, whose protein product calcium/calmodulin-dependent serine protein kinase (CASK) plays a role in presynaptic scaffolding, is one of them. Mutations in the *CASK* gene not only produce ONH, but also microcephaly and intellectual disability. Investigating the mechanism of *CASK*-linked ONH will provide critical data to understand the molecular basis of optic nerve formation and maturation. Here we have used the *CASK* heterozygous knockout mouse model to replicate the ONH and microcephaly seen in female human patients. We discovered that the onset of *CASK*-linked ONH corresponded to the late third trimester developmental stage in humans, thus ONH is developmental in nature. ONH pathologies include thinning of optic nerves, axonal atrophy, and synaptopathy. In contrast to the postnatal death of constitutive CASK loss of function in mice, CASK ablation in adult mice did not lead to lethality. *CASK* deletion also delays neuronal myelination. Overall, our results indicate that CASK is critical for postnatal maturation of the central nervous system and mutations of the *CASK* gene is sufficient to lead to ONH. Early intervention and proper gene therapy may treat *CASK*-linked ONH.

Acknowledgements

I would like to extend my special gratitude to Dr. Konark Mukherjee for being my mentor in my Ph.D. studies. Being extremely supportive and always accessible, he guided me with not only the experimental techniques, but also taught me the ideology that will help me succeed in the research field. One thing that I will remember very clearly is that a researcher should think critically about published work, and focus on how experimental results were interpreted to reach the conclusion.

I would like to thank Dr. Michael Fox for his valuable advice during "CASK meetings" and committee meetings for projects on which we are collaborating. His knowledge in neuroscience and neuroanatomy was critical for pursuing my work. I am also very thankful for the suggestions from Dr. Gregorio Valdez and Dr. Robert Gourdie in my committee meetings.

I often consulted and got help from my colleagues at Virginia Tech Carilion Research Institute (VTCRI). Alicia Kerr has been my collaborator in this study and it has been valuable experience to work with her. Dr. Leslie LaConte was present in all our lab meetings and provided valuable insights. Dr. Vrushali Chavan helped me learn a lot of molecular biology techniques. Helen Clark and Sidney Stewart helped me learn biochemistry and mouse experiments. Paras Patel helped me with the language of the dissertation draft. I am also indebted to Dr. Jianmin Su, Dr. Aboozar Monavarfeshani, Dr. Jianping Wu, Dr. Iskander Ismailov, Dr. Alexei Morozov, Dr. Wataru Ito, and many

others for their time. I thank the Department of Biological Sciences and VTCRI for providing me with the opportunity to carry out my dissertation research.

I am very grateful to my parents, Xuefeng Zhu and Jie Liang. They have always been supporting me in my life and encouraging me when I am depressed. I really enjoy the dinner every time I go back home.

I also would like to thank my friends Shengchuang, Zhuoya, and Yi for the get-togethers in Roanoke and Blacksburg.

Table of Contents

Abstract ii

General Audience Abstract iv

Acknowledgements v

Table of Contents vii

List of Figures x

List of Publications xii

Chapter 1: Introduction 1

1.1 Anatomy, function, and development of retinal cells 1

1.2 Optic Nerve Hypoplasia (ONH) 4

1.3 CASK mutations and ophthalmic disorders 7

Chapter 2: Methods 11

2.1 Mouse breeding 11

2.2 Genotyping 12

2.3 Immunohistochemistry (IHC) 13

2.4 Immunoblotting 13

2.5 Optic nerve samples preparation for toluidine blue staining and transmission electronic microscopy (TEM) 14

2.6 G-ratio distribution spectra 14

2.7 Serial block-face scanning electron microscopy 15

2.8 Intraocular injections of anterograde tracers and quantification 15

2.9 Cell counts and lamina quantification 16

2.10 Description of coarse and fine axons 17

Chapter 3: Results 17

3.1 Optic nerve in CASK$^{(+/-)}$ mice is not only thin, but is comprised of atrophic retinal axons, and displays reactive astrogliosis 17

3.1.1 Mutations in CASK gene are associated with ONH 17

3.1.2 CASK$^{(+/-)}$ mice mimic the human MICPCH phenotype 20

3.1.3 Heterozygous deletion of CASK in mice produces optic nerve pathology 24

3.1.4 Axonopathy is present in optic nerves of CASK$^{(+/-)}$ mice 27

3.1.5 Retinogeniculate synaptopathy is observed in CASK$^{(+/-)}$ mice 31

3.1.6 RGC numbers are reduced in CASK$^{(+/-)}$ mice 34

3.2 ONH is developmental in nature and CASK is not required for survival of adult mice 37

3.2.1 ONH develops postnatally in CASK$^{(+/-)}$ mice 37

3.2.2 CASK is not essential for survival after maturity 40

3.3 CASK plays a valuable role in neuron but CASK-linked ONH is not always coupled to microcephaly 44

3.3.1 Cerebellum hypoplasia but no ONH was observed in adult CASK^{floxed} mice 44

3.3.2 MICPCH pathology is not purely neuronal in origin 47

3.3.3 CASK neuronal knockout is lethal and produces optic nerve myelination retardation 54

Chapter 4: Discussion 57

Appendix Chapter 1: Examining a methodology for targeting neurons for future therapy 63

Appx. 1.1 Introduction 63

Appx. 1.1.1 Scavenger receptor (SR) mediated endocytosis: a novel approach to drug targeting to neurons 63

Appx. 1.2 Methods 64

Appx. 1.2.1 Cell culture and internalization assay 64

Appx. 1.2.2 Texas-red maleylated BSA generation 64

Appx. 1.2.3 Acute cortical slice experiment 65

Appx. 1.3 Results 65

Appx. 1.4 Discussion 71

Summary 71

References 72

List of Figures

Figure 1: Development of retinal cells with time. 4

Figure 2: Representative funduscopic images of ONH diagnosis. 5

Figure 3: Methods of measuring DM:DD ratio. 6

Figure 4: A model of neurexin phosphorylation by CASK. 8

Figure 5: CASK interacts with a large number of molecules. 9

Figure 6: Brain images show that CASK mutations are associated with MICPCH. 10

Figure 7: Genetic, brain and retinal alterations associated with a heterozygous CASK mutation. 19

Figure 8: Generation of CASK$^{(+/-)}$ heterozygous mutant mice. 21

Figure 9: CASK$^{(+/-)}$ mice display postnatal microcephaly, cerebellar hypoplasia, and ONH. 24

Figure 10: CASK$^{(+/-)}$ mice optic nerves display reduced axons and increased astrogliosis. 26

Figure 11: CASK$^{(+/-)}$ mice optic nerves display axonal thinning 30

Figure 12: CASK$^{(+/-)}$ mice display a decreased number of retinogeniculate synapses and a reduced number of active zones in the remaining synapses. 33

Figure 13: Decreased number of retinal ganglion cells in CASK$^{(+/-)}$ mice. 35

Figure 14: Retinal lamination remains the same among genotypes. 36

Figure 15: CASK$^{(+/-)}$ mice optic nerves display the secondary reduction in size. 40

Figure 16: Tamoxifen successfully induced expression of tdTomato in CreER tdTomato mice. 41

Figure 17: Adult tamoxifen-induced CASK knockout ($CASK^{iKO}$) displayed no abnormalities. 43

Figure 18: Characterization of adult wild type and $CASK^{floxed}$ brain and optic nerve. ... 46

Figure 19: Deletion from neurons and characterization of female heterozygous mice with neuron-specific CASK deletion. 49

Figure 20: Normal brain formation in CASK neuronal knockout mice. 53

Figure 21: Characterization of CASK neuronal knockout ($CASK^{NKO}$) mice. 57

Figure 22: Cortical neurons internalize MBSA. 69

Figure 23: PolyG but not polyA can be internalized by cortical neurons. 70

List of Publications

1. Liang, Chen*, Alicia Kerr*, Yangfengzhong Qiu, Francesca Cristofoli, Hilde Van Esch, Michael A. Fox, and Konark Mukherjee. "Optic Nerve Hypoplasia Is a Pervasive Subcortical Pathology of Visual System in Neonates." ***Investigative Ophthalmology & Visual Science*** 58, no. 12 (2017): 5485-5496. (*Contributed equally)
2. Liang, Chen, Vrushali Chavan, and Konark Mukherjee. "Internalization of scavenger receptor ligands by cortical neurons." ***Matters*** 3, no. 5 (2017): e201703000006.
3. Srivastava, Sarika, Ryan McMillan, Jeffery Willis, Helen Clark, Vrushali Chavan, Chen Liang, Haiyan Zhang, Matthew Hulver, and Konark Mukherjee. "X-linked intellectual disability gene *CASK* regulates postnatal brain growth in a non-cell autonomous manner." ***Acta neuropathologica communications*** 4, no. 1 (2016): 30.
4. LaConte, Leslie EW, Vrushali Chavan, Chen Liang, Jeffery Willis, Eva-Maria Schönhense, Susanne Schoch, and Konark Mukherjee. "CASK stabilizes neurexin and links it to liprin-α in a neuronal activity-dependent manner." ***Cellular and Molecular Life Sciences*** 73, no. 18 (2016): 3599-3621.

Chapter 1: Introduction

1.1 Anatomy, function, and development of retinal cells

The vertebrate retina, as a structure sensing light signals, lies in between the choroid and the vitreous body of the eye (Marieb and Hoehn 2007). Three types of neuronal cells, photoreceptors (PR), bipolar cells (BC), and retinal ganglion cells (RGC), are the major players of "light to neural visual signal" conversion (Marieb and Hoehn 2007). From the outermost to the innermost, there are total ten layers in retina (Figure 1A): the retinal pigment epithelium (RPE), the layer of rods and cones (or photoreceptor, PR), the outer (or external) limiting membrane (OLM), the outer nuclear layer (ONL), the outer plexiform layer (OPL), the inner nuclear layer (INL), the inner plexiform layer (IPL), the layer of ganglion cells (GC), the nerve fiber layer (NFL), and the inner limiting membrane (ILM) (Gray 1878). Each layer contains different cell types or subcellular structures. Enveloping the PR, the RPE cells absorb scattered light and protect the retina from photo-oxidation (Strauss 2005). The RPE has a single layer of cuboidal cells with the presence of melanin pigments in melanosomes in each cell (R Sparrrow, Hicks et al. 2010). The PR contains the outer and inner segments of the PRs: rods and cones (Marieb and Hoehn 2007). The photopigments rhodopsin and conopsin are located on the membrane shelves in the outer segment of rods and cones, respectively (Guyton and Hall 1992). The inner segment of PRs is rich in mitochondria (Guyton and Hall 1992). The peak absorbance wavelength of light for rod cells in both human and mouse is at 498 nm (Bowmaker and Dartnall 1980). There are only two subtypes (maximum sensitivity: purple and green) of cones in mouse but three subtypes in human (maximum sensitivity: blue (S), green (M), and red (L)) with exact peak absorbance varying for different individuals (Bowmaker and Dartnall 1980). The highest number of cones

are present in the macular and only cones can be found in the central region of the macula (Kolb 1995). The central region is called the fovea (Kolb 1995). The OLM is considered to be collectively formed by the apical processes of Müller glial cells (Omri, Omri et al. 2010). The ONL consists of the cell body of PRs, where the cell bodies of cones are closer to the OLM while cell bodies of rods are evenly distributed within the layer (Gray 1878). The OPL has the synapses mostly between BCs and PRs, and some are between horizontal cells and PRs (Gray 1878). The INL has cell bodies of BCs, horizontal cells and amacrine cells and Müller cells (Gray 1878). Horizontal cells are responsible for the lateral inhibition to generate the center-surround receptive field (Luo 2015). Amacrine cells contribute to the asymmetric inhibition of direction-selectivity, detection of directional motion and circadian rhythm (Balasubramanian and Gan 2014). The functions of Müller cells are structurally supporting the retina and regulating the extracellular environment of the retina (Newman and Reichenbach 1996). There are two major types of BCs, ON bipolar and OFF bipolar (Luo 2015). They are either depolarized (ON) or hyperpolarized (OFF) in the presence of light (Luo 2015). The outer part of IPL harbors the synapses formed by OFF BCs and RGCs, while the inner part of IPL is abundant in the synapses of ON BCs and RGCs (Luo 2015). Somas and axons of RGCs form the layer of GC and NFL, respectively, and are covered by ILM mainly formed by footplates of Müller cells (Gray 1878). RGCs are responsible for collecting and transmitting visual signals inputs from BCs to the thalamus or superior colliculus (Erskine and Herrera 2014). There are five groups of RGCs based on their morphologies: U, V, W, X, and Y (Sümbül, Song et al. 2014). Some RGCs containing melanopsin play a role in synchronizing the circadian rhythm according to the day and night cycle (Do and Yau 2010).

Together with horizontal cells, amacrine cells, and cones, RGCs are among the first batch of neuronal cells to be born within the optic cup (the precursor of neural retina) at embryonic day 11.5 (E11.5) for mouse, and the process of RGC generation lasts until postnatal day 2 (P2) (Bassett and Wallace 2012). It takes an average of four days for the axons of RGCs to grow along the optic stalk and reach the brain to form the major part of the optic nerve (Graw 2010). The formation of horizontal cells, amacrine cells, and cones end before E15.5, P3, and E17.5, respectively (Zhang, Serb et al. 2011). Rods and BCs come later than RGC but the time frame of generation is longer (Zhang, Serb et al. 2011). Hallmarks of birth of the cells are the expression of certain transcription factors: Atoh7 for RGCs, Six3 for amacrine cells, Vsx2 for BCs, Foxn4 for horizontal cells, Nrl for rods, Sall3 for cones, just to name a few (Figure 1B) (Bassett and Wallace 2012).

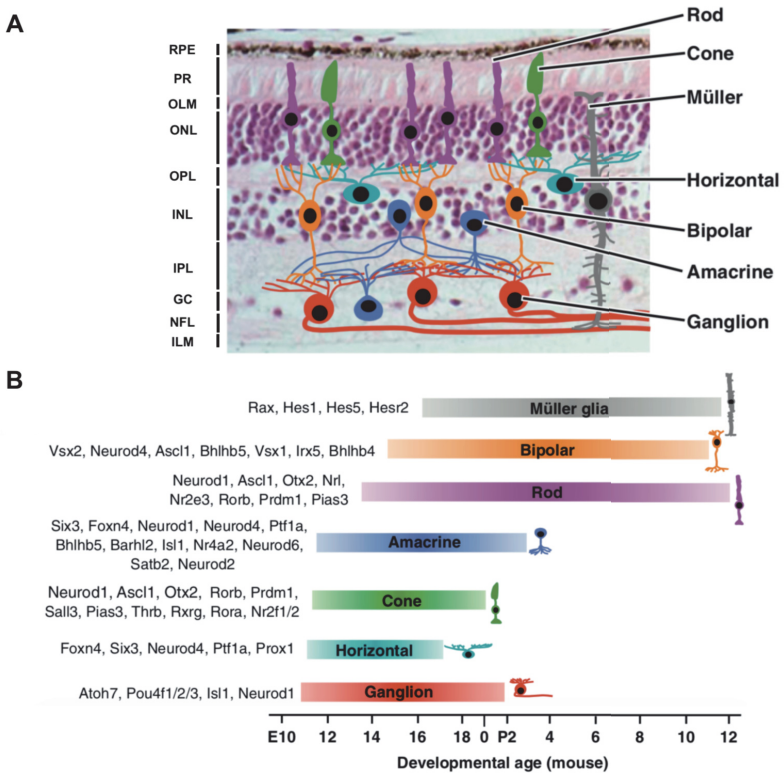

Figure 1: Development of retinal cells with time.

A) The layering of a vertebrate (mouse) retina. A schematic diagram overlaid with a histological image. B) Again, using the mouse as an animal model, the chronological order of retinal cell birth is displayed with the expression of transcription factors as hallmarks. (Adapted from (Bassett and Wallace 2012))

1.2 Optic Nerve Hypoplasia (ONH)

As the second pair of cranial nerves, the optic nerve is responsible for visual signal transmission from retina to the brain described by Vilensky, Robertson et al. (2015). The underdevelopment (hypoplasia) of the optic nerve leads to severe medical conditions like vision loss. Around 15% childhood blindness cases were documented with ONH in developed countries (Kaur, Jain et al. 2013). Diagnosed by a small pale optic disc in a boy, the first case of ONH was described 1884 by H. Magnus (Magnus 1884). 31 years later, O. Schwarz provided the completed illustrations of optic disc appearance in 1915 (Schwarz 1915). In modern ages, besides a small optic disc with a double ring structure (Figure 2A, B) (Garcia-Filion and Borchert 2013), an increased ratio of disc-macula to disc diameter (DM:DD) also serves to determine the presence of ONH (Kaur, Jain et al. 2013).

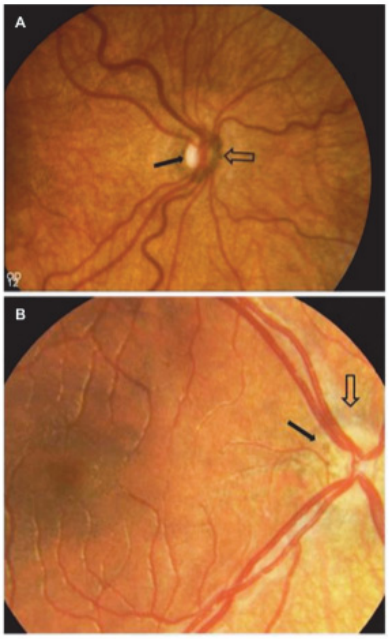

Figure 2: Representative funduscopic images of ONH diagnosis.

A) ONH (filled arrow) with a pigmented double ring (unfilled arrow). B) ONH (filled arrow) with a hypopigmented double ring (unfilled arrow). (Adapted from (Garcia-Filion and Borchert 2013))

DM:DD ratio can be measured by two major methods. The first method is shown as below:

$$DM{:}DD = \frac{a+b}{2a},$$

where a is the horizontal radius of the optic disc, b is the disc-macula measurement (Figure 3A) (Mok and Lee 2002). In order to reduce the error of disc diameter measurement, the second method was invented as:

$$DM{:}DD = \frac{D_{ft}+\frac{D_1}{2}}{\frac{D_1+D_2}{2}},$$

where D_{ft} is the disc-macula measurement, D_1 is the diameter of optic disc toward the fovea, D_2 is the diameter of optic disc perpendicular to D_1 (Sato 2017) (Figure 3B).

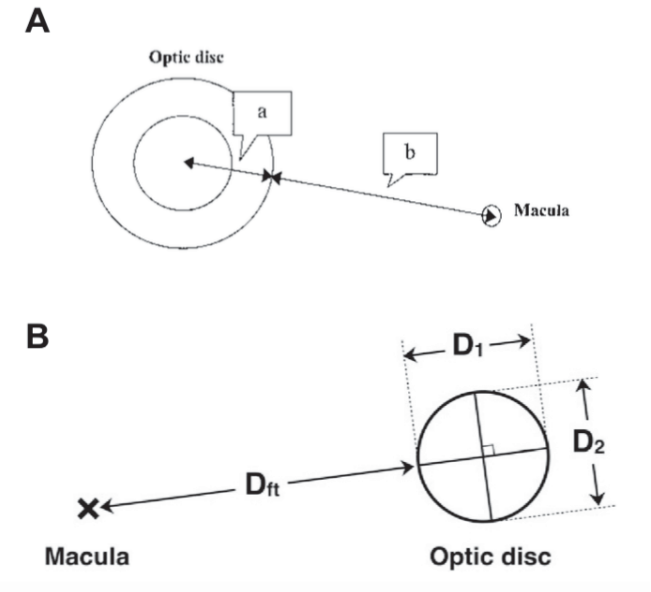

Figure 3: Methods of measuring DM:DD ratio.

A) The first method. (Adapted from (Mok and Lee 2002)) B) the second method. (Adapted from (Sato 2017))

ONH can occur as isolated or syndromic, and are thus categorized into three subforms: I) ONH simplex, II) septo-optic dysplasia (SOD), and III) septo-optic-pituitary dysplasia (Kaur, Jain et al. 2013). The term SOD, or de Morsier's Syndrome, was first described by G. de Mosier, and further supported by clinical cases from W. Hoyt, as ONH with the absence of the septum pellucidum (De Morsier 1956, Hoyt, Kaplan et al. 1970). If the abnormally small size of hypopituitary can also be observed in SOD cases, then such cases are named as septo-optic-pituitary dysplasia (Hoyt, Kaplan et al. 1970). Other ophthalmological diagnoses and co-

morbidities, such as microphthalmia, aniridia, nystagmus, and strabismus, are also reported to commonly co-occur with ONH (Zeki, Dudgeon et al. 1991). Bilateral ONH is also frequently (~65%) associated with other brain manifestations.

Both non-genetic and genetic factors contribute to the etiopathogenesis of ONH. Statistics have shown that young maternal age and primiparity highly increase the risk of ONH in infants (Garcia-Filion and Borchert 2013). Mutations in transcription factors (TFs), such as *HESX1*, *PAX6*, *SOX2*, *NR2F1*, *OTX2*, *VAX1,* and *ATOH7* are clinically linked to ONH (Chen, Yin et al. 2017). However, the association is not inclusive, since these TFs function not only in the development in the eye, but in more organs during the embryonic development. ONH associated with these genes is more likely to be an extended pathology of other developmental and/or ophthalmological disorders, such as anophthalmia, anencephaly, corpus callosum defects, and astigmatism. Other genes functioning in chromatin remodeling, RNA splicing, and scaffolding are also shown to be linked to ONH (Chen, Yin et al. 2017). The calcium/calmodulin-dependent serine protein kinase (*CASK*) gene is one of the genes whose mutations may contribute to the pathology of ONH (Moog, Kutsche et al. 2011).

1.3 CASK mutations and ophthalmic disorders

CASK is a multi-domain protein involved in a variety of molecular functions. The human *CASK* gene is located on the short arm of X chromosome (Xp11.4), which encodes a protein of 926 amino acids (105 kD) in full length (Dimitratos, Stathakis et al. 1998). The mouse *CASK* gene is also on the X chromosome (mouse: X 8.43 cM) (Blair, Reed et al. 2000) and encodes a protein the same length as human (Huang and Hsueh 2017). As a protein belonging to the membrane-associated guanylate kinases (MAGUK) family, CASK contains two L27 (lin-2/lin7) domains, a

PDZ (PSD-95/Dlg-1/ZO-1) domain, an SH3 (Src homology 3) domain, a guanylate kinase domain, and CASK harbors a unique calcium/calmodulin-dependent kinase (CAMK) domain at its N-terminus that can phosphorylates the neurexin C-terminal tail (Figure 4) (Mukherjee, Sharma et al. 2008).

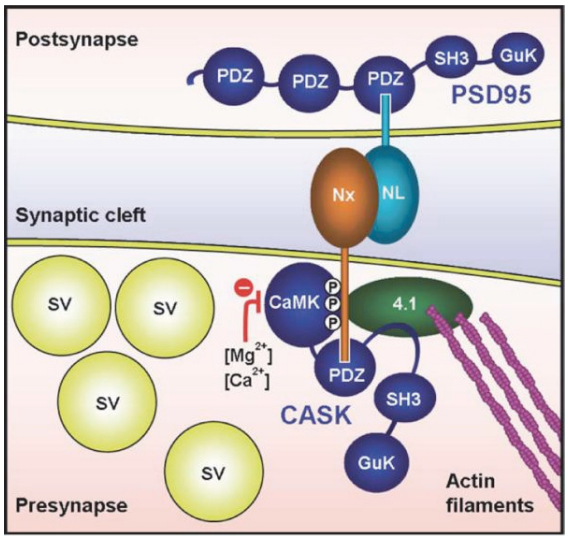

Figure 4: A model of neurexin phosphorylation by CASK.

CASK (Ca^{2+}/calmodulin dependent kinase domain (CaMK), lin-2, lin7 domains (L27), a PSD-95, dlg, ZO-1 domain (PDZ), a Src homology 3 domain (SH3) and guanylate kinase domain (GuK)) is recruited to the cytosolic C-tail of neurexin (Nx) via the CASK PDZ-domain, and phosphorylates the neurexin C-terminal tail. (Adapted from (Mukherjee, Sharma et al. 2008))

CASK gene evolved early in animal kingdom even before the origin of three distinct germ layers, and in mammals it is expressed nearly ubiquitously in all tissues (Hata, Butz et al. 1996, Mukherjee, Sharma et al. 2010). Not only found in different tissues, CASK proteins are also able to bind to a number of other proteins besides neurexin (Hata, Butz et al. 1996), such as

membrane bound adhesion molecules SynCAMs (Biederer, Sara et al. 2002), and syndecans (Cohen, Woods et al. 1998), scaffolding molecule like Veli and Mint1 (Butz, Okamoto et al. 1998), regulatory molecules like calmodulin (Hata, Butz et al. 1996), cytoskeletal protein, protein 4.1 (Biederer and Sudhof 2001), nuclear transcription factors like Id1 and Tbr-1 (Hsueh, Wang et al. 2000, Qi, Su et al. 2005), ion channels, mitochondria associated proteins like parkin, glutaminase, isocitrate dehydrogenase and several kinases (Figure 5) (Fallon, Moreau et al. 2002, Olsen, Liu et al. 2002, Mukherjee, Slawson et al. 2014, LaConte, Chavan et al. 2016, Srivastava, McMillan et al. 2016). CASK protein also may have a variety of functions in organization of cell junctions (including presynapse and postsynapse) (Butz, Okamoto et al. 1998, Hsueh, Yang et al. 1998), regulation of transcription (Hsueh, Wang et al. 2000), protein trafficking (Leonoudakis, Conti et al. 2004), regulation of ion channels (Maximov, Sudhof et al. 1999), cell proliferation (Qi, Su et al. 2005), polarity (Caruana 2002) and motility, development and wound healing (Marquez-Rosado, Singh et al. 2012).

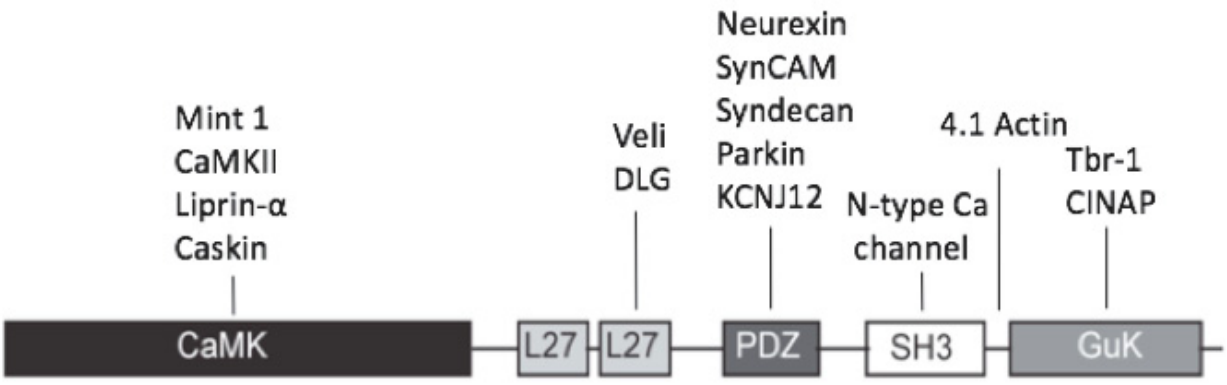

Figure 5: CASK interacts with a large number of molecules.

The figure depicts the domain arrangement of CASK and some of the known interactors.

Deletion mutations, insertion mutations, and copy number variations are associated with a complex neurodevelopmental disorder called mental retardation and microcephaly with pontine and cerebellar hypoplasia (MICPCH) (Figure 6) (Najm, Horn et al. 2008, Moog, Kutsche et al. 2011).

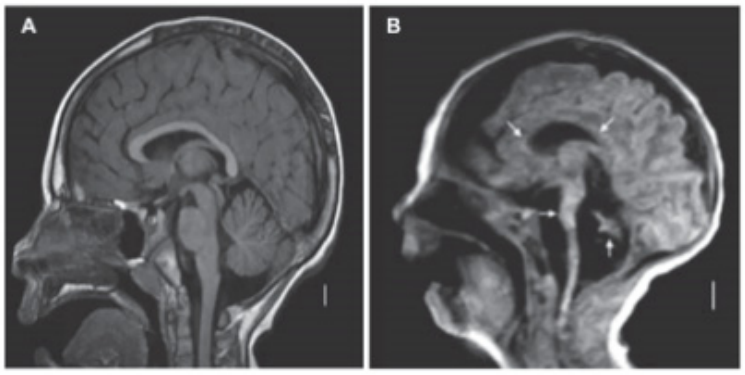

Figure 6: Brain images show that *CASK* mutations are associated with MICPCH.
A) A normal individual as a control. B) A boy (CASK 915G>A mutation) with MICPCH. (Adapted from (Najm, Horn et al. 2008))

Missense mutations in boys, however, are frequently found in cases of X-linked intellectual disability (Hackett, Tarpey et al. 2010). *CASK* mutations in boys, as well as girls, are frequently associated with ophthalmic conditions like nystagmus, strabismus, hyperopia, myopia, macropappila, megalocornea, glaucoma, salt and pepper retinopathy, persistent hyperplastic primary vitreous, ONH, and optic nerve atrophy (ONA) (Burglen, Chantot-Bastaraud et al. 2012, Moog, Bierhals et al. 2015). Since the ocular manifestations with CASK haploinsufficiency can be classified both as developmental (ONH) (Moog, Kutsche et al. 2011) or degenerative (ONA and glaucoma) (Burglen, Chantot-Bastaraud et al. 2012), we asked following questions:

1) What are the hallmarks of the optic nerve pathology associated with CASK haploinsufficiency?
2) Is *CASK*-linked optic nerve pathology developmental in nature? Is it a true ONH?
3) Is *CASK*-linked optic nerve pathology independent of the overall microcephaly?

To answer these questions, we decided to:

1) determine the microscopic and ultrastructural optic nerve pathology associated with CASK haploinsufficiency;

2) elucidate the timing of optic nerve pathology in *CASK* mutated mice;

3) determine if ONH and microcephaly are always coupled.

The answers to these three questions will shed light on the function of CASK in the formation and maintenance of the subcortical visual pathway. Besides, we also decided to look for potential targets to help develop gene therapy strategies and rescue the function of CASK.

Chapter 2: Methods

2.1 Mouse breeding

The original *CASK*^{floxed} mice have been obtained from the laboratory of Prof. Thomas Südhof and maintained in a C57Bl6 background. The mouse was designed by flanking the exon1 of *CASK* gene by LoxP sites. A neomycin selection cassette was introduced into the intron 3' of exon1. A third LoxP site follows the neomycin cassette. Cre expression therefore splices of both exon1 and neomycin cassette producing a knockout. The *CASK*^{floxed} mice itself however is a hypomorph due to pronounced selection cassette interference on *CASK* gene expression. *CASK*^{floxed} mice were crossed with ZP3-Cre transgenic mouse line which expresses Cre-recombinase specifically in oocytes (Lewandoski, Wassarman et al. 1997). Females from this

cross carrying *CASK* deletion in oocytes were used to generate $CASK^{(+/-)}$ mouse line. Neuron-specific knockouts were generated by crossing $CASK^{floxed}$ mice with mouse line carrying Cre-recombinase under synapsin-1 promoter obtained from the Jackson Laboratory (Zhu, Romero et al. 2001). LsL-tdTomato transgenic strain, an indicator line for Cre-recombinase activity was a kind gift from Dr. Alexei Morozov. Whole body time-dependent inducible knockout was derived by crossing $CASK^{floxed}$ mice with estrogen-Cre transgenic line (CAGGCre-ERTM) obtained from the Jackson Laboratory (Hayashi and McMahon 2002). *CASK* can be deleted acutely by administering tamoxifen intraperitoneally.

2.2 Genotyping

Primer pair 1 (F: tttggggactagatgggtgtggtg, R: cttggtcgcagcttgggagta) are used for detecting $CASK^{(+/-)}$ mouse line, primer pair 2 (F: gcattaccggtcgatgcaacgagtgatg, R: gagtgaacgaacctggtcgaaatcagtg) are used for detecting Cre mouse line and primer pair 3 (F: acctcagcagctgcaacc, R: actaaccctcctcccttcg) are used for $CASK^{floxed}$. A toe of a P5 mouse pup is digested in 100 µl of tail buffer (50 mM NaCl, 10 mM Tris-HCL with pH=9, 0.4% TritonX-100, 0.4% Tween 20) with Proteinase K (1:50 dilution, AG Blog) at 55°C for 5 hours. Proteinase K is inhibited by incubation at 100°C for 15 min. Each PCR reaction cycle is composed of three stages: 94°C 30s (melting), 64°C 30s (annealing) and 72°C 30s (extension), and the volume of each reaction is 25.5 µl (9.5 µl H2O, 1.25 µl of forward primer (20 µM), 1.25 µl reverse primer (20 µM), 12.5 µl 2X Master Mix (Apex) and 1 µl template). PCR products are separated on 2% agarose gel.

2.3 Immunohistochemistry (IHC)

All experiments are done using VT IACUC guidelines. Mice were anesthetized and perfused with first chilled PBS (phosphate buffered saline) and then 4% paraformaldehyde (PFA). Brain, retina or optic nerve were dissected and postfixed in 4% PFA. Tissues were cryopreserved in 30% sucrose before embedding in Neg50 matrix and cryosectioned using Leica Cryostat to generate 16 - 25 μm-thick tissue sections. Sections were permeabilized and blocked with 0.25% TritonX-100 and 5% BSA in PBS. Immunostaining weas performed using primary antibodies at an appropriate concentration followed by labeling with fluorophore conjugated secondary antibodies. Primary antibodies include: Calretinin (Rabbit polyclonal Ab, Millipore, Cat# AB5054, 1:2000), RBPMS (Rabbit polyclonal Ab, PhosphoSolution, Cat# 1830, 1:500), GFAP (mouse monoclonal Ab, Neuromab, Cat# 75240, 1:1000), and Liprin- α3 (4396) (rabbit monoclonal Ab, a kind gift from Dr. Thomas Südhof, 1:200), and Synaptophysin (rabbit monoclonal Ab, Sigma, Cat# SAB4502906, 1:100). Secondary antibodies include: Alexa Fluor 488 (Goat anti-rabbit, Invitrogen, Cat# A-11008, 1:1000) and Dylight 633 (anti-mouse IgG, Thermo Scientific, Cat# 35512, 1:1000). Sections were mounted with Vectashield containing DAPI (Vector Laboratories, Burlingame, CA, USA) and were imaged using a Zeiss 700 or 710 laser scanning confocal microscope.

2.4 Immunoblotting

Optic nerves dissected from young female wildtype and *CASK*$^{(+/-)}$ mice (postnatal day 40) were boiled in sample buffer and proteins separated on an 8% SDS-PAGE (sodium dodecyl sulfate-polyacrylamide gel electrophoresis). Proteins were then transferred onto nitrocellulose membrane and blocked in 5% skimmed milk for 2 hours and incubated using appropriate primary and secondary antibodies. For quantitative immunoblots, secondary antibodies

conjugated with fluorophore were used and images were captured using an appropriate filter in Chemidoc™ (Biorad). Antibodies used are CASK (mouse monoclonal Ab, NeuroMab, Cat# 75000, 1:1000), Neurofilament-associated antigen (NFAA) (mouse monoclonal Ab, DSHB, Cat# 3A10, 1:1000), Liprin- α3 (4396) (rabbit monoclonal Ab, a kind gift from Dr. Thomas Südhof, 1:2000), Synaptophysin (rabbit monoclonal Ab, Sigma, Cat# SAB4502906, 1:5000), PSD-95 (mouse monoclonal Ab, NeuroMab, Cat# 75-028,1:1000) and tubulin (mouse monoclonal Ab, DSHB, Cat# 12G10 anti-alpha-tubulin, 1:1000).

2.5 Optic nerve samples preparation for toluidine blue staining and transmission electronic microscopy (TEM)

Mice were anesthetized and perfused with PBS and then sodium cacodylate (NaCa) buffer (2% glutaraldehyde/2% PFA (2G/2PF) in 0.1M sodium cacodylate in PBS, pH 7.4). After perfusion, optic nerves were dissected and immersed in NaCa buffer overnight and then put in 2% O_sO_4 for 2 hours for post fixation. Dehydration was achieved by sequentially adding 15%-100% ethanol. Samples were embedded in 100% Epoxy resin for 24 hours and then placed in an oven at 58°C for 2 days. Sectioning of samples and successive toluidine blue stain or TEM was performed at Virginia-Maryland College of Veterinary Medicine at Virginia Tech.

2.6 G-ratio distribution spectra

G-ratios, defined as the ratio of inner axonal diameter to the outer axonal diameter (including myelin sheath) (Guy, Ellis et al. 1989), of 240 optic nerve axons were measured on TEM images (4000X) using ImageJ. The measurements of inner and outer axonal diameters (d) were calculated from inner and outer axonal areas (a), respectively, to reduce error since the sections were not perfectly round in shape, where $d \approx 2\sqrt{\frac{a}{\pi}}$. The probability density distribution of G-

ratio values was plotted based on a smooth kernel density estimate by using the function "SmoothHistogram" offered in the software of Mathematica. The smooth kernel density estimate based probability density function is given by a linearly interpolated version of

$$\frac{1}{nh}\sum_{i=1}^{n} k\left(\frac{x-x_i}{h}\right),$$

where x is the value of the G-ratio, n is the sample size, bandwidth h is selected as "Automatic" and kernel smoothing function $k(x)$ was given by "Gaussian" $\left(\frac{1}{\sqrt{2\pi}} e^{-\frac{u^2}{2}},\ u \in \mathbb{R}\right)$ in Mathematica. Above functions can be found in any advanced level statistics textbook. The Kolmogorov-Smirnov test was used to determine if the two probability density distributions are from the same population.

2.7 Serial block-face scanning electron microscopy

Control and *CASK*$^{(+/-)}$ mice were transcardially perfused with PBS and 4% paraformaldehyde / 2% glutaraldehyde in 0.1M cacodylate buffer. Brains were removed, 300 μm coronal sections were obtained using a vibratome and the dLGN were dissected. Tissues were stained, embedded, sectioned and imaged as described previously (Mukherjee, Clark et al. 2016) by Renovo Neural Inc. (Cleveland, OH). Images were acquired at a resolution of 6 nm/pixel and image sets included > 200 serial sections (with each section representing 65 nm in the z axis). Data sets were analyzed in TrakEM2 (Cardona et al. 2012) and retinal terminals were unequivocally identified by the presence of synaptic vesicles and pale mitochondria (Hammer, Monavarfeshani et al. 2015, Mukherjee, Clark et al. 2016).

2.8 Intraocular injections of anterograde tracers and quantification

Intraocular injection of cholera toxin subunit B (CTB) conjugated to AlexaFluor 555 (Invitrogen) was performed as described previously (Su, Haner et al. 2011). After 2 days, mice were

euthanized, perfused with 4% PFA and brains were dissected and postfixed in 4% PFA overnight. 80–100μm coronal slices were sectioned on a vibratome and mounted using VectaShield (Vector Laboratories, Burlingame, CA, USA). Confocal Z-stack images from coronal dLGN sections were acquired on a Zeiss LSM 700 confocal microscope (Oberkochen, Germany). Z-stacks were obtained with a Zeiss 20x Plan-Apochromat objective and contained 14-20 optical sections (in 3μm steps). Confocal Images were obtained from 4 adult *CASK*$^{(+/-)}$ mutants and 4 littermate controls. The size and quantity of synapses in each dLGN (from the center of its rostral-caudal extent), was performed in ImageJ, blind to the genotype of the sample. Five images of each dLGN Z-stacks were randomly selected, images were manually thresholded, and the quantity and surface area of the isolated puncta was measured. Data was exported into Microsoft Excel, binned by size, and plotted as a histogram.

2.9 Cell counts and lamina quantification

Cell counts were performed on 16 μm cryosectioned 4% PFA-fixed retinal tissue as described in (Fox, Sanes et al. 2007, Su, Stenbjorn et al. 2012). Slides were stained with DAPI (diluted 1:5000 in PBS) for 60 seconds and then mounted with VectaShield (Vector Laboratories, Burlingame, CA, USA). Images of the central retina were acquired on a Zeiss LSM 700 confocal microscope (Oberkochen, Germany) or a Zeiss Axio Imager A2 fluorescent microscope. All DAPI and RBPMS-positive cells in the ganglion cell layer were counted manually under 20x objective. Cell counts were analyzed from at least 4 animals for each age and genotype. Five images per retina per mouse were analyzed. Retinal lamination was quantified for each genotype in the central retina in DAPI-stained retinas using ImageJ.

2.10 Description of coarse and fine axons

Since the axons in *CASK*$^{(+/-)}$ mice are overall small, it is difficult to apply the same threshold for fine and coarse axons on these mice as with those of the wildtype. On examining the distribution of the axonal area, we found they are distributed in a bimodal manner (two different slopes) (Figure 5C). Since the *CASK*$^{(+/-)}$ axons were smaller we applied a different threshold for each genotype, the value of the threshold was the point where the data points start to lose linearity.

Chapter 3: Results

3.1 Optic nerve in CASK$^{(+/-)}$ *mice is not only thin, but is comprised of atrophic retinal axons, and displays reactive astrogliosis*

3.1.1 Mutations in CASK gene are associated with ONH

Mutations in the *CASK* gene have been previously associated with ONH, ONA and glaucoma (Moog, Kutsche et al. 2011, Burglen, Chantot-Bastaraud et al. 2012). Here we describe a 3-year-old girl with a heterozygous splice site mutation in *CASK* (NM_001126054:exon24:c.2233+1G>A) leading to skipping of exon 24 who exhibits microcephaly, global developmental delays, and spastic quadriparesis (Figure 7A, B, C and personal communication). Magnetic resonance imaging did not reveal any specific midline structural defect as seen in septo-optic dysplasia or any white matter lesion (Figure 7D, E). Although truncated proteins may be generated in the subject from the mutated *CASK* allele, they are unlikely to be functional in absence of the Hook motif and the guanylate kinase domain, especially since the interdomain interaction with the guanylate kinase domain is critical for proper folding and function of MAGUK proteins (Tavares, Panepucci et al. 2001, Li, Wei et al.

2014). Furthermore, the transcripts with premature stop codon are likely to get degraded due to non-sense mediated decay. Thus, the pathogenic mutation described here is likely to produce haploinsufficiency. The girl displays ONH and other ophthalmic conditions including hyperopia, nystagmus, and infantile esotropia. Fundoscopy revealed a bilaterally normal anterior segment, however both optic discs were pale, small and hypoplastic (Figure 7F) compared with a normal person (Figure 7G). Hypoplastic optic nerves have also been observed in both MRI and fundoscopic examination of a second girl with heterozygous nonsense mutation in the N-terminal calcium/calmodulin-dependent kinase domain of *CASK* (c.661G>T; p.G221X (het)) (personal communications). This highly premature stop codon would either result in a non-functioning small peptide or no CASK protein product due to nonsense-mediated decay. The second girl displays severe visual impairment as well as nystagmus and intermittent exotropia (personal communications). These observations, and previously published reports, indicate that heterozygous loss of function mutations of *CASK* gene associates with ONH.

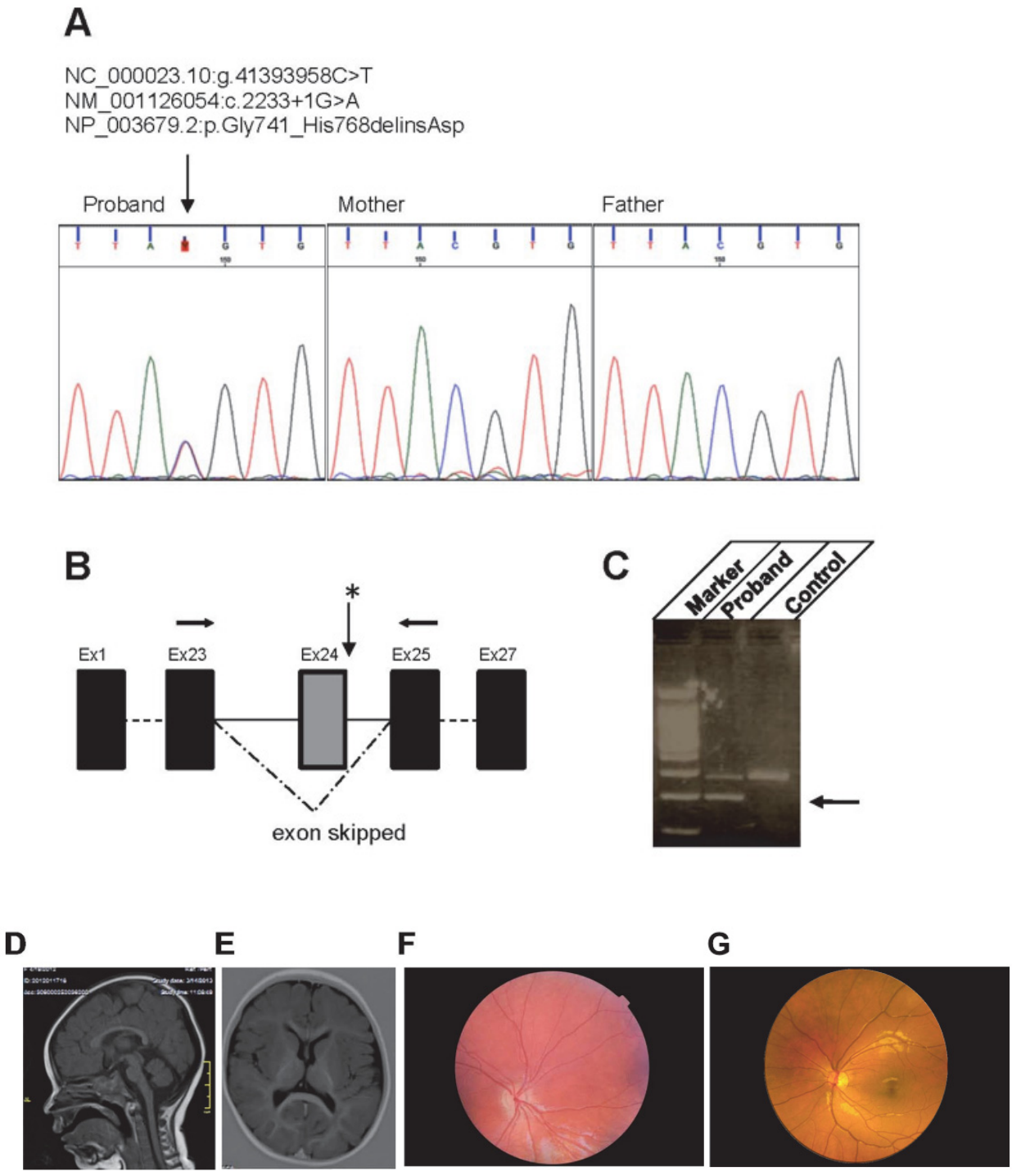

Figure 7: Genetic, brain and retinal alterations associated with a heterozygous *CASK* mutation.

A) Sanger sequences showing the de novo heterozygous splice variant in exon 24 (NM_001126054:exon24:c.2233+1G>A), B) The schematic of exon skipping C) *CASK* RT-PCR with primers (arrows in panel B) in exons 25 and 23 on cDNA of the patient and subsequent sequencing confirmed exon 24 skipping (a lower band indicated by the arrow compared with control). D, E) MRI images of brain indicate no specific midline structural defect or white matter lesion. F) A fundoscopic image from this haploinsufficient 3-year-old girl who was diagnosed with ONH. Note the pale, hypoplastic optic disc, as compared with G) a fundoscopic image from a 3.5-year-old girl without ONH.

3.1.2 CASK$^{(+/-)}$ mice mimic the human MICPCH phenotype

Since *CASK*-related neurological disorders occur due to deletion of a single *CASK* allele in females, we engineered a *CASK*$^{(+/-)}$ mouse line to model the neurodevelopmental defects (Methods section and Figure 8).

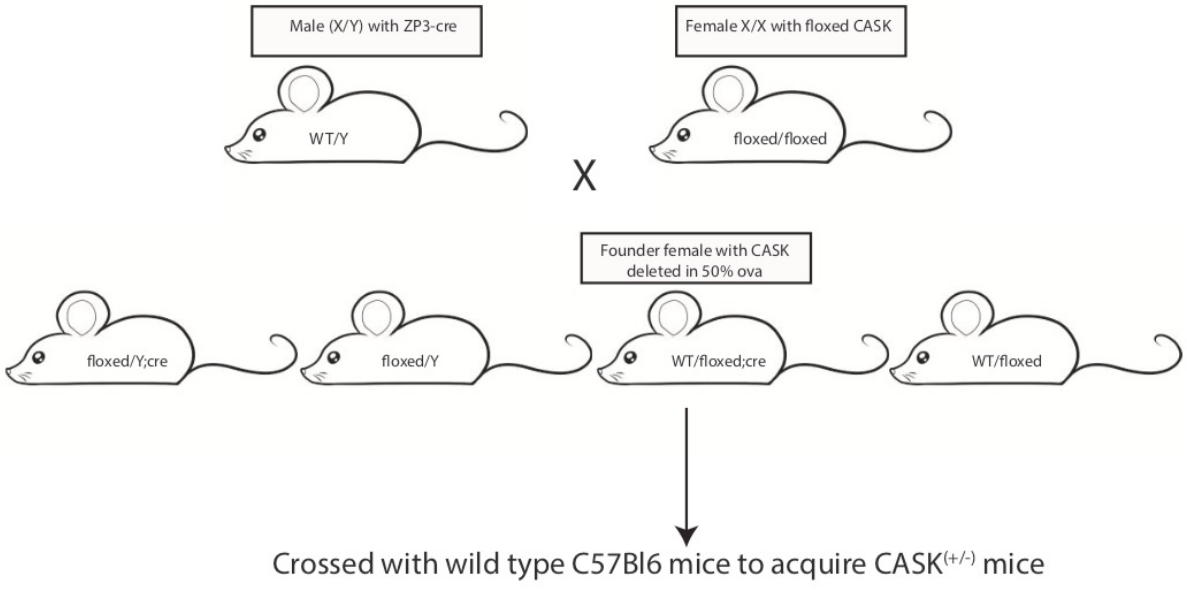

Figure 8: Generation of *CASK*$^{(+/-)}$ heterozygous mutant mice.

Schematic diagram of crosses for generating founder mice for the *CASK*$^{(+/-)}$ colony. Female mice with *CASK* deleted in ova were crossed with the wild type C57Bl6 males to generate *CASK*$^{(+/-)}$ colony.

Similar to the *CASK*$^{(-/-)}$ complete knock-out mice, the brains of *CASK*$^{(+/-)}$ knockout mice were indistinguishable from their wild-type littermates at birth (Figure 9A) (Atasoy, Schoch et al. 2007). However, pronounced microcephaly was observed beginning one week after birth, and the brains of adult *CASK*$^{(+/-)}$ females were ~ 25 % smaller in weight compared to sex-matched wild-type littermate controls (Figure 9A, B). The hematoxylin and eosin (H&E) staining of brain sections showed no significant change in hippocampal size and layering of cells in the *CASK*$^{(+/-)}$ mice (Figure 9C, I), but a marked decrease in cerebellar size (Figure 9D, I) and number of cells in the cerebellum (Figure 9E) was observed in the *CASK*$^{(+/-)}$ mice compared to the *CASK*$^{(+/+)}$ mice, suggesting disproportionate cerebellar hypoplasia. In contrast to lissencephaly (Goldowitz, Cushing et al. 1997), the *CASK*$^{(+/-)}$ cerebellum exhibited normal layering of cells (Figure 9D, E). Examination of the cerebella of 5-day-old *CASK*$^{(+/-)}$ mice revealed that the thickness of the external granular layer (where granule cells are formed) remains unchanged (Figure 5F, G).

These data are consistent with our previous findings that lack of CASK increases cell loss by apoptosis rather than by producing any deficiency in the formation of cells (Atasoy, Schoch et al. 2007). Similar to *CASK* heterozygous deletion mutation patients, the *CASK*$^{(+/-)}$ mice displayed ONH; the optic nerve diameter was significantly reduced compared to sex-matched *CASK*$^{(+/+)}$ littermate controls (Figure 9H, I). Although we observed a trend toward microphthalmia in *CASK*$^{(+/-)}$ mice, the optic globe size difference did not reach a statistical significance (Figure 9H,

I). ONH is frequently accompanied by malformation of the brain midline (Birkebaek, Patel et al. 2003), but we did not observe such an anomaly in the *CASK*$^{(+/-)}$ mice, suggesting that ONH associated with CASK heterozygous deletion mutation has a distinct pathology.

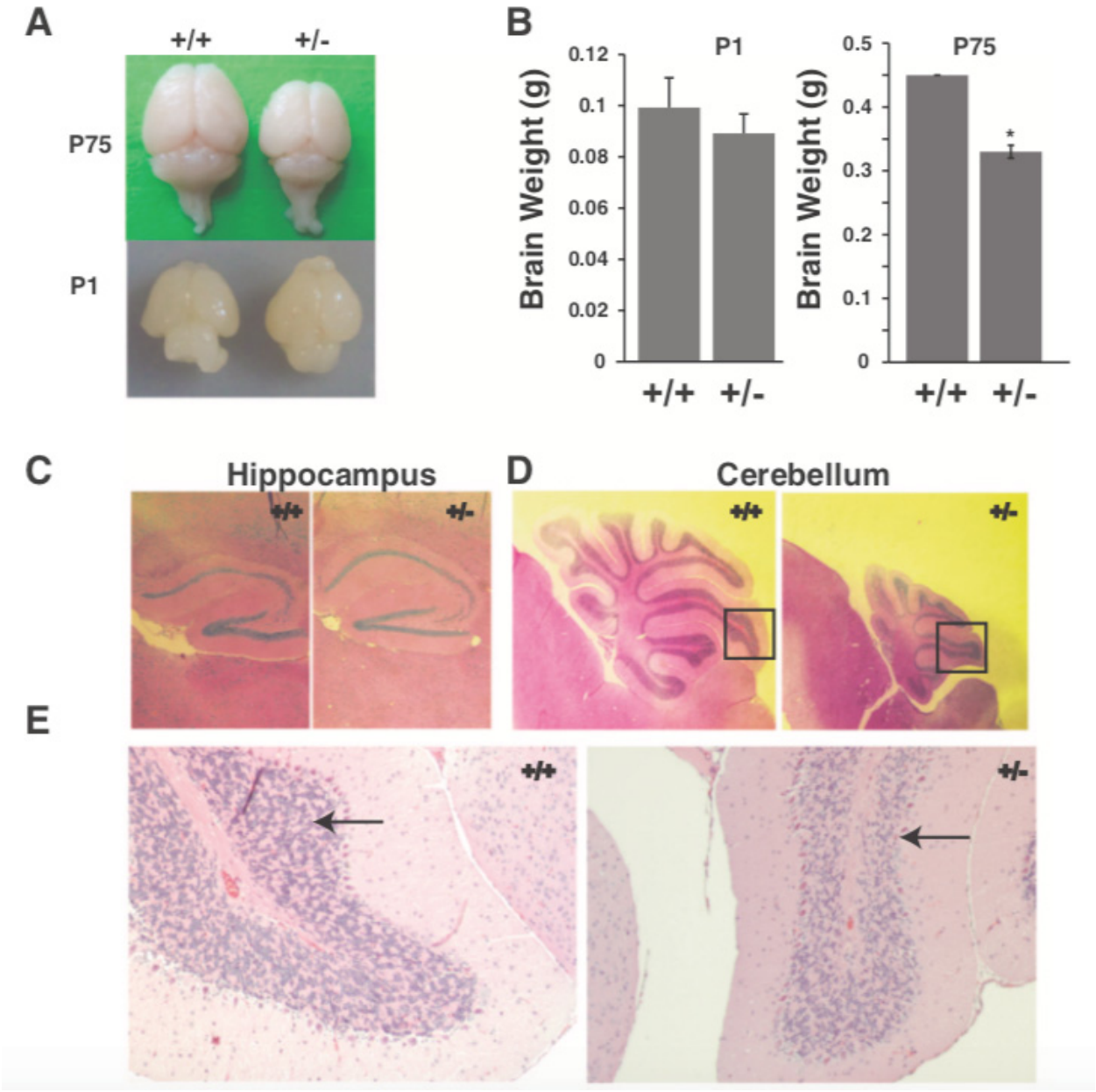

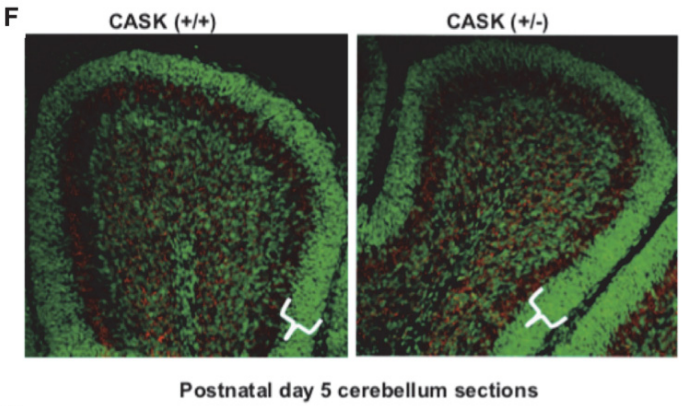
F
CASK (+/+)
CASK (+/-)
Postnatal day 5 cerebellum sections

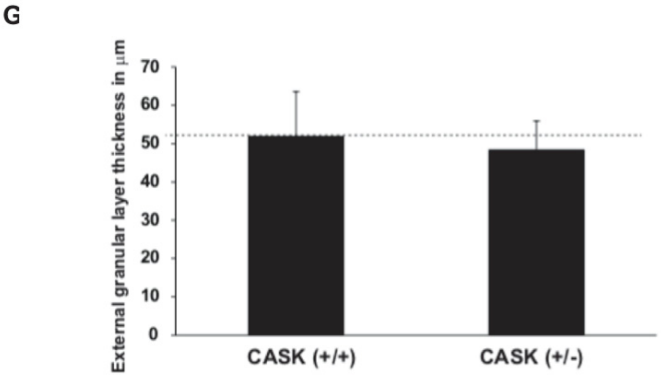
G
External granular layer thickness in μm
70
60
50
40
30
20
10
0
CASK (+/+)
CASK (+/-)

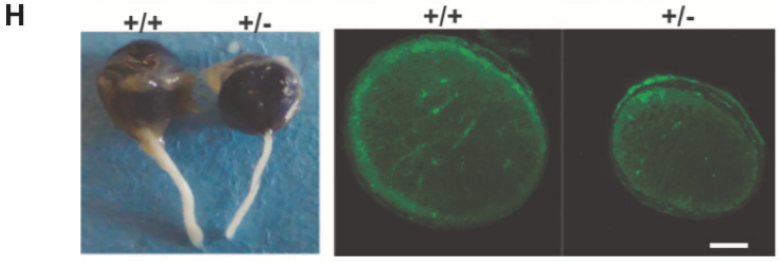
H
+/+
+/-
+/+
+/-

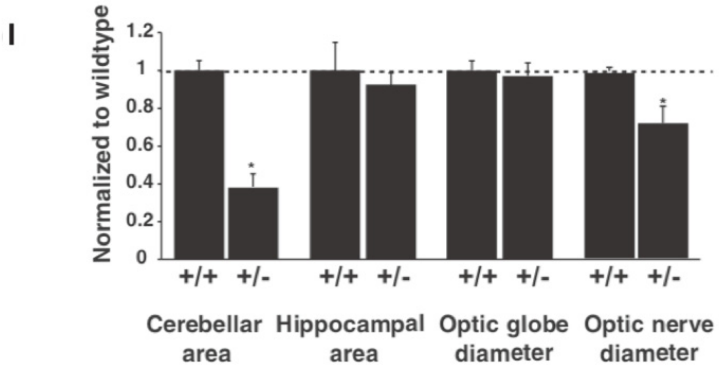
I
Normalized to wildtype
1.2
1
0.8
0.6
0.4
0.2
0
+/+ +/-
+/+ +/-
+/+ +/-
+/+ +/-
Cerebellar area
Hippocampal area
Optic globe diameter
Optic nerve diameter

Figure 9: *CASK*$^{(+/-)}$ mice display postnatal microcephaly, cerebellar hypoplasia, and ONH.

A) Representative brain images of the sex-matched *CASK*$^{(+/+)}$ and *CASK*$^{(+/-)}$ mutant littermates at postnatal day 1 and day 75 (P1 and P75), respectively. B) Quantitation of brain weights from *CASK*$^{(+/+)}$ and *CASK*$^{(+/-)}$ mice at P1 and P75 (* indicates $p < 0.05$, $n = 4$). C) Hematoxylin and eosin (H&E) stained sections of hippocampus derived from *CASK*$^{(+/+)}$ and *CASK*$^{(+/-)}$ mice at P75; note the hippocampi sizes are comparable. D) H&E stained sections of the cerebellum at P75 showing pronounced cerebellar hypoplasia in *CASK*$^{(+/-)}$ mice relative to the *CASK*$^{(+/+)}$ control. E) High magnification of the indicated square regions from panel D showing relatively fewer cells in the cerebellar folia of *CASK*$^{(+/-)}$ mice compared to the *CASK*$^{(+/+)}$ control. F) Cerebella from the postnatal day 5 mouse pups were dissected and fixed in PFA. Parasagittal sections were stained with a green nucleic acid stain to reveal the external granular layer (EGL). G) Quantitation of thickness of EGL is plotted as mean ± SEM, $n = 3$. H) Left panel shows representative images of the optic globe and optic nerve derived from three month old *CASK*$^{(+/+)}$ and *CASK*$^{(+/-)}$ mice . Right panel shows the optic nerve cross section stained with anti-tubulin antibody from *CASK*$^{(+/+)}$ and *CASK*$^{(+/-)}$ mice; note the decrease in optic nerve diameter. Scale bar = 100 μm. I) Quantification of the cerebellar and hippocampal areas and the optic nerve and optic globe diameters obtained from *CASK*$^{(+/+)}$ and *CASK*$^{(+/-)}$ mice. Measurements were made using Image J software and normalized to the sex-matched wild-type littermate controls. Bar graphs are plotted as mean ± SEM (* indicates $p < 0.05$, $n = 4$).

3.1.3 Heterozygous deletion of CASK in mice produces optic nerve pathology

We next examined the optic nerve carefully to test whether heterozygous mutation of *CASK* is sufficient to alter the architecture of optic nerve and subcortical visual system in mice. We analyzed female mouse mutants with a single allele of *CASK* deleted (*CASK*$^{(+/-)}$ mice). We

examined optic nerves following toluidine blue staining of semithin cross-sections - a method that labels myelin and allows the quantification of myelinated retinal axons in the optic nerve. Surprisingly besides being small (Figure 10A, B), the optic nerve displayed an overall decrease in axonal density (Figure 10C, D). The number of axons in a given area was reduced by ~25% and the interaxonal space was expanded (Figure 10E). Histopathology on a single optic nerve hypoplasia case suggested that there may be an increase in number of astrocytes in ONH (Saadati, Hsu et al. 1998). We therefore examined the optic nerve of *CASK*$^{(+/-)}$ mice for levels of glial fibrillary acidic protein (GFAP), a marker of astrocytes. We found a large increase in the GFAP staining in the optic nerve of *CASK*$^{(+/-)}$ mice compared to sex-matched littermate controls suggesting that haploinsufficiency of *CASK* gene may be associated with increased astrocytes in optic nerve (Figure 10F, G).

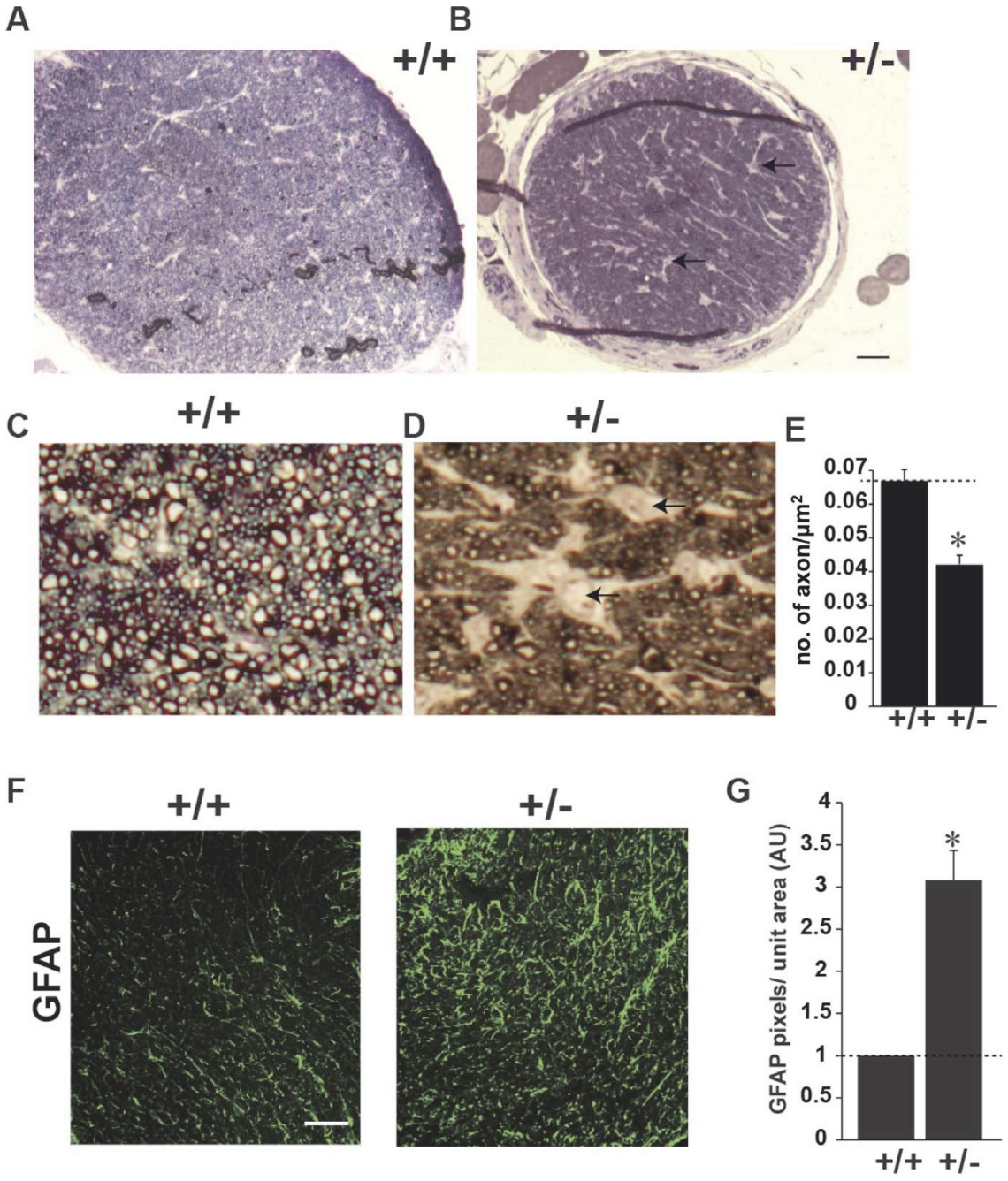

Figure 10: *CASK*$^{(+/-)}$ mice optic nerves display reduced axons and increased astrogliosis.

A and B) representative images of semithin cross section of optic nerves from indicated genotype stained with toluidine blue. Scale bar = 100 µm. C and D) higher magnification of toluidine blue stained semithin optic nerve sections of indicated genotype. Note that *CASK*$^{(+/-)}$ optic nerve has

lesser axonal density and increased interaxonal space (indicated by arrows). E) Axonal density from optic nerve of 4 different mice is quantified, plotted as mean±SEM. (*: $p<0.05$). F and H) Panels showing fluorescence microscopy of cryosections of optic nerve of indicated genotypes. Green panel represents fluorophore tagged cholera toxin B subunit (CTB-Alexa488), red panel represents immunostaining with GFAP. Scale bar = 50 μm. G) Quantification of pixels of GFAP per unit area of optic nerve has been plotted as mean±SEM, n=4.

3.1.4 Axonopathy is present in optic nerves of CASK$^{(+/-)}$ mice

A reduced axonal density in the *CASK*$^{(+/-)}$ mice optic nerve may reflect not only a loss of RGC axons, but also a thinning of individual axons of RGCs. Very small atrophic axons may escape counting from toluidine blue stained semi-thin sections. We therefore performed transmission electron microscopy on cross sections of optic nerves and quantified axons in *CASK*$^{(+/-)}$ mutants (Figure 11A, B). Indeed, our data indicate that the cross-sectioned area of individual axons was significantly decreased in *CASK*$^{(+/-)}$ mice (Figure 11A, B, C, D), with the presence of many very small axons in mutant optic nerves. Since optic nerves contain populations of coarse and fine retinal axons (Guillery, Polley et al. 1982, Williams and Chalupa 1983), we measured the area of coarse and fine axons separately. Our data demonstrate that the area of both the types of axons are decreased in *CASK*$^{(+/-)}$ mice (Figure 11E, F).

We next turned our attention to myelin content in mutant optic nerves, to assess whether the reduction in optic nerve diameter reflects myelin loss. G-ratio distribution spectra, which assess the ratio of axonal diameter to the diameter of the myelinated axon (Guy, Ellis et al. 1989), were applied to compare myelin of wild type littermate mice to that of the *CASK*$^{(+/-)}$ mice. The probability density distribution of G-ratios in mutant mice appears shifted to the left, indicating a

higher myelin-to-axon ration compared to controls (Figure 11G). We interpret these results to indicate that while *CASK* haploinsufficiency influences axon diameter it does not appear to limit the development of compact myelin on these axons.

Because *CASK* is an X-linked gene and is therefore subject to X-linked random inactivation, two types of RGCs exist in *CASK*$^{(+/-)}$ mutant mice, those which produce *CASK* and those which do not. Differences in axonal diameter of *CASK*$^{+}$ and *CASK*$^{-}$ RGCs should produce an increased variability in axonal diameter within the optic nerve in these studies. We therefore measured the mean of deviation (how far on average all values are from the mean), which is a measure of variability of the axonal areas. Surprisingly, the mean deviation for the axonal area in *CASK*$^{(+/-)}$ optic nerve is smaller than the wildtype indicating a tighter distribution (Figure 11H). Overall, the distribution of the area of individual axons was smaller but roughly parallel in *CASK*$^{(+/-)}$ mice and their sex-matched wild type littermate indicating random inactivation of deleted *CASK* allele had no bearing on the development or health of individual axons (Figure 11C). Indeed we have previously documented that *CASK* promotes postnatal brain growth in a non-cell-autonomous manner (Srivastava, McMillan et al. 2016), i.e. *CASK*$^{+}$ and *CASK*$^{-}$ cells are equally affected. We therefore tested if there is specific loss of only *CASK* negative axons in *CASK*$^{(+/-)}$ mice. Specific loss of axons from cells which are *CASK* negative will lead to an artificial skewing of RGCs towards being *CASK* positive. To determine if such is the case, we blotted optic nerve homogenates for CASK, an axonal marker neurofilament associated antigen (NFAA), and a general cellular marker tubulin-α (Figure 11I). Our data suggest that there is a slight reduction in NFAA which did not reach a statistical significance (Figure 11J). Our data thus indicate that the decrease in axonal count from toluidine blue stained section may indeed be an overestimate due

to omission of very small gauge atrophic axons. However, the CASK content within optic nerve was ~47%. Secondary selection of *CASK* positive RGCs would have produced a favorable skewing of X-chromosome inactivation among RGCs (Sharp, Robinson et al. 2000). Under such circumstances we would not expect to see a decrease in CASK protein amount. Therefore our data suggest that ONH in *CASK*$^{(+/-)}$ mice may not be due to specific loss of *CASK* negative axons.

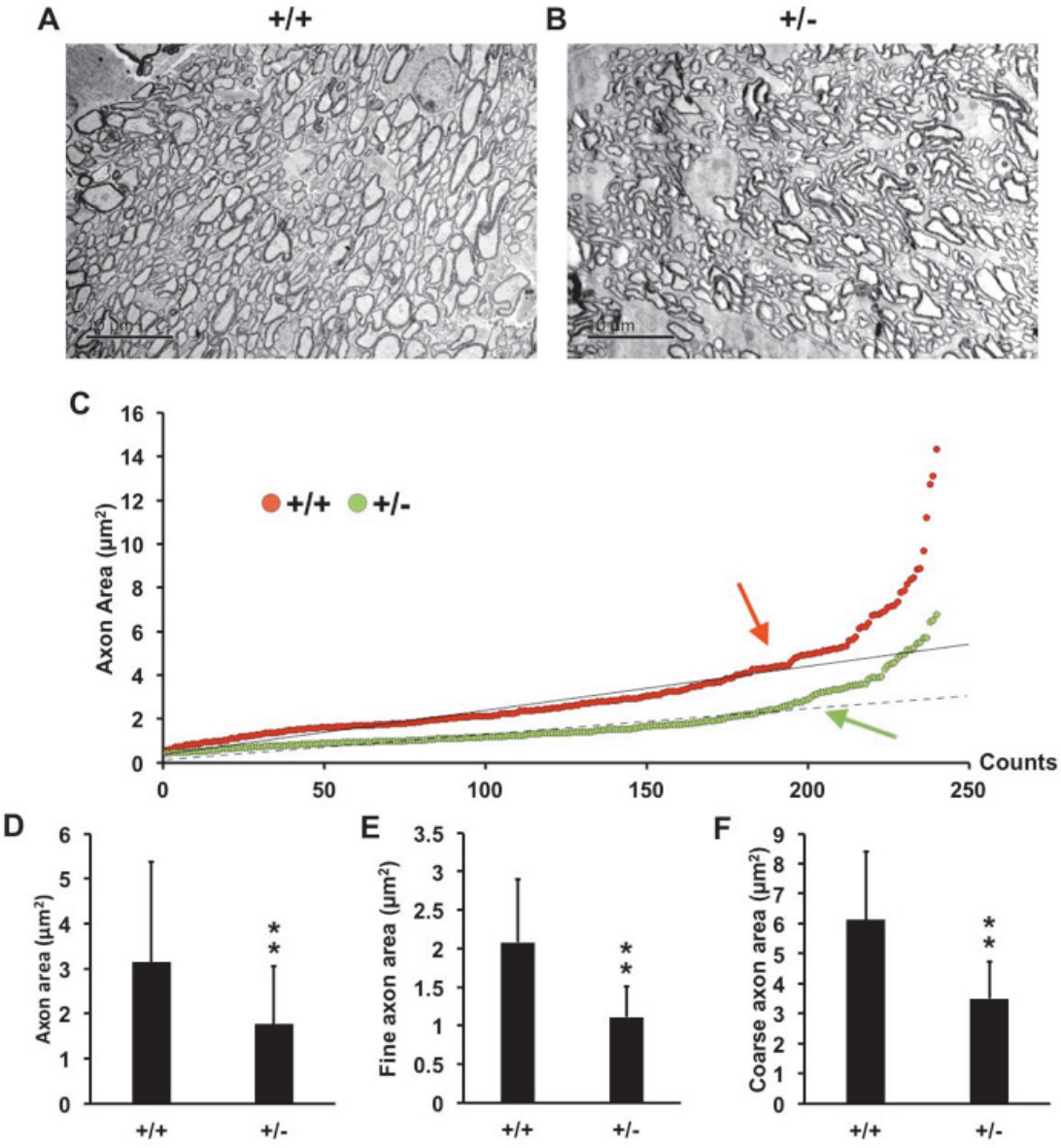

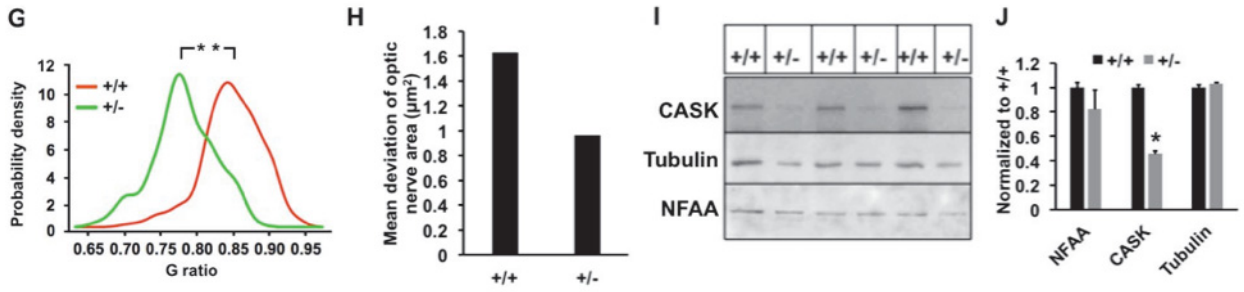

Figure 11: *CASK*$^{(+/-)}$ mice optic nerves display axonal thinning.

A and B) Representative transmission electron micrograph of optic nerve thin sections from indicated genotype. C) Scattered plot of individual axonal area from anonymized images obtained from 3 mice in each group in optic nerves showing two linear regressions for +/+ and +/-. Arrows indicate the threshold where the data points start to lose linearity (correlation coefficient R^2 value starts and continue decreasing). Axons with area values that are greater than or equal to the threshold are considered as coarse axons, and axons with volume values that are smaller than the threshold are considered as fine axons. Threshold value for +/+ is 4 and +/- is 2 (μm^2). D) Mean and standard deviations of all axons from (C) are plotted, N=240. E and F) Comparisons of fine and coarse axons area changes from anonymized images obtained from 3 mice in each group (+/+ and +/-), data are plotted as mean±SD; N=240. G) G-ratio probability density distributions of myelinated optic nerve axons of +/+ and +/-, N=240. H) Mean deviation of optic nerve area is plotted for both genotypes. Mean deviation is a measure of variation and calculated with following formula: mean deviation= $\Sigma (x-\mu)/N$, where x represents each value, μ is the mean and N= number of values. I) Immunoblot of optic nerves from six randomly selected animals of indicated genotype. The antigens are indicated, NFAA is neurofilament associated antigen which is axonal marker. J) Quantitation of the blots normalized to ponceau staining, the

wild-type amount is considered to be 1.0. Data are plotted as mean ±SEM, n=3. (all panels, *: $p<0.05$, **: $p<0.01$)

3.1.5 Retinogeniculate synaptopathy is observed in CASK$^{(+/-)}$ mice

Axonopathy may alter axonal transport and produce defects in synapse formation (Sterman and Sposito 1984). *CASK* has also been shown to be both a trafficking molecule (Wei, Zheng et al. 2011) and a synaptic scaffolding protein. It is also known to interact and phosphorylate presynaptic adhesion molecule neurexin in an activity dependent manner (Mukherjee, Sharma et al. 2008, Mukherjee, Sharma et al. 2010). Neurexins are synaptogenic (Scheiffele, Fan et al. 2000), therefore, we examined retinogeniculate synapses in *CASK*$^{(+/-)}$ mice. It is pertinent to note in previous animal model studies involving worms, flies, and mice, deletion of *CASK* did not produce defects in synapse formation (Hoskins, Hajnal et al. 1996, Atasoy, Schoch et al. 2007, Slawson, Kuklin et al. 2011). We initially examined RGC terminals in thalamus by anterogradely labeling RGCs with intraocular injection of fluorescently conjugated cholera toxin subunit B. We found that there is a significant reduction in small diameter RGC terminals in *CASK*$^{(+/-)}$ mice compared to wild-type littermate (Figure 12A). Because of this change in terminal populations, we examined the ultrastructure of RGC terminals using serial block face scanning electron microscopy. With this technique, retinal terminals can be unequivocally identified based on their ultrastructural morphology (Atasoy, Schoch et al. 2007). Overall synapse volume in *CASK*$^{(+/-)}$ mice remained largely unchanged (Figure 12B, C, D). In order to test if the defect associated with CASK haploinsufficiency is restricted to smaller synapses only or not, we carefully analyzed the ultrastructure of all reconstructed RGC terminals. Our data demonstrate that the number of active zones (release sites) per unit volume of RGC terminals are reduced in *CASK*$^{(+/-)}$ (Figure 12E, F). Furthermore, smaller terminals have significant increase in volume (Figure 12G,

H). Thus, besides the thinning of axons produced by *CASK* haploinsufficiency we also observed defects in retinogeniculate synapse morphology and ultrastructure.

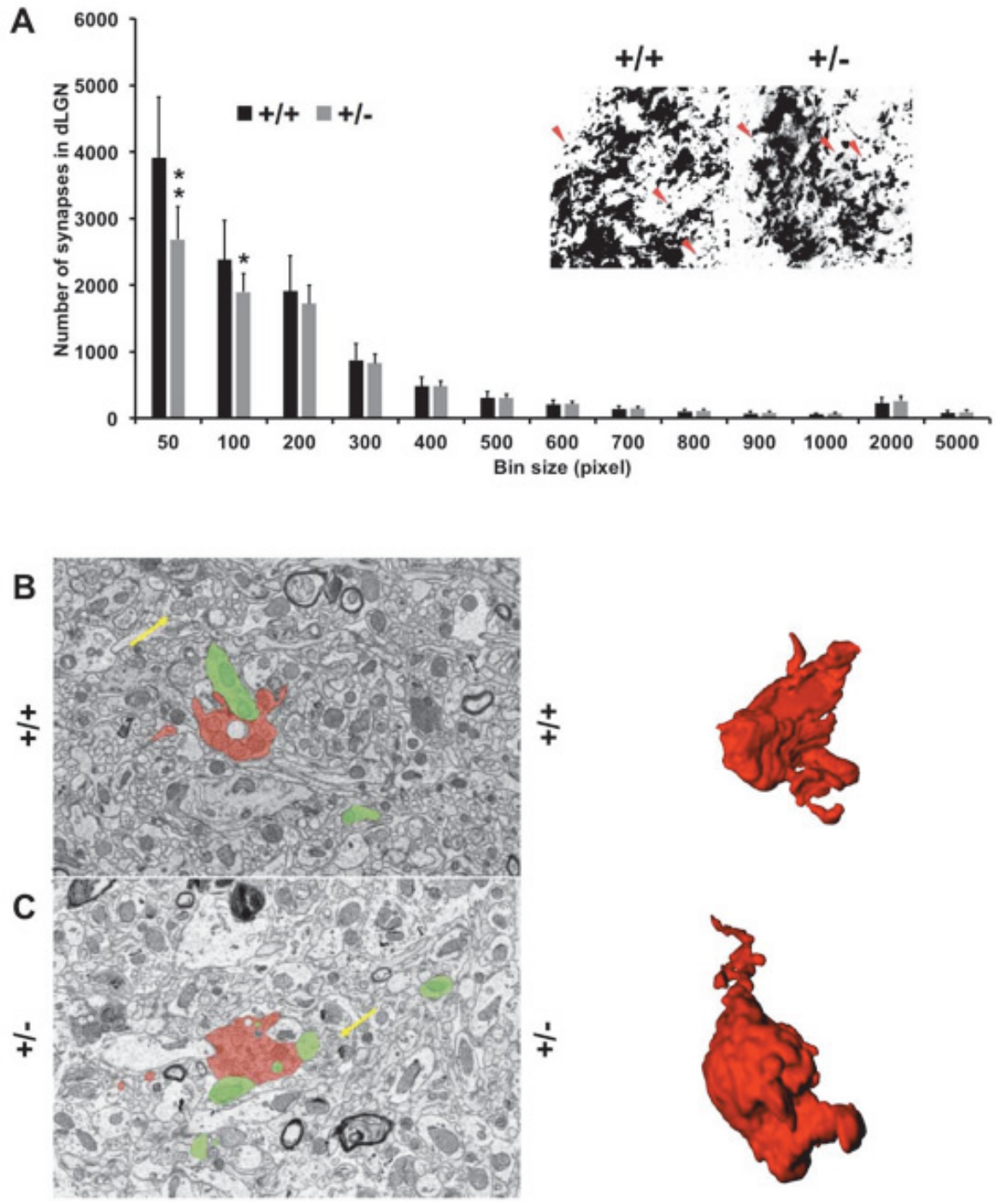

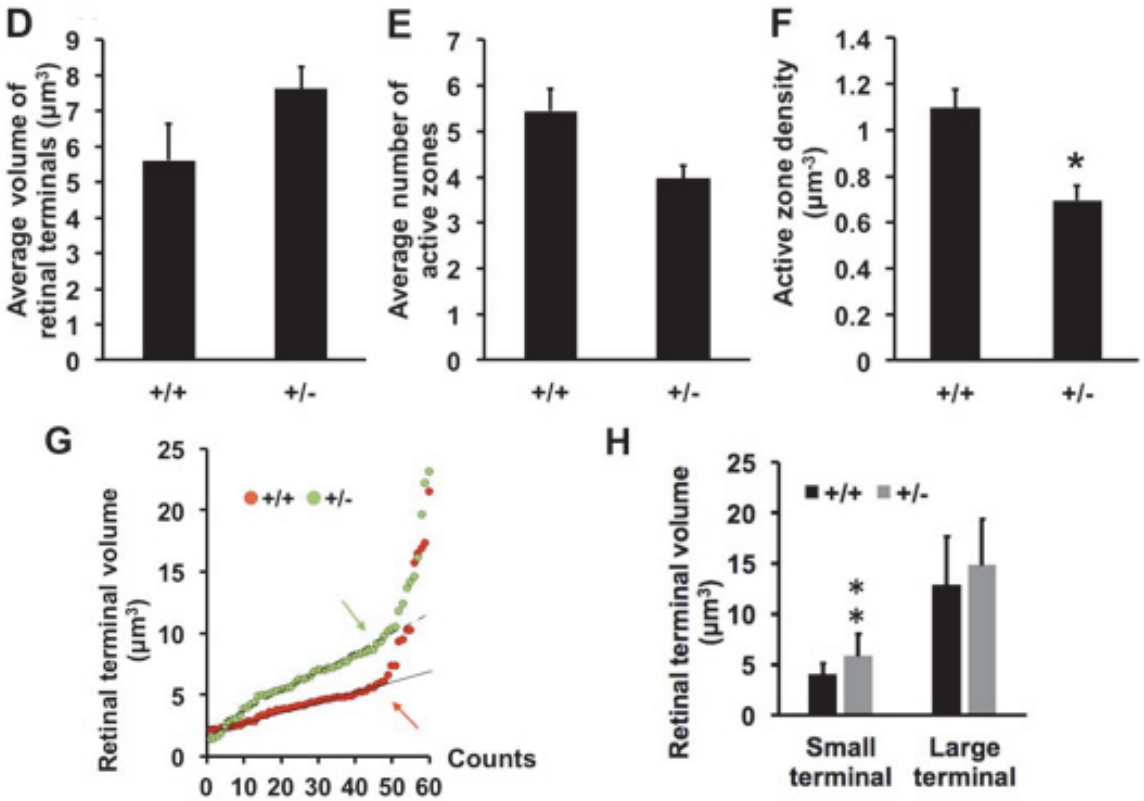

Figure 12: *CASK*$^{(+/-)}$ mice display a decreased number of retinogeniculate synapses and a reduced number of active zones in the remaining synapses.

A) Quantification of the area of terminals in the shell of the dLGN by anterograde labeling of CTB with showing of representative images of dLGN of mice of indicated genotype injected with an anterograde fluorescent tracer (CTB-Alexa488) to label the retinal nerve endings. Red arrows represent distinct terminals of different sizes. Data represents mean±SEM, n=4. B and C) Representative image of SBFSEM ultramicrograph with a retinogeniculate presynapse (identified by presence of pale mitochondria indicated with yellow arrows) labeled red and a postsynapse labeled green. Examples of reconstructed retinal terminals from a series of SBFSEM micrographs are shown on the right, the general volume of reconstructed synapse seems unperturbed. Volumetric quantitation (D), number of active zones (E) and active zone density (F),

of the presynaptic boutons from 60 reconstructed presynapses (SBFSEM analysis) from three different mice in each group are plotted. Data represent mean±SEM, n=3. (*: $p<0.05$, **: $p<0.01$). G) Scattered plot of terminal volumes showing two linear regressions for +/+ and +/-. Arrows indicate the threshold where the data points start to lose linearity (correlation coefficient R^2 value starts and continue decreasing). Terminals with volume values that are greater than or equal to the threshold are considered as large terminals, and terminals with volume values that are smaller than the threshold are considered as small terminals. Threshold value for +/+ is 7 and +/- is 10 (μm^3). H) Comparisons of small and large axons between *CASK*$^{(+/+)}$ and *CASK*$^{(+/-)}$ by terminal volume (bouton), data are plotted as mean±SD; n=3.

3.1.6 RGC numbers are reduced in CASK$^{(+/-)}$ mice

CASK is present in all retinal cells (Anjum, Ayoubian et al. 2014) and since we detected both a thinner optic nerve and a lowered axonal density in optic nerve of *CASK*$^{(+/-)}$ mice, we next examined if there was also a loss of retinal integrity or RGCs in *CASK*$^{(+/-)}$ mice. Immunolabeling mutant and control retinal cross-sections with antibodies against Calretinin (Calr) (Figure 13A), revealed that the general cytoarchitecture and laminated structure of the retina was preserved in the absence of CASK. To assess whether there was a specific loss of retinal ganglion cells in *CASK*$^{(+/-)}$ mice we counted the total number of cells within the ganglion cell layer of the retina, by labeling nuclei with DAPI and staining for RBPMS, an RNA binding protein selectively expressed by RGCs in the rodent retina (Samuels, Hsueh et al. 2007) (Figure 13B). Together these data reveal a significant loss of RGCs in *CASK*$^{(+/-)}$ mutants (Figure 13A, B, C). Taken together, we find that ONH in *CASK*$^{(+/-)}$ mice is a complex developmental disorder involving a decrease in the number of RGCs, thinning of individual axons, reactive astrogliosis within the optic nerves, and alterations in retinogeniculate synapses. Thus, mutation of *CASK* appears to

phenocopy many of the features observed in human patients with ONH and therefore represents an appropriate mouse model to elucidate the mechanisms underlying ONH.

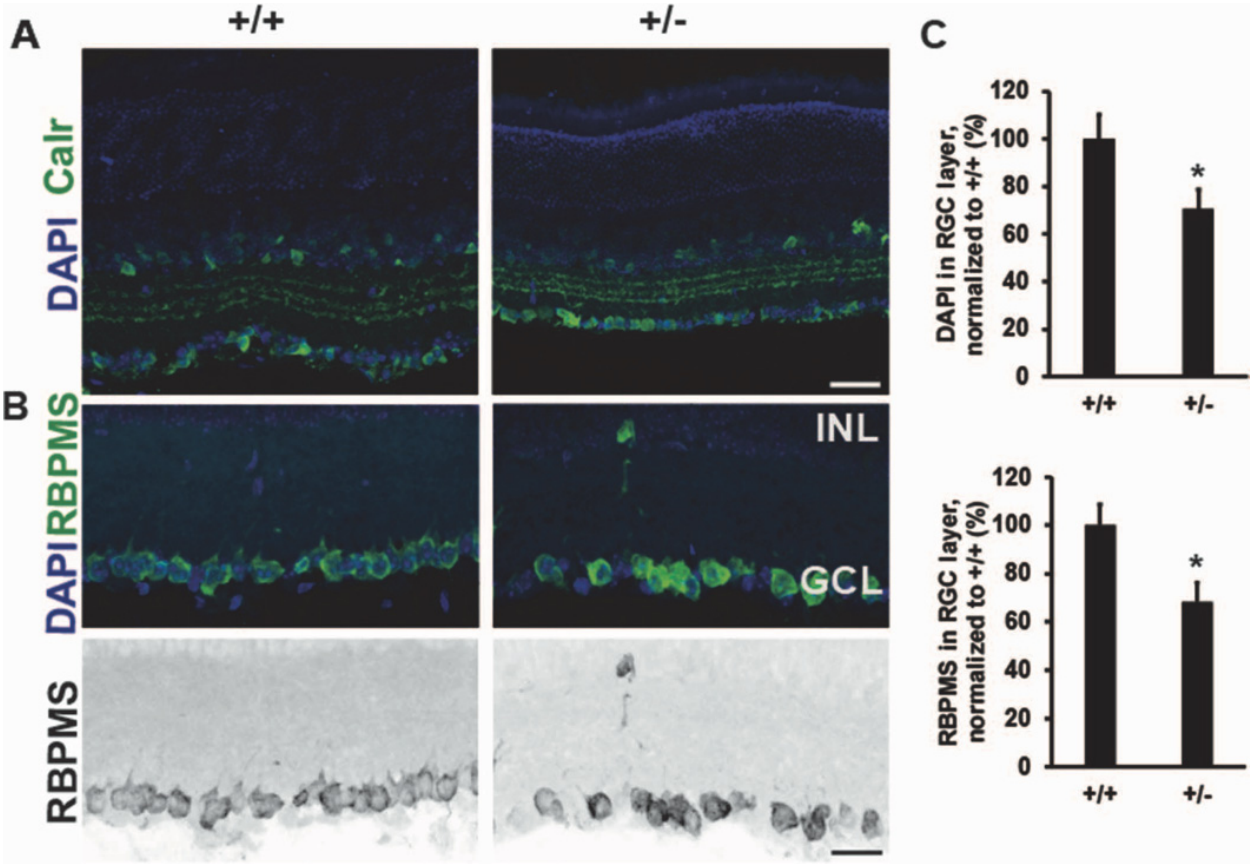

Figure 13: Decreased number of retinal ganglion cells in *CASK*$^{(+/-)}$ mice.

A) Immunostaining of retina with antibodies against calretinin reveals normal lamination in *CASK*$^{(+/-)}$ mutants at P26. B) Representative images of retinas stained with DAPI and RNA-Binding Protein with Multiple Splicing (RBPMS) reveal a significant loss of cells in the ganglion cell layer in *CASK*$^{(+/-)}$ mutants compared to controls. Scale bar = 25 µm. Lower panel is a grey scale image for better visualization. C) Quantition of cells in the ganglion cell layer in indicated staining (mean ± SEM, *: $p<0.05$).

In an order to be comprehensive in our analysis we also measured the thickness of other layers of the retina to evaluate if these layers are affected by CASK loss. Our data indicate the lamination of retinal layers is not perturbed in *CASK*$^{(+/-)}$ mice (Figure 14A, B).

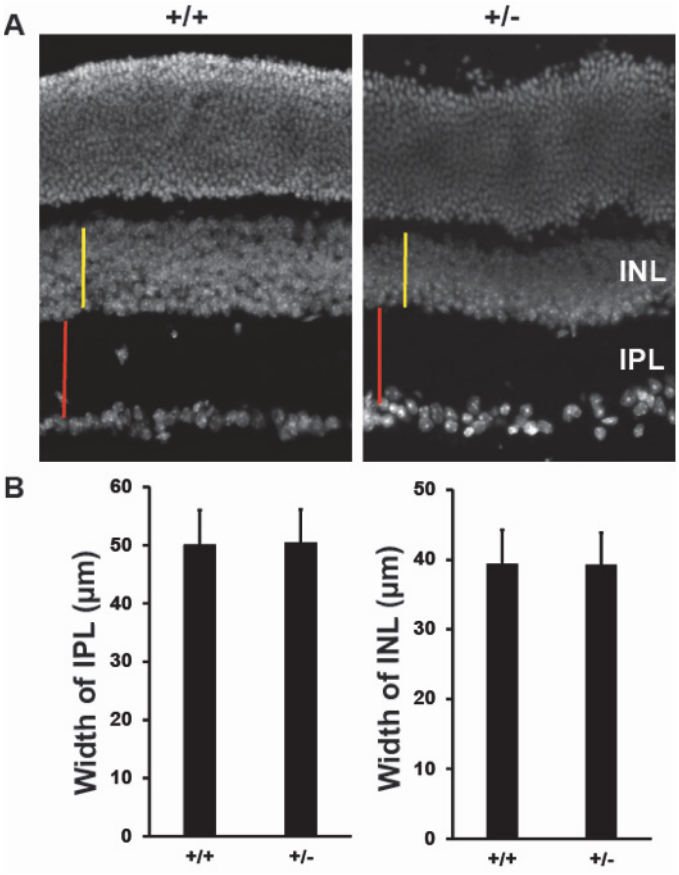

Figure 14: Retinal lamination remains the same among genotypes.

A) Representative images of retinas taken with confocal microscope. These images were imported to Image J, lines were drawn for the Inner Plexiform Layer (IPL), shown with red lines, as well as the Inner Nuclear Layer (INL), shown with yellow lines. Lengths of red and yellow lines were quantified for each image (several locations per image, n = 5 mice per genotype). B) Quantification of width for IPL and INL (plotted as mean ± SEM).

3.2 ONH is developmental in nature and CASK is not required for survival of adult mice

3.2.1 ONH develops postnatally in CASK$^{(+/-)}$ mice

The first mechanistic question regarding ONH pathogenesis that has eluded our understanding is when exactly the disease is initiated. The decrease in RGCs and their axons could occur pre- or postnatally. While it is difficult to parse these differences out in humans, in this mouse model the difference can be studied by observing optic nerve diameter throughout development. We therefore examined toluidine blue stained semi-thin section of *CASK*$^{(+/-)}$ and control optic nerves during the first three weeks of postnatal mouse development (Figure 15A). It is important to point out that the first two postnatal weeks of rodent development correspond to developmental milestones that occur in the third trimester of human fetal development (Dobbing and Sands 1979). Moreover, neonatal mice do not open their eyes until the end of the second postnatal week of development. Surprisingly, the optic nerves of P1 *CASK*$^{(+/-)}$ mice were of similar size to that of the wildtype controls (although, a slight trend towards being smaller was observed). A more clear and significant difference between the size optic nerves became apparent by the end of the first week of postnatal development and the difference from the wildtype reaches the difference observed in adults by P22 (Figure 15B). Although myelinogenesis starts around P5 in mouse optic nerves, it peaks during the third and fourth postnatal week (Dangata and Kaufman 1997). By P22 myelinated axons are easily quantifiable in the optic nerve. To confirm that the decrease in axonal density occurs at an early age and not as a part of later degeneration, we examined the number of axons in P22 optic nerve per unit area. Our data indicate that axonal density is already reduced (at par as noted in adults, Figure 10C) by this stage suggesting that *CASK*-linked ONH can clearly be classified as a developmental and not a degenerative process (Figure 15C). Since, we observed thinning of optic nerve only from P6, we repeated the measurement of RGCs at P6.

Our data indicates that at P6 there is no reduction in RGC numbers in *CASK*$^{(+/-)}$ mice, indicating a potential loss of RGCs early in development (Figure 15D, E). However, the apoptosis *in situ* detection assay on P6 retinas shows *CASK*$^{(+/-)}$ has an increased number of apoptotic cells in both the internal nuclear layer and the RGC layer, indicating a reduction in RGC number in the later development, which corresponds with our RGC counting results at P22 (Figure 15F, G, H). Overall, our data demonstrate that ONH in *CASK*$^{(+/-)}$ mice occurs early in postnatal development (P6-P22), prior to the full maturation of the subcortical visual system.

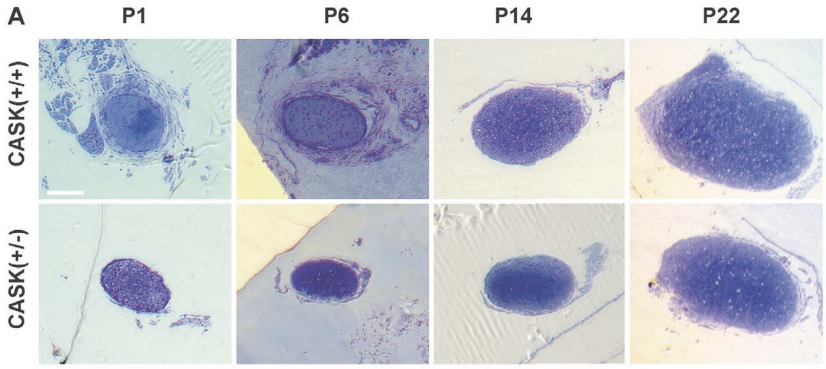
A
P1
P6
P14
P22
CASK(+/+)
CASK(+/-)

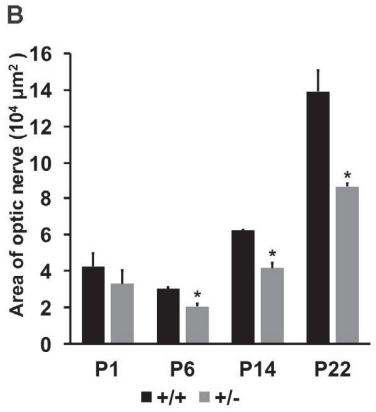
B
Area of optic nerve (10⁴ μm²)
16
14
12
10
8
6
4
2
0
P1
P6
P14
P22
+/+
+/-

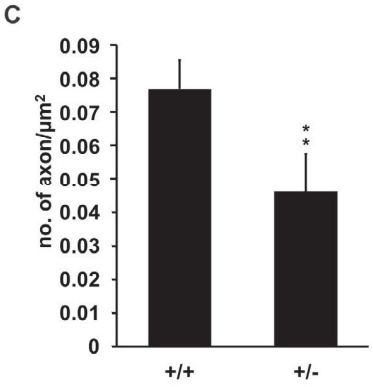
C
no. of axon/μm²
0.09
0.08
0.07
0.06
0.05
0.04
0.03
0.02
0.01
0
+/+
+/-

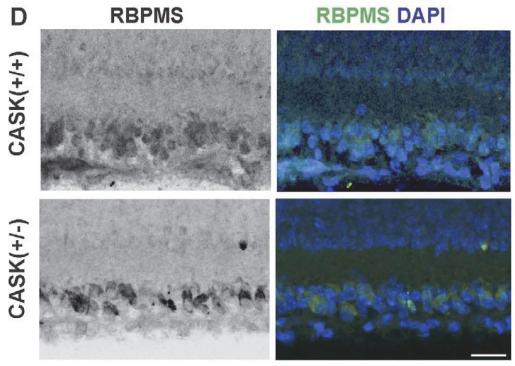
D
RBPMS
RBPMS DAPI
CASK(+/+)
CASK(+/-)

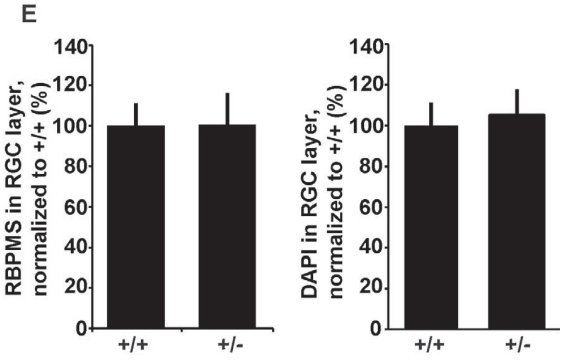
E
RBPMS in RGC layer, normalized to +/+ (%)
DAPI in RGC layer, normalized to +/+ (%)
140
120
100
80
60
40
20
0
+/+
+/-

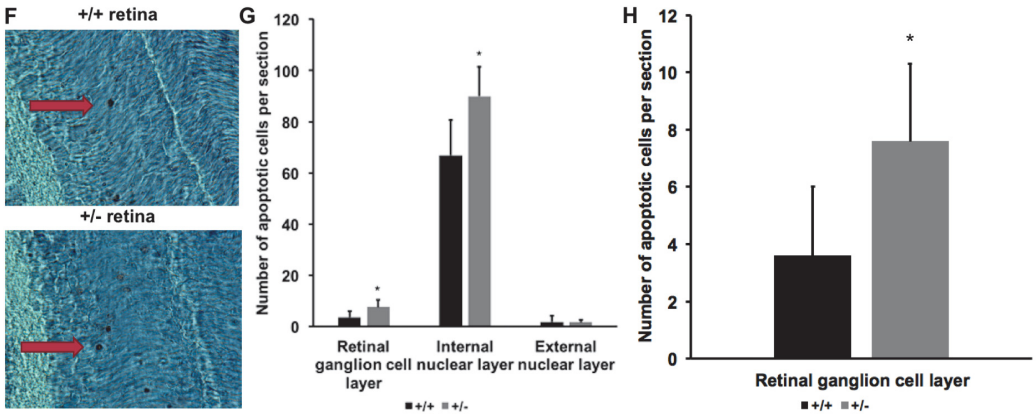

Figure 15: *CASK*$^{(+/-)}$ mice optic nerves display the secondary reduction in size.

A) Representative images of toluidine blue stained semithin-sections derived from optic nerve of indicated age and genotypes (P=postnatal). Scale bar = 100 µm. B) Quantitation of optic nerve areas from mice of indicated age and genotype, data are plotted as mean±SEM, n=3. C) Quantitation of axonal density, data are plotted as mean ±SD. (*: $p<0.05$; **: $p<0.01$). D) Representative images of retinas from P6 mice stained with DAPI and RNA-Binding Protein with Multiple Splicing (RBPMS) reveal no change of cells in the ganglion cell layer in *CASK*$^{(+/-)}$ mutants compared to controls. Left panels are in grey scale for better visualization. Scale bar = 25 µm. E) Quantition of cells in the ganglion cell layer in P6 retina. F) TUNEL assay (Neurotacs II, Trevigen) for *CASK*$^{(+/+)}$ and *CASK*$^{(+/-)}$ retinas results show apoptotic cells as black dots (red arrows). G) Quantification of apoptotic cells in different retinal layer, showing number of cells per cryosection slice (mean±SEM, *: $p<0.05$). H) Enlarged image of the quantification of apoptosis in retinal ganglion cell layers (mean±SEM, *: $p<0.05$).

3.2.2 CASK is not essential for survival after maturity

Cerebellar growth in mouse is largely postnatal, with both area and volume increasing till adulthood (Goldowitz, Cushing et al. 1997). Therefore, to investigate the role of CASK in

mature brain, after development of cerebellum we generated inducible *CASK* knockout mice (*CASK*^{iKO}) by crossing the *CASK*^{floxed} mice to a mouse line expressing estrogen receptor fused Cre recombinase ubiquitously. In the resulting male mice, *CASK* can be acutely deleted using tamoxifen injection. Experiments with indicator mouse expressing recombination dependent tdTomato expression suggest that there is considerable degree of leakiness in Cre-recombination activity even in absence of tamoxifen. In some areas, up to 8~20% cells expressed tdTomato. However, upon a single dose of tamoxifen 90~95% cells exhibited recombination in all major organs including brain within a week (Figure 16A, B, C).

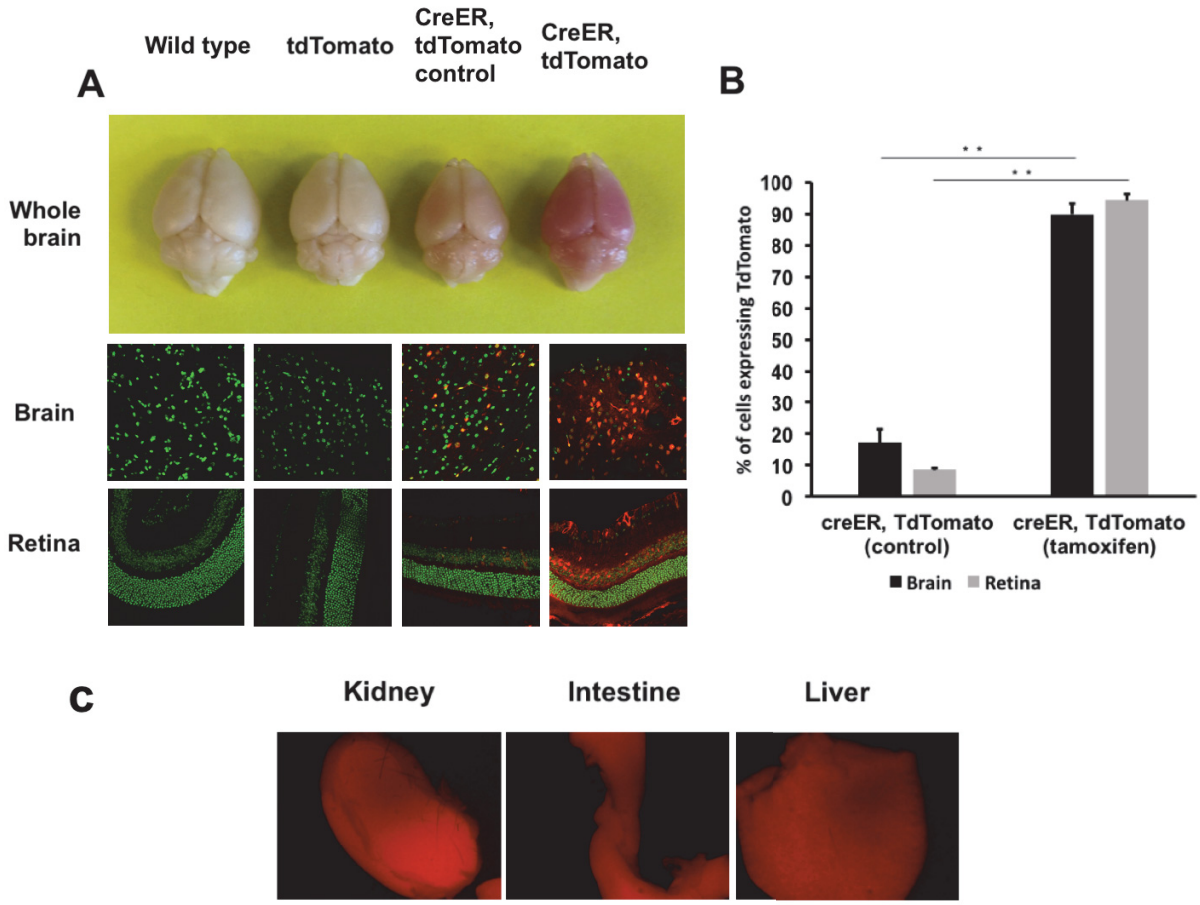

Figure 16: Tamoxifen successfully induced expression of tdTomato in CreER tdTomato mice.

A) representative images showing red (tdTomato signal) brain and red cells under confocal microscope as an indication of Cre recombinase expression. Nuclei were stained with DAPI and shown as green. B) quantifications of the percentage of cells that are red in color from brain and retina (inner nuclear layer) (mean±SD, N=3). C) Kidney, intestine, and liver are also red under fluorescence microscope.

Four *CASK*^{iKO} mice were followed for 47 days. Mice did not exhibit any major abnormal behavior phenotypes. Beginning 47th day mice received 5 daily doses of tamoxifen by intraperitoneal injection. None of the mice exhibited any phenotypic response to tamoxifen injection up to 2 months of initial injection (Figure 17A). Mice were then sacrificed and brains were examined. Our data indicate that as expected the mouse brains had less than 5% of CASK remaining (Figure 17B). However, there is no change in synaptic protein synaptophysin, active zone organizer liprin-α or astrogliosis marker GFAP (Figure 17C). Nissl granule staining indicated although the brain of the CASK null mice is smaller due to presumably smaller size of the mice, there is no obvious pathological changes (Figure 17D). Toluidine blue staining of wild type, *CASK*^{floxed} and *CASK*^{iKO} mice showed no differences in optic nerve diameter (Figure 17E). Thus, the dominant role of CASK manifests only during the postnatal phase and loss of CASK function is not essential for survival or optic nerve maintenance past maturity.

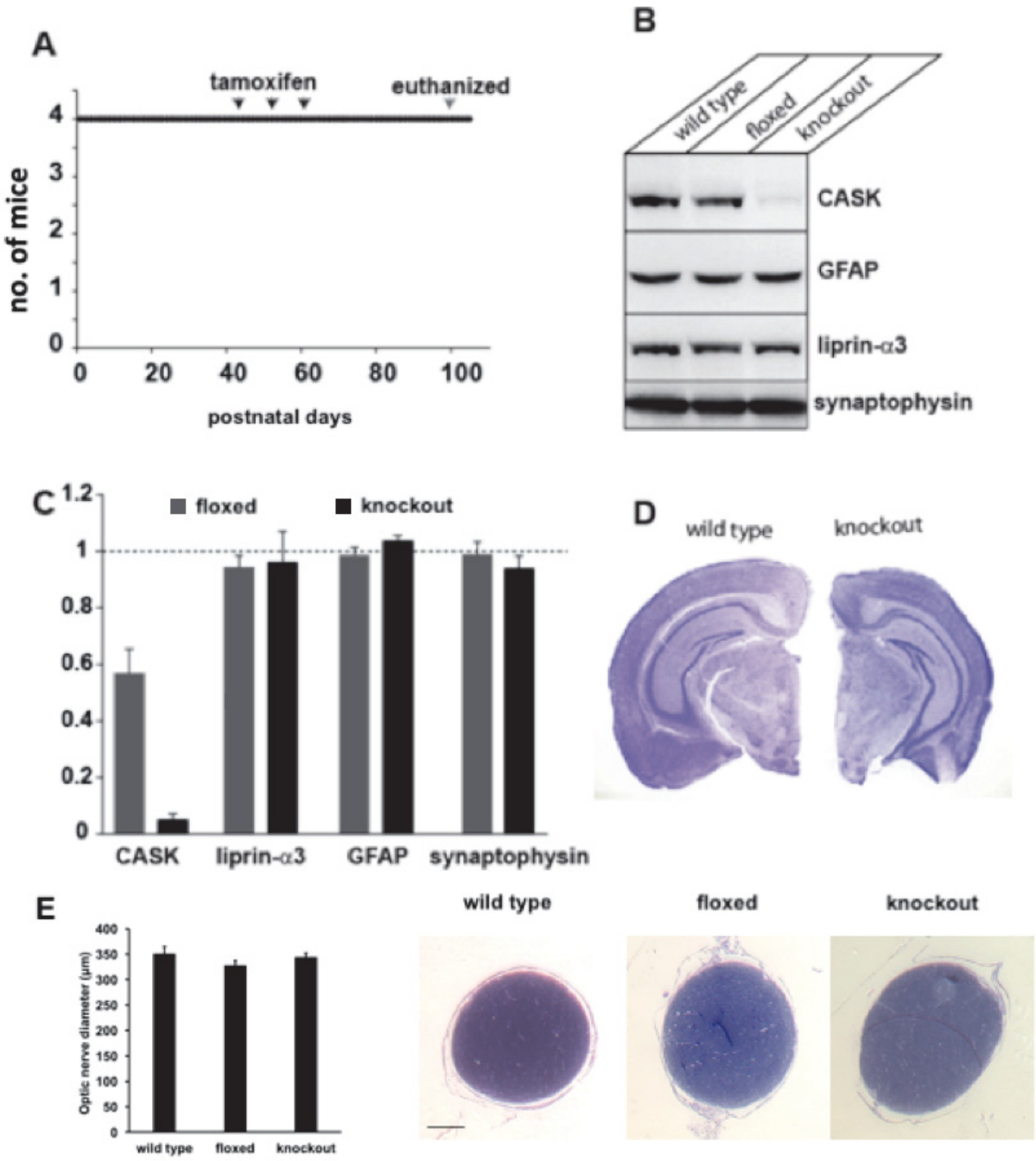

Figure 17: Adult tamoxifen-induced *CASK* knockout (*CASK*^{iKO}) displayed no abnormalities.

A) days and numbers of adult knockout mice that survived after tamoxifen injection. B) immunoblotting for CASK and indicated proteins on wild type, *CASK*^{floxed} and *CASK*^{iKO} brain lysates. C) Quantification of the immunoblotting result, normalized to wild type (mean±SEM, n=4). D) Representative images of wild type and *CASK*^{iKO} brain nissl staining slices. E) Optic nerve cross section diameters of wild type, *CASK*^{floxed} and *CASK*^{iKO} mice with toluidine blue staining representative images (mean±SEM, n=3). Scale bar = 100 μm.

3.3 CASK plays a valuable role in neuron but CASK-linked ONH is not always coupled to microcephaly

3.3.1 Cerebellum hypoplasia but no ONH was observed in adult CASK^{floxed} mice

The brain of the *CASK*^{floxed} mice is structurally normal but displayed a much smaller cerebellum (Figure 18A, B, C, D). Although overall the weight of the brain is smaller in the CASK hypomorph mice, the ratio of brain weight to lean body mass remained unchanged indicating these mice have a brain which is appropriate for their body size (Figure 18E, F). The weight of the cerebellum however appeared to be 10% smaller when compared to the rest of the brain indicating that *CASK*^{floxed} mice have a specific cerebellar hypoplasia (Figure 18G). We therefore examined the cerebella more closely, section of *CASK*^{floxed} cerebella indicated the area of cerebellum is overall small (Figure 18H); however there is no change in vermis to cerebellar hemisphere ratio, or folia formation indicating a global cerebellar hypoplasia (Srivastava, McMillan et al. 2016). Unlike *CASK*$^{(+/-)}$ mice, *CASK*^{floxed} mice didn't have ONH, shown as no changes in optic nerve diameter or RGC axon density (Figure 18I, J). Overall the data do not indicate presence of any specific optic nerve pathology.

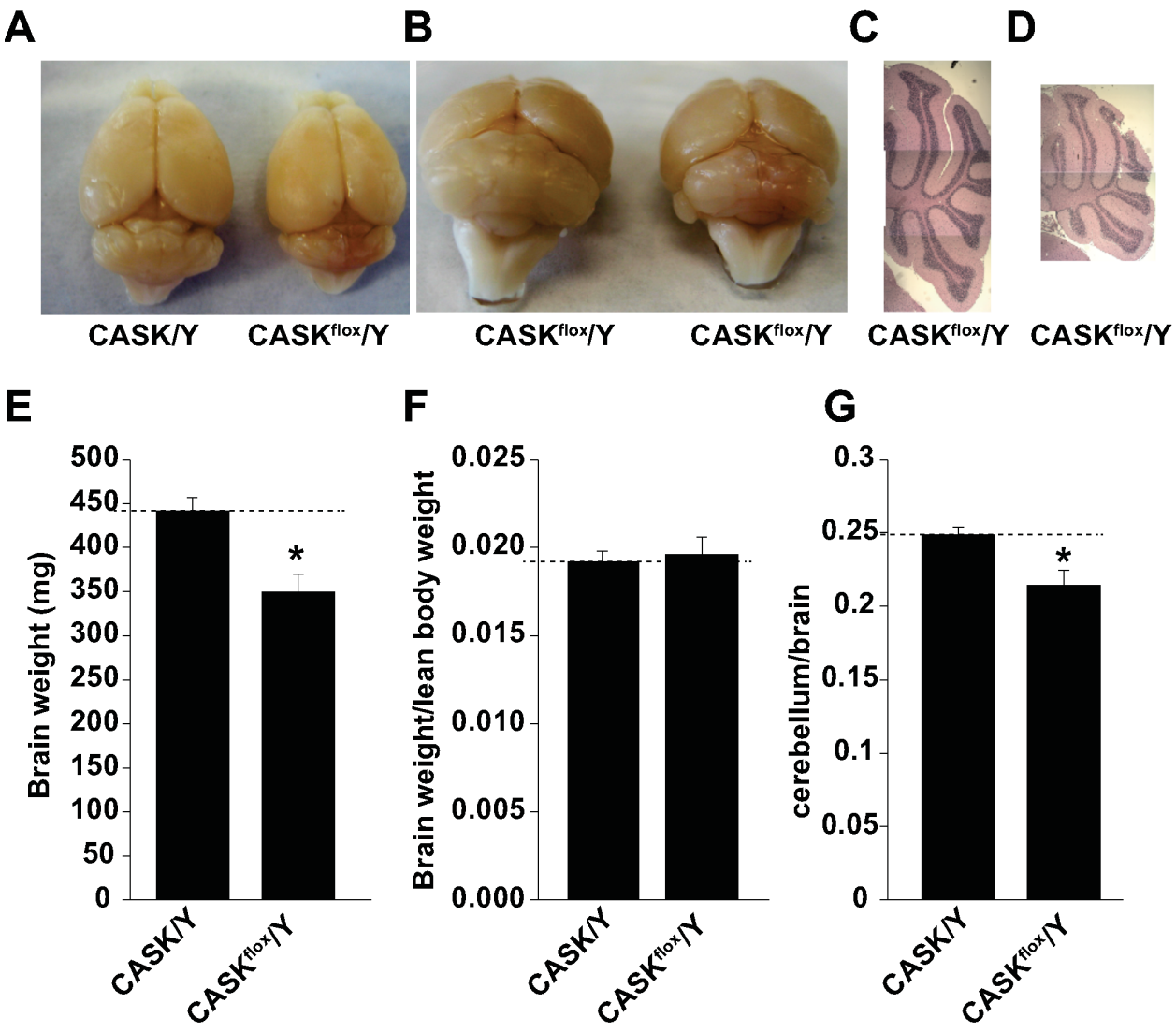
A
B
C
D
CASK/Y
CASKflox/Y
CASKflox/Y
CASKflox/Y
CASKflox/Y
CASKflox/Y
E
F
G
Brain weight (mg)
500
450
400
350
300
250
200
150
100
50
0
*
CASK/Y
CASKflox/Y
Brain weight/lean body weight
0.025
0.020
0.015
0.010
0.005
0.000
CASK/Y
CASKflox/Y
cerebellum/brain
0.3
0.25
0.2
0.15
0.1
0.05
0
*
CASK/Y
CASKflox/Y

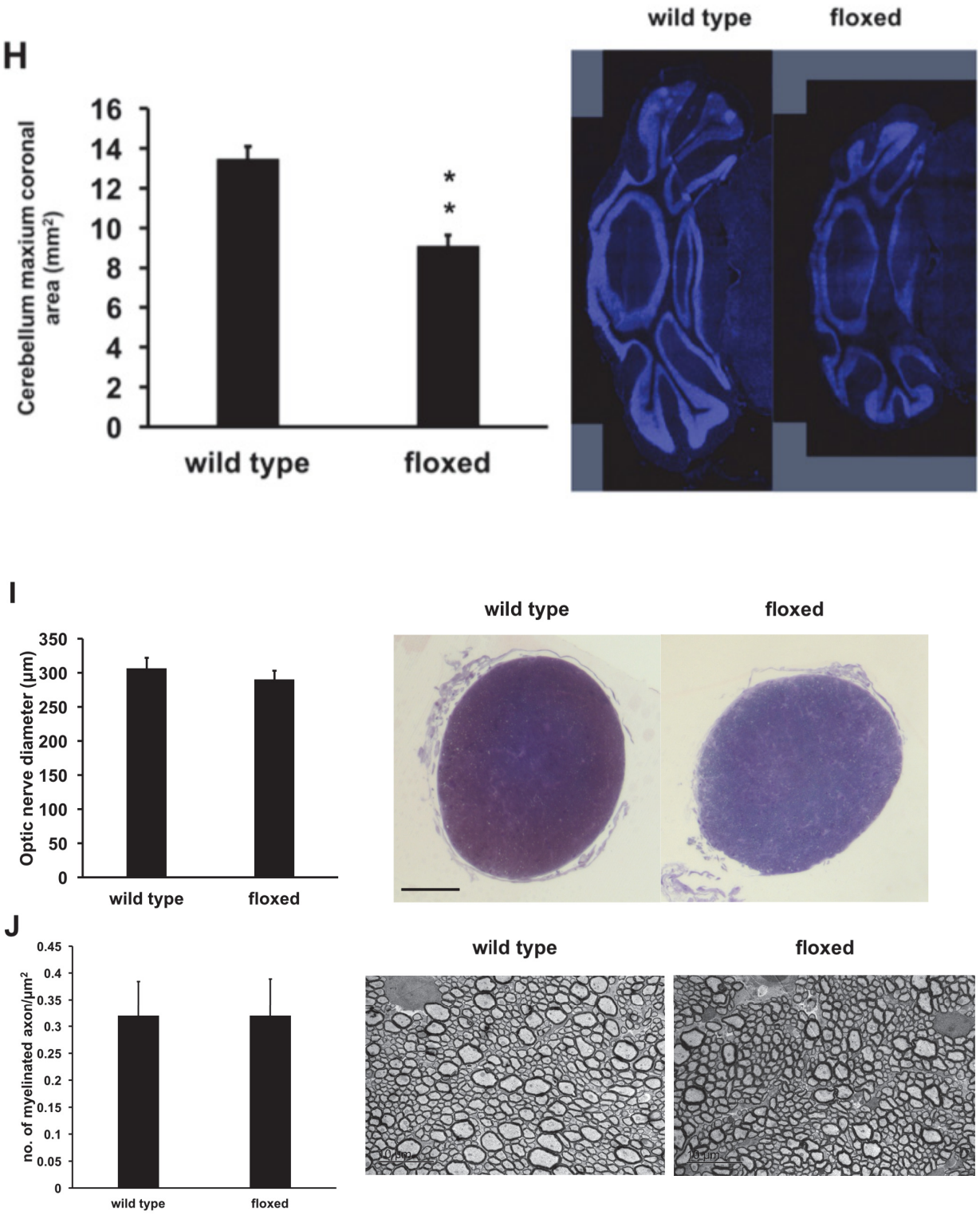

Figure 18: Characterization of adult wild type and *CASK*^{floxed} brain and optic nerve.

A, B) representative images of wild type and *CASK*^{floxed} cerebellum. C, D) Hematoxylin and eosin (H&E) staining of wild type and *CASK*^{floxed} cerebellar sagittal sections. E, F, G) Measurements of brain weight, brain to lean body weight ratio and cerebellum to whole brain weight ratio of wild type and *CASK*^{floxed} mice. H) Quantifications show cerebellar coronal section area of *CASK*^{floxed} cerebellum is less than wild type. Representative confocal images of cerebellar area, stained with DAPI, are shown on the right. I) Optic nerve cross sectional diameters of wild type and *CASK*^{floxed} with representative toluidine blue staining images. Scale bar = 100 μm. J) Optic nerve density of wild type and *CASK*^{floxed} with TEM representative images (mean±SD).

3.3.2 MICPCH pathology is not purely neuronal in origin

A large body of literature suggests that CASK may have a potential synaptic function (Reviewed in (Hsueh 2006)), abnormality in which may lead to death of brain cells. Previously, attempt to generate brain specific *CASK* knockout mice was done using transgenic mice expressing Cre recombinase driven by nestin promoter to delete *CASK* from embryonic brain. The resultant mice exhibited postnatal lethality like the constitutive *CASK* knockout mice (personal communication with Prof. Susanne Schoch McGovern). However, besides neurons, nestin is also expressed in non-neuronal brain cells and even in extra-neuronal tissue which made it difficult to interpret this data (Wagner, Wagner et al. 2006, Walker, Goings et al. 2010). We have therefore generated the pan-neuronal-specific *CASK* knockout mice by crossing *CASK*^{floxed} mice (Atasoy, Schoch et al. 2007) with a synapsin1-Cre line which expresses Cre exclusively in post-mitotic neurons (Schoch, Cibelli et al. 1996, Zhu, Romero et al. 2001). In parallel, we also crossed the synapsin-Cre mice with the reporter mouse line that expresses tdTomato in a Cre-dependent manner. Our experiments confirmed the previous findings that Cre-mediated recombination in these mice

occurs in nearly all neurons at an embryonic stage (as early as E12.5) (Zhu, Romero et al. 2001) and Figure 19A, B). Since most CASK-associated patients are females harboring a heterozygous mutation in *CASK*, we initially examined female mice heterozygous for deletion of *CASK* pan-neuronally. Surprisingly, female mice heterozygous for neuron-specific *CASK* deletion exhibit no major phenotype and have normal-sized brains, including the cerebellum (Figure 19C, D, E, F). This observation strongly suggests that *CASK*-associated MICPCH in humans is not specifically a neuronal pathology.

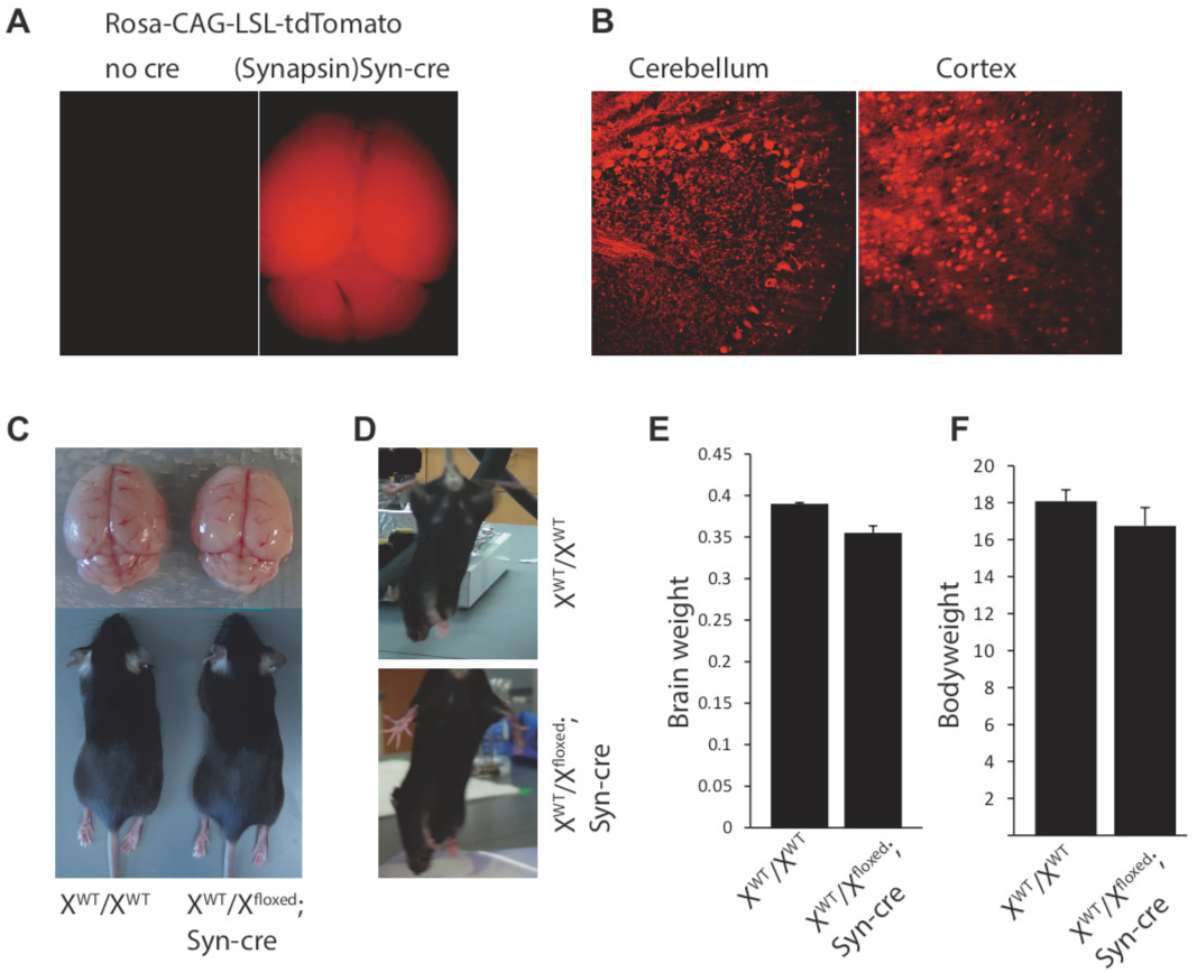

Figure 19: Deletion from neurons and characterization of female heterozygous mice with neuron-specific *CASK* deletion.

A) Representative brain images of Rosa-CAG-LSL-tdTomato mice with or without synapsin-Cre; note the ubiquitous expression of tdTomato with synapsin-Cre. B) Sections from cerebellum and cortex showing Cre-mediated recombination in most neurons. C) Representative images of brain from mice with indicated genotypes (the mice are shown in lower panel). D) Shows that mice heterozygous for neuron-specific *CASK* deletion do not exhibit hind-limb clasping phenotype. E) Comparison of brain weight of mice with indicated genotypes. Bar graphs are plotted as mean ± SEM, n = 4. F) Comparison of body weight of mice with indicated genotypes.

Consistent with this assumption, complete deletion of *CASK* from all neurons did not produce the neonatal lethality observed in the constitutive *CASK* knockout mice (Atasoy, Schoch et al. 2007) (Figure 20A). The CASK neuronal-null mice are indistinguishable from their wild-type littermates until ~10-12 days after birth and maintain mobility until 21 days after birth, indicating that they have functional synapses ((Srivastava, McMillan et al. 2016)). After 10 days of birth, the CASK neuronal-null mice begin to exhibit a slower growth rate and by ~ 20 days of age, CASK neuronal-null mice are less than half the size of the control $CASK^{floxed}$ mice or wild-type littermates (Figure 20B). Brain weight is also significantly reduced in the *CASK* neuronal knockout pups, although the cerebellum appears normal compared to $CASK^{floxed}$ mice and wildtype mice (Figure 20C). True microcephaly has been defined by some studies as an adult brain which is not only small but small for body weight (Edvardson, Shaag et al. 2007, Hong and Mah 2015). We therefore next measured the ratio of brain weight to body weight in CASK neuronal-null mice. The brain weight to body weight ratio is however significantly increased in

the *CASK* neuronal-knockout mice compared to the control *CASK*^{floxed} mice or wildtype mice (Figure 20D), suggesting that the reduction in brain weight is secondary to overall growth retardation. Brain lamination is unaltered, and the neuronal arrangement in *CASK* neuronal knockout hippocampi and cerebella are comparable to control mice (Figure 20E and Figure 20F). *CASK* neuronal knockout mice express ~ 15 % of wild-type CASK in the brain (Figure 20G, H), which may be due to CASK expression in other cell types including astrocytes (Marquez-Rosado, Singh et al. 2012) and oligodendrocytes (Anitei, Ifrim et al. 2006). Although CASK is deleted from most neurons at the embryonic stage, the levels of pre-synaptic and post-synaptic markers are unchanged, consistent with the previous study that demonstrated synapse formation is unaltered in *CASK* knockout mice (Atasoy, Schoch et al. 2007). The level of glial fibrillary acidic protein (GFAP) is also unaltered, indicating that although CASK is specifically deleted in neurons, there is no reactive gliosis and the ratio of neurons to astroglia may be unaltered (Figure 20G, H). It has to be however considered that the CASK neuronal-null mice are produced on the *CASK*^{floxed} mice background, so glial cells are generating only ~ 33 % of CASK. The strong phenotype in the CASK neuronal-null mice therefore may indicate a combination of effect from CASK-null neurons and CASK-hypomorphic glial cells. Altogether, these data suggest that although loss of CASK function in neurons contributes to some components of the phenotypic spectrum of CASK-associated pathology (e.g. growth retardation), it does not contribute to microcephaly or cerebellar hypoplasia. Many *CASK* missense mutations in human males are associated with intellectual disabilities and growth retardation in the absence of microcephaly, clearly indicating that these phenotypes are not interdependent and may represent loss of different molecular functions of CASK (Hackett, Tarpey et al. 2010).

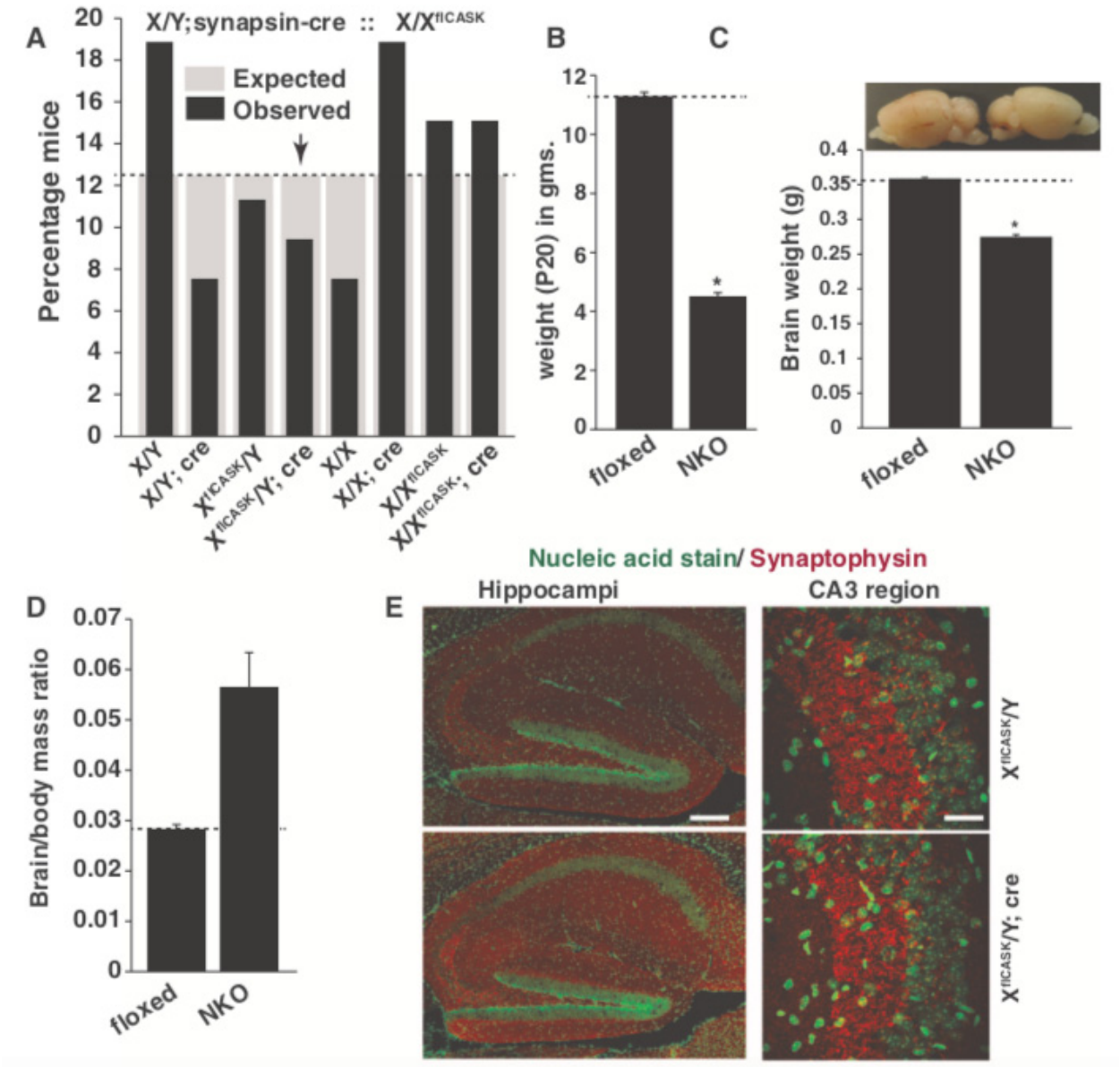
A
X/Y;synapsin-cre :: X/X^flCASK
Expected
Observed
Percentage mice
X/Y
X/Y; cre
X^flCASK/Y
X^flCASK/Y; cre
X/X
X/X; cre
X/X^flCASK
X/X^flCASK; cre
B
weight (P20) in gms.
floxed
NKO
C
Brain weight (g)
floxed
NKO
D
Brain/body mass ratio
floxed
NKO
E
Nucleic acid stain/ Synaptophysin
Hippocampi
CA3 region
X^flCASK/Y
X^flCASK/Y; cre

F

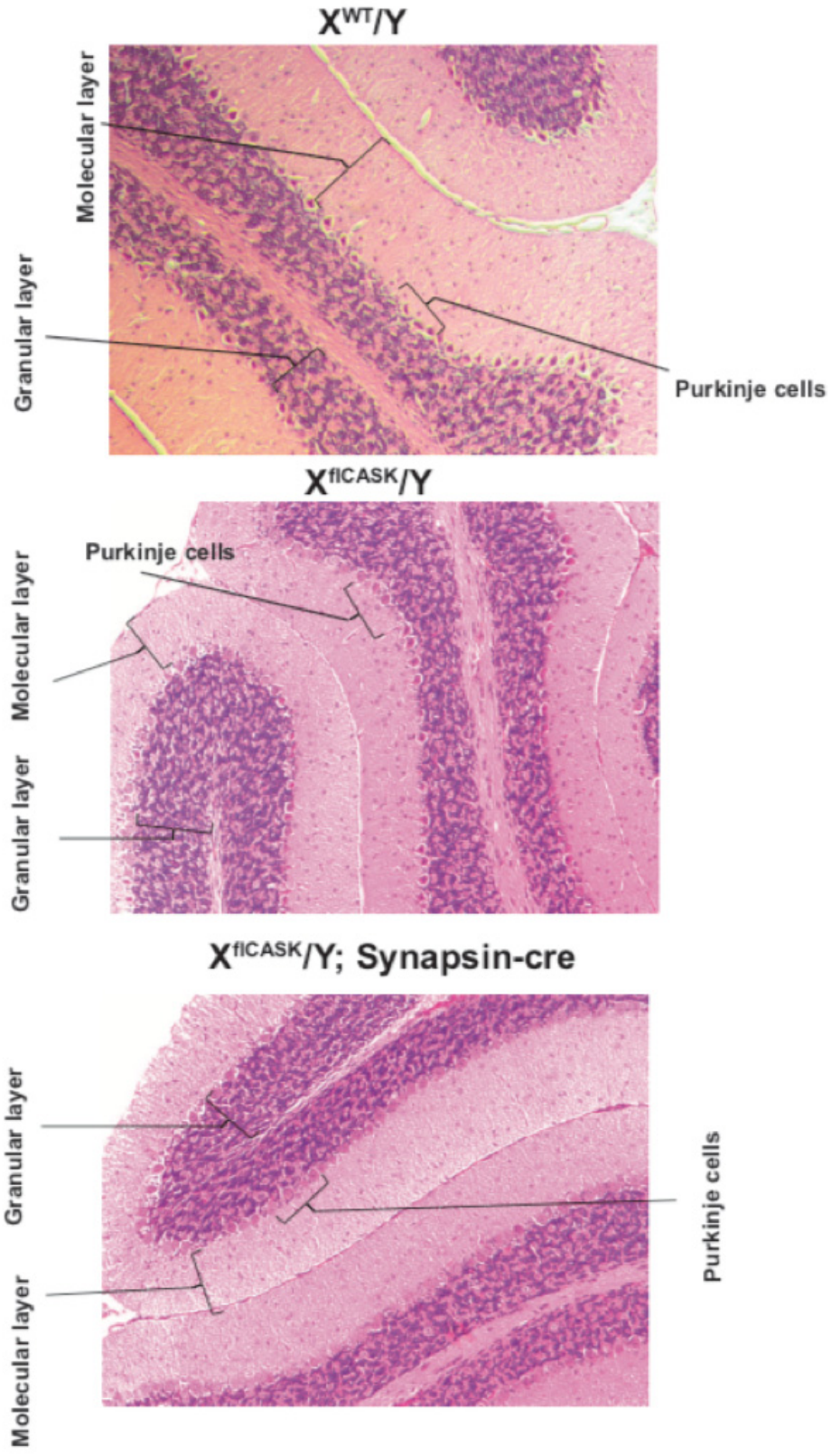
X^WT/Y
Molecular layer
Granular layer
Purkinje cells
X^flCASK/Y
Purkinje cells
Molecular layer
Granular layer
X^flCASK/Y; Synapsin-cre
Granular layer
Molecular layer
Purkinje cells

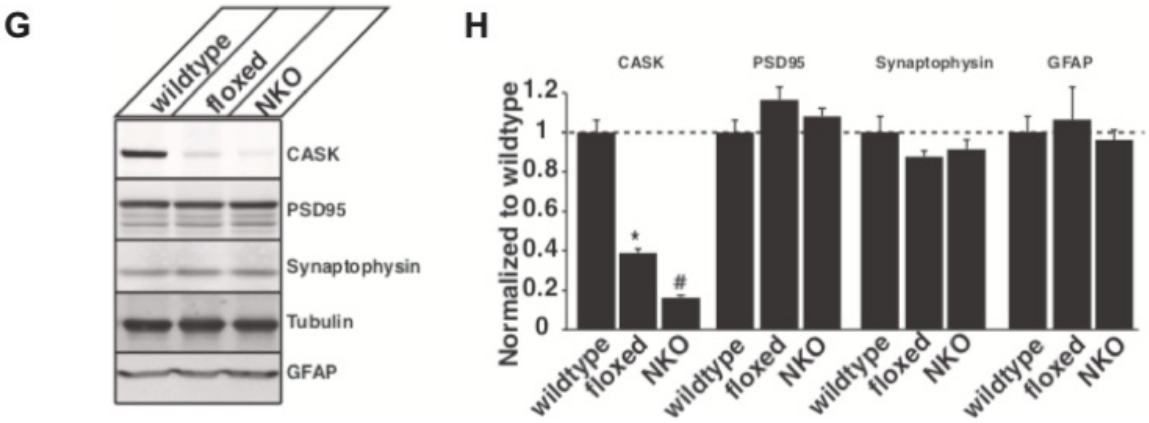

Figure 20: Normal brain formation in *CASK* neuronal knockout mice.

A) Shows the expected (grey bar) and observed (black bar) percentage of mice with each genotype obtained from crossing the X/Y; synapsin-Cre males with X^{flCASK}/X females; n = 62. Arrow indicates the *CASK* neuronal knockout group. B) Weight of $CASK^{floxed}$ (floxed) and *CASK* neuronal knockout male mice (NKO) at 20 days of age (* indicates $p < 0.05$, n = 5). C) Representative brain halves and brain weight at 21 days of age from *CASK* (X^{flCASK}/Y) (floxed) and *CASK* neuronal knockout (NKO) mice. (* indicates $p < 0.05$; n = 4). D) Ratio of brain to body weight of *CASK* (X^{flCASK}/Y) (floxed) and *CASK* neuronal knockout mice (NKO). (* indicates $p < 0.05$; n = 4). E) Image showing hippocampus from 21-day-old $CASK^{floxed}$ and NKO mice. Green staining indicates nucleic acid and red staining indicates synaptophysin. Note that there is no significant change in the lamination and CA3 region synaptophysin staining in *CASK* neuronal knockout mice. F) Representative images of H&E stained cerebella from mice of indicated genotype, demonstrating that *CASK* neuronal knockout mice have properly layered cerebella which are indistinguishable from the control mice. G) Representative Western blot

showing endogenous levels of CASK, PSD95, synaptophysin and tubulin from 21-day-old mice. H) Western blot protein quantitation where data is normalized to tubulin and expressed relative to wild-type levels. Bar graphs are plotted as mean ± SEM. (* indicates $p < 0.05$; $n = 3$). Wild-type represents littermate mice with unperturbed *CASK* gene, floxed indicates *CASK*^{floxed} mice and NKO indicates neuron-specific *CASK* knockout mice.

3.3.3 CASK neuronal knockout is lethal and produces optic nerve myelination retardation

Beginning around 17-18 days of age, these mice suffer from progressively increasing bouts of epileptic seizures and spasms, which often prove fatal before 23 - 24 days of age (Srivastava, McMillan et al. 2016)). We observed that there is a gender difference in days of survival. Female pups live on average 2 days longer than male pups (Figure 21A). We also monitored body weight of wild type, *CASK*^{floxed} and *CASK*^{NKO} pups from P6 to P21. We found body weight of *CASK*^{NKO} pups peaked and started to decrease at P14 (Figure 21B). Typically, the pups died of dehydration and malnutrition/metabolic disorders, which suggests CASK has a critical function in neuronal cells. To examine the role of neuronal CASK on optic nerve development, we first examined the diameter of *CASK*^{NKO} optic nerve stained with liprin-α3 antibody. The diameter of optic nerve is reduced by 22%. (Figure 21C). Together with the data from the previous section, deletion of CASK from neuron has profound effect on body growth, brain growth and optic nerve maturation. How does the deletion of CASK from neuronal cells affects optic nerve ultrastructure? We examined the TEM image of P12 *CASK*^{NKO} optic nerve and compared it with wild type and *CASK*^{floxed}. We found that only very small numbers of axons are myelinated in *CASK*^{NKO} optic nerve (Figure 21D, E). The number of myelinated axons did increase at P18 in *CASK*^{NKO} pups, but was still below *CASK*^{floxed} and wild type. This indicates that *CASK*^{NKO} mice

exhibit delayed myelination. Overall our data indicate that neuronal CASK plays a wide-ranging role in neuronal maturation.

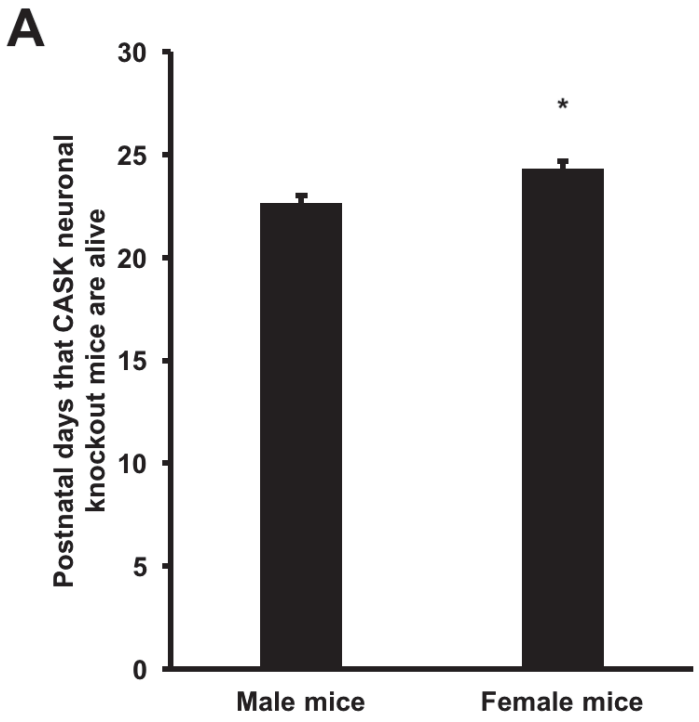

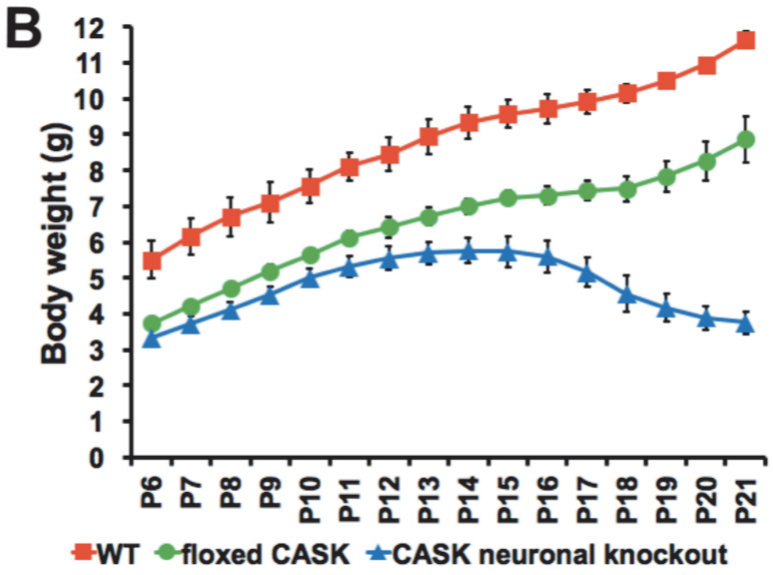

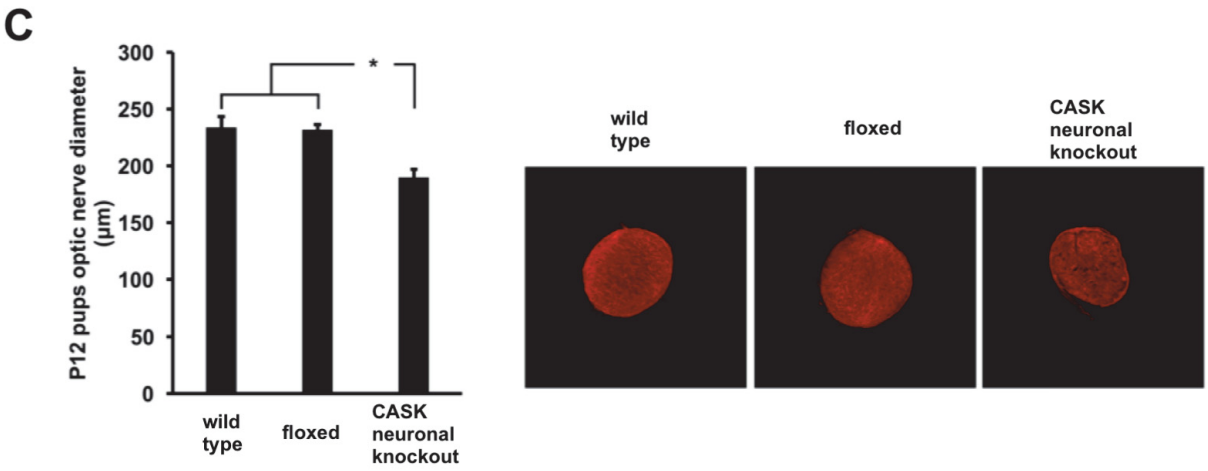
C
P12 pups optic nerve diameter (µm)
300
250
200
150
100
50
0
*
wild type
floxed
CASK neuronal knockout
wild type
floxed
CASK neuronal knockout

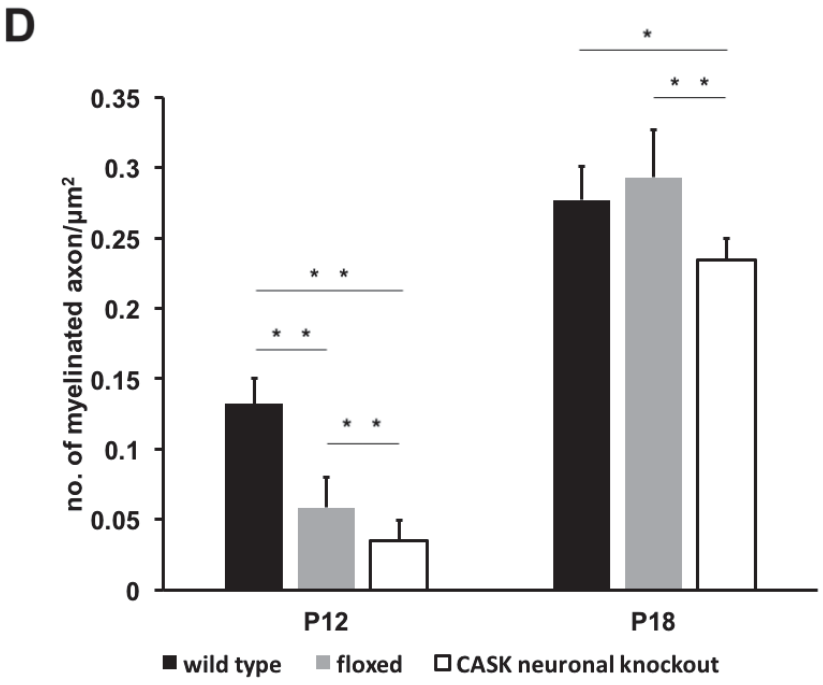
D
no. of myelinated axon/µm²
0.35
0.3
0.25
0.2
0.15
0.1
0.05
0
* *
* *
* *
*
P12
P18
wild type
floxed
CASK neuronal knockout

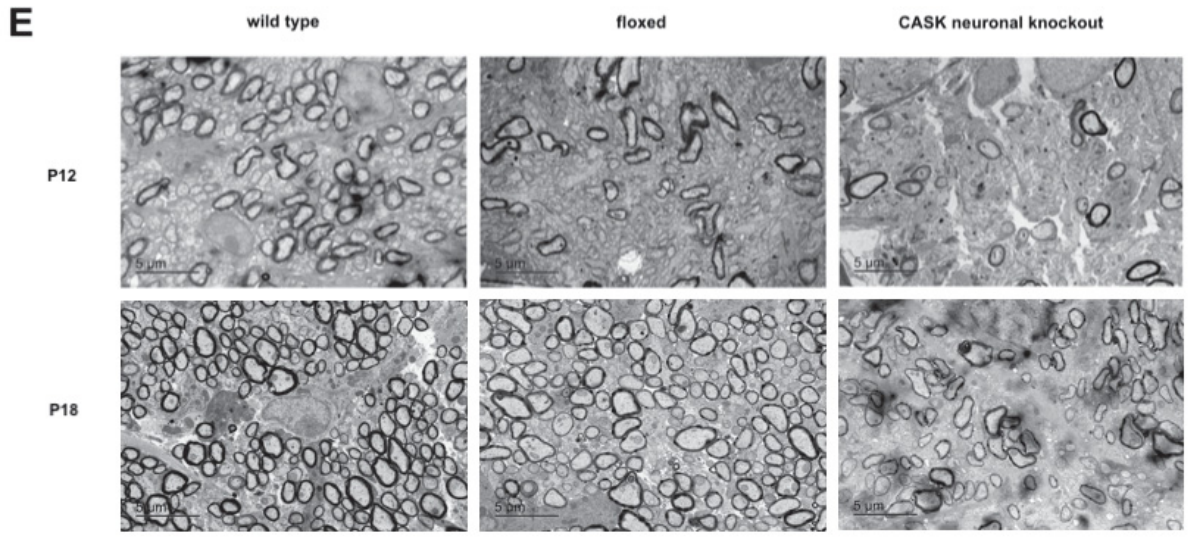

Figure 21: Characterization of *CASK* neuronal knockout (*CASK*^{NKO}) mice.

A) days that a *CASK*^{NKO} can sruvive (mean±SEM, *: p<0.05, n = 3). B) Body weight of wild type, floxed and *CASK*^{NKO} change with time from P6 to P21, in 1 day incremet (mean±SEM, n = 4). C) Optic nervecross section diameters of P12 wild type, floxed and *CASK*^{NKO} with representative images, immunostained for liprin- α3 (mean±SEM, *: p<0.05, n = 3). D) Quantifications of optic nerve axon density of P12 and P18 wild type, floxed and *CASK*^{NKO} with E) TEM optic nerve cross section representative images (mean±SD, N=18 (P12 wild type and floxed), N=11 (P12 *CASK*^{NKO}), N=6 (P18 wild type and floxed), N=3 (P18 *CASK*^{NKO})).

Chapter 4: Discussion

ONH is the commonest cause of childhood blindness in developed nations, and its prevalence is growing at an alarming rate (Hackett, Tarpey et al. 2010). A validated genetic animal model of ONH recapitulating the clinical condition will serve not only as a necessary tool to understand the mechanism of disease pathogenesis, but also to test potential therapeutic interventions. ONH

may occur with midline defects as observed in SOD, with other brain malformations like atrophic brain or even as isolated condition (Garcia-Filion and Borchert 2013). The co-incidence of ONH with other brain malformation is not surprising given that the retina and optic nerves are a part of our central nervous system and subject to the same developmental processes as the brain. Therefore, a clear understanding of ONH may also help unlock the pathophysiology of other neurodevelopmental disorders. In fact, subjects with ONH display a high incidence of autistic phenotype such as stereotypy (Ek, Fernell et al. 2005, Parr, Dale et al. 2010). In this regard mutations in *CASK* gene as a causal factor for ONH is particularly important since *CASK* mutations are also known to produce autistic traits (Hackett, Tarpey et al. 2010). *CASK* directly binds and phosphorylates neuronal adhesion molecule neurexin (Mukherjee, Sharma et al. 2008, Mukherjee, Sharma et al. 2010). It is pertinent to note that mutations in both neurexins and their trans-synaptic interacting partners also are associated with autism (Cao and Tabuchi 2017). Despite known interactions between CASK and neurexin, no synaptic ultrastructural defect has been shown to be associated with *CASK* mutation in any animal model. Here, we therefore show for the first-time clear morphological defects at retinogeniculate synapse involving changes in size and number of release site. Such changes align with the idea that CASK may be involved in trafficking of molecules and/or acts as a molecular scaffold at the synapse. Although it may also be possible that changes in synapses reflect the atrophy in axons. Mutations in the *CASK* gene are also associated with postnatal microcephaly (Srivastava, McMillan et al. 2016). It is possible to argue that ONH may simply be a part of microcephaly. However other monogenic syndromes associated with postnatal microcephaly such as Rett syndrome or Angelman syndrome do not present with ONH (Saunders, Mcculloch et al. 1995, Michieletto, Bonanni et al. 2011). Furthermore, not all CASK linked microcephaly are associated with ONH in humans presumably

due to preservation of some CASK functions. Consistent with this idea *CASK*^{floxed} hypomorphic mice exhibit smaller brain but not ONH. Overall the data indicates that ONH is an independent manifestation of *CASK* mutation.

CASK is a membrane-associated guanylate kinase protein which interacts with a large number of protein molecules. Specifically, *CASK* has been considered to be a synaptic scaffolding molecule both at the pre-and post-synaptic compartments (Samuels, Hsueh et al. 2007, Hu, Umemori et al. 2016). We have recently made two independent observations: 1) CASK stabilizes neuronal adhesion molecule neurexin and links it to the signaling molecule liprin-α (LaConte, Chavan et al. 2016). Liprin-αs are critical for photoreceptor axonal targeting in drosophila (Hofmeyer, Maurel-Zaffran et al. 2006) as well as for forming active zones (Zhen and Jin 1999). Neurexins themselves may play a critical role in intercellular adhesion and signaling (Graf, Zhang et al. 2004). A reduction in neurexin signaling and defect in axonal targeting may produce ONH, secondary to defect at the retinogeniculate synapses due to retrograde degeneration (Mosier, Lieberman et al. 1978). 2) CASK may regulate cellular metabolism including mitochondrial respiration (Srivastava, McMillan et al. 2016). Retina and optic nerve are highly susceptible to metabolic defects, and mitochondrial damage and mutations in mitochondrial genes are frequently associated with optic neuropathies (Carelli, Ross-Cisneros et al. 2004). In fact as many as 12% cases of non-syndromic mitochondrial cytopathies may display ONH (Taban, Cohen et al. 2006). Thus a change in metabolic status of retinal cells may also lead to ONH in *CASK*$^{(+/-)}$ mice and *CASK* haploinsufficient girls.

Mutations in *CASK* have been associated with diagnosis of both ONH and ONA. The difference between these two conditions is often blurred and it has been speculated that better imaging techniques may differentiate these conditions. Many authorities even suggest that both ONH and ONA may be similar pathology with the only difference being in their timing (Hoyt and Good 1992). What does our study reveal regarding the pathology of optic nerve? First of all, we present case reports of *CASK* haploinsufficiency displaying ONH, confirming the genetic associations. Secondly, using a rodent model, we are able to causally link ONH with *CASK* haploinsufficiency. Due to a common underlying biology (CASK haploinsufficiency) and similar optic nerve pathology $CASK^{(+/-)}$ mice satisfies the criteria for 'face validity' of an animal model. Previous rodent models of ONH using alcohol produced thinning of optic nerve only during adulthood (after 9 weeks) (Parson, Dhillon et al. 1995). In contrast, significant decrease in optic nerve area in $CASK^{(+/-)}$ mice was observed as early as P6 which corresponds to late third trimester in human fetal development (Dobbing and Sands 1979). The time period of optic nerve pathology in $CASK^{(+/-)}$ mice is indeed developmental in nature and is therefore a superior rodent model of ONH. Consistent with this idea deletion of CASK after maturity did not produce obvious ONA. Several histopathological hallmarks of atrophy however are present in ONH such as astrogliosis and thinning of axons. A detailed examination of optic nerve, retina and dLGN in $CASK^{(+/-)}$ mice undermine the idea that simply better imaging tool may be able to distinguish between ONH and ONA in human patients, these optic neuropathies may not be amenable to straightforward binary classification simply by morphology. We suggest that mutations in *CASK* is typically associated with ONH, the diagnosis of ONA may simply stem from the timing when originally uncovered. In fact, many infants that are diagnosed with ONA may actually have ONH which was not diagnosed earlier.

Our study indicates that CASK is not essential for survival after maturity. Till date the lethality of CASK deletion in mammals have been difficult to reconcile with non-lethal phenotypes in invertebrates like flies and worms. Our data provides the first possible step in explaining this paradox. The embryonic and immediate postnatal development of mammals is extremely different than those of invertebrates. Most likely CASK plays a highly specialized role during postnatal brain development of mammals. Further examination of this critical development period in mammals will unravel the function of CASK.

In our previous work, we speculated that a disproportionate cerebellar hypoplasia may be due to postnatal timing of *CASK*-linked pathology since cerebellum has a large postnatal developmental component. However, our current data suggest that cerebellum may be particularly sensitive to CASK loss of function. Cerebellum has certain unique features in metabolism compared to the rest of the brain. Aerobic glycolysis occurs in cerebellum at a much lower level than the rest of the brain. Cerebellar hypoplasia in cats and dogs can be commonly seen in cases of malnutrition. One reason for different metabolic features of cerebellum may be due to the neuronal population itself. Cerebellar granule cells are one of the smallest and yet most abundant kind of neurons in the brain, these neurons are excitatory in nature and any change in metabolism with alteration of neurotransmitter milieu may assert excitotoxicity and cell death. However, deletion of CASK specifically from some cerebellar cells did not produce any obvious effect. CASK is expressed at high levels even in embryonic brain; one possibility may be that to observe the effect CASK has to be deleted in cerebellar progenitor cells rather than post-mitotic neurons. Another possibility

could be that the mitochondrial deficit observed in cerebellum is systemic indirect effect of CASK reduction.

The *CASK*$^{(+/-)}$ female mice and the *CASK*^{floxed} male mice both have reduced level of CASK in their brain, but due to the unique biology of X-linked genes the pattern of expression in these two mice are completely different. Whereas the *CASK*$^{(+/-)}$ female brain is constituted of 50% cells expressing the full complement of CASK and 50% cells without any CASK, *CASK*^{floxed} male mice have reduced levels of CASK expression uniformly in all cells. This difference in expression pattern produces interesting differences in phenotype observed. Reduction of CASK in male mice produced cerebellar hypoplasia and overall growth retardation without manifestation of ONH. We also observed the cerebellar hypoplasia in homozygous female *CASK*^{floxed} mice indicating that gender itself do not play a role in the differences of CASK-linked pathology that we observe between these mice. This notion is further supported by the fact that boys with mosaic *CASK* mutation due to somatic mutation during embryogenesis also exhibit MICPCH like female patients.

Although the neuron-specific *CASK* heterozygous knockout mice did not exhibit any major phenotype, the complete *CASK* neuronal knockout mice exhibited pronounced growth retardation and delayed myelination. Since, the CASK neuronal-null mutants are made on a hypomorphic background, at present it is not possible to specifically point out the consequences of deleting CASK only from neurons. However, our data suggests that the disruption of neuronal CASK function does contribute to the overall CASK mutation-related phenotypes.

Appendix Chapter 1: Examining a methodology for targeting neurons for future therapy

Appx. 1.1 Introduction

Appx. 1.1.1 Scavenger receptor (SR) mediated endocytosis: a novel approach to drug targeting to neurons

Since we found CASK plays a critical role in neuronal maturation, we planned to test if we could target neurons in vivo for future therapeutic intervention. SRs were identified in the laboratory of Goldstein and Brown due to their ability to endocytose modified low density lipoproteins, modified proteins like maleylated albumin and nucleotides (polyguanylic and polyinosinic acid) (Goldstein, Ho et al. 1979, Brown, Basu et al. 1980). At present, at least 10 different classes of SRs are known (Zani, Stephen et al. 2015). SRs are versatile receptors and play numerous physiological and pathological roles and have also been successfully used for drug targeting specifically in macrophages (Mukhopadhyay, Chaudhuri et al. 1989, Mukherjee, Parashuraman et al. 2002). Most studies till date have focused on immunological (Plüddemann, Mukhopadhyay et al. 2011) and cardiovascular role of SRs. SRs also play a crucial role in lipid transport. Although SRs are known to be expressed in brain tissue, limited number of studies have focused on their function in the brain. Microglia, astrocytes and brain macrophages express SRs (Alarcon, Fuenzalida et al. 2005). It has been demonstrated that SRs are involved in uptake of amyloid β (Aβ) and thus play a role in Alzheimer's disease (Zhang, Su et al. 2014). Some members of the SR family are also expressed in neurons (Zani, Stephen et al. 2015), however functional studies to characterize neuronal SRs have not been extensively performed. In this study, we probed acute mouse cortical slices with two independent fluorophores labeled SR-ligands, maleylated-BSA (MBSA) and polyguanylic acid (polyG) to examine their cell-type-specific uptake.

Appx. 1.2 Methods

Appx. 1.2.1 Cell culture and internalization assay

Raw 264.7 cells were kind gift from Prof. Liwu Li, they were maintained in DMEM containing 10% FBS at 37˚C and 5% CO_2. For internalization assay, RAW 264.7 cells transduced with lentivirus expressing GFP were plated on poly-lysine coated glass bottom tissue culture plate. 24 hours later, cells were exposed to 2 μM MBSA-Texas red for 4 minutes at 37˚C. Cells were imaged using an inverted Zeiss laser scanning microscope (LSM 880) with a 63X oil immersion lens. For pulse-chase experiments Raw 264.7 cells were plated on polylysine coated glass bottom tissue culture plate. 24 hours later cells were pulsed with 2 μM MBSA-Texas red for 4 minutes washed and fresh media added. Cells were incubated at 37˚C for 65 minutes, lysotracker was added to the cells and they were returned to the incubator for additional 25 minutes. Live cells were imaged using 63X oil immersion lens in an inverted Zeiss laser scanning microscope (LSM 880).

Appx. 1.2.2 Texas-red maleylated BSA generation

BSA (Sigma) was incubated with NHS-Texas red (ThermoFisher) at pH 8.5 in a 1:3 ratio for half an hour at 4˚C. Conjugation was stopped using Tris and the protein was dialyzed against PBS (phosphate buffered saline) exhaustively. The ratio of texas red to BSA was found to be ~1:2.2. BSA-Texas red was then maleylated using maleic anhydride following a protocol described earlier (Mukherjee, Parashuraman et al. 2002); briefly maleic anhydride was added to BSA-texas red with constant stirring, the pH was maintained above 8.5 using 5 N NaOH. This was followed by dialysis against PBS overnight. 10 mer polyG and polyA conjugated with FAM were acquired from IDT (Integrated DNA Technology).

Appx. 1.2.3 Acute cortical slice experiment

200 μm thick coronal brain slices from an adult mouse (35 days old) were cut under a vibratome, which was adapted from Wu and Hablitz, 2005 (Wu and Hablitz 2005). Slices were then incubated in a 24-well plate containing 5 μM MBSA-Texas Red (5 μM BSA-Texas Red as control) or 10 μM polyG (10 μM polyA as control) in 1ml artificial cerebrospinal fluid (ACSF, Cold Spring Harbor Protocols) at 4˚C with continuing oxygen supply for 30 min to allow binding. Afterward, oxygen supply was cut off and the plate was incubated at 37 ˚C for 8 min to allow internalization. The brain slices were washed with phosphate buffered saline (PBS) three times and fixed with 4% paraformaldehyde (PFA). Neuronal marker NeuN (Novus Biologicals, dilution ratio 1:150) antibody was used for immunostaining as needed. The slices were permeabilized overnight with 0.2% TritonX-100 in PBS, slices were blocked for 1hour in blocking buffer (0.2% TritonX-100 in PBS with 5% horse serum). Slices were incubated with NeuN antibody diluted in blocking buffer for an hour followed by incubation for 30 min with Alexa 488 or Alexa 546 anti-Rabbit (Abcam) secondary antibody (1:500). Slices were then washed mounted on slides using Vectashield® with DAPI.

Appx. 1.3 Results

MBSA has been widely used as a ligand for SRs. We generated Texas-red labeled MBSA and tested it on a macrophage cell line RAW264.7 which is known to express scavenger receptors. Our data indicate that MBSA-Texas red was rapidly internalized by RAW264.7 cells. Internalization of BSA was negligible during the same time (Figure 22A, B). To ensure that the internalized MBSA was indeed transported to endo-lysosomal compartment, we did a pulse chase experiment on RAW264.7 cells. Within 90 minutes, MBSA-Texas- red co-localized with lysotracker indicating that indeed MBSA is transported to endo-lysosomal compartment (Figure

22C). We next examined the uptake of MBSA-Texas red on acute cortical slices generated from adult mice. MBSA was rapidly taken up by some but not all the cortical cells, counterstained with nucleic acid stain DAPI, indicating that not all the cells efficiently internalized MBSA (Figure 22D). We therefore counterstained cortical slices with the neuronal marker NeuN, the astrocytic marker, GFAP (glial fibrillary acidic protein) and the microglial marker Iba1. Our data clearly demonstrate that only cells positive for the neuronal marker NeuN efficiently internalized MBSA (Figure 22E, F, G, H). This indicates that the cells which robustly endocytosed MBSA were neurons. To confirm that MBSA enters endocytic vesicles within neurons, we acquired higher magnification images, our data reveal that even in diffraction limited confocal microscopy, clear punctate structures can be observed in somatodendritic region which likely represents endocytic vesicles (Figure 22I).

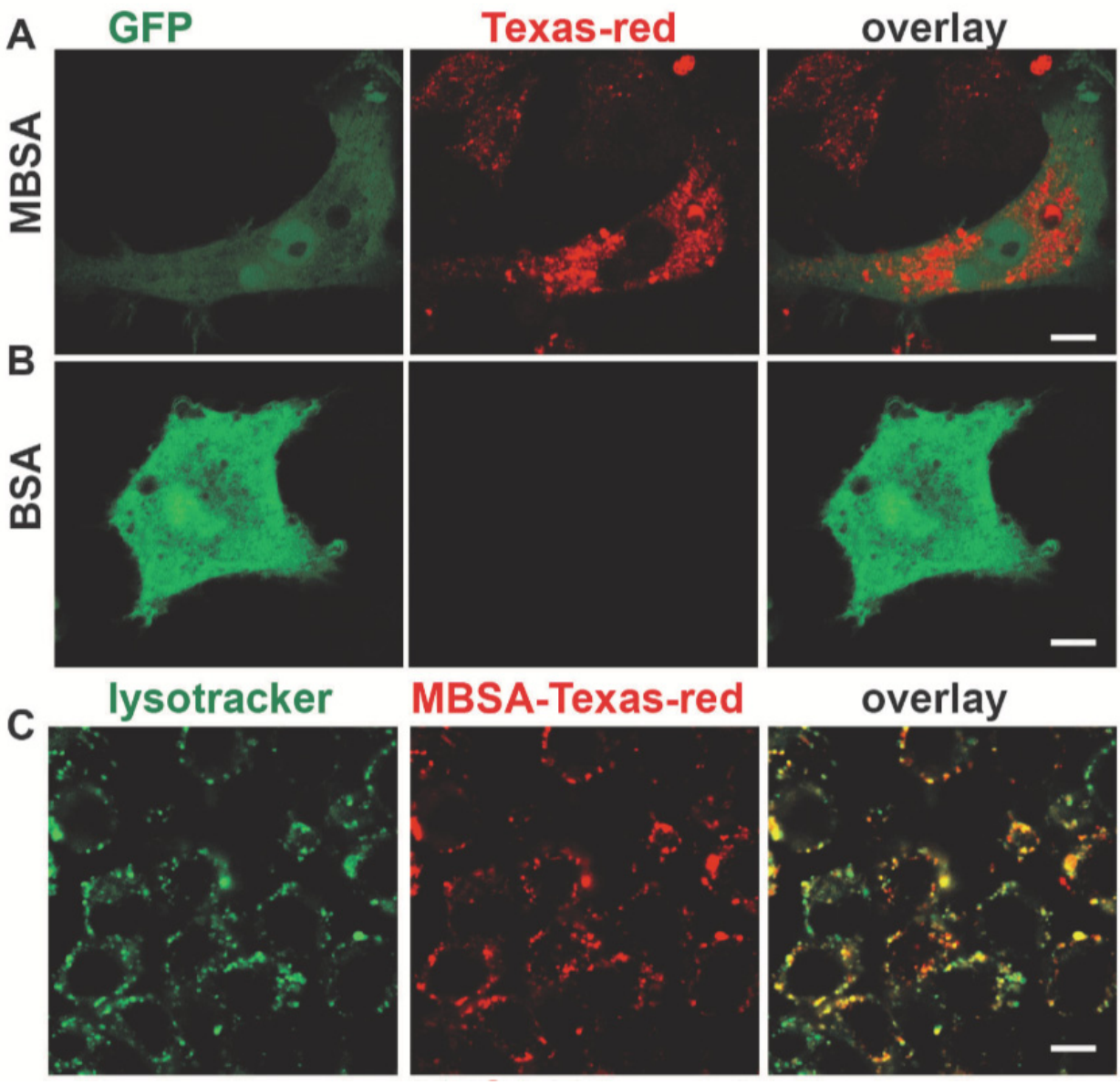
A
GFP
Texas-red
overlay
MBSA
B
BSA
C
lysotracker
MBSA-Texas-red
overlay

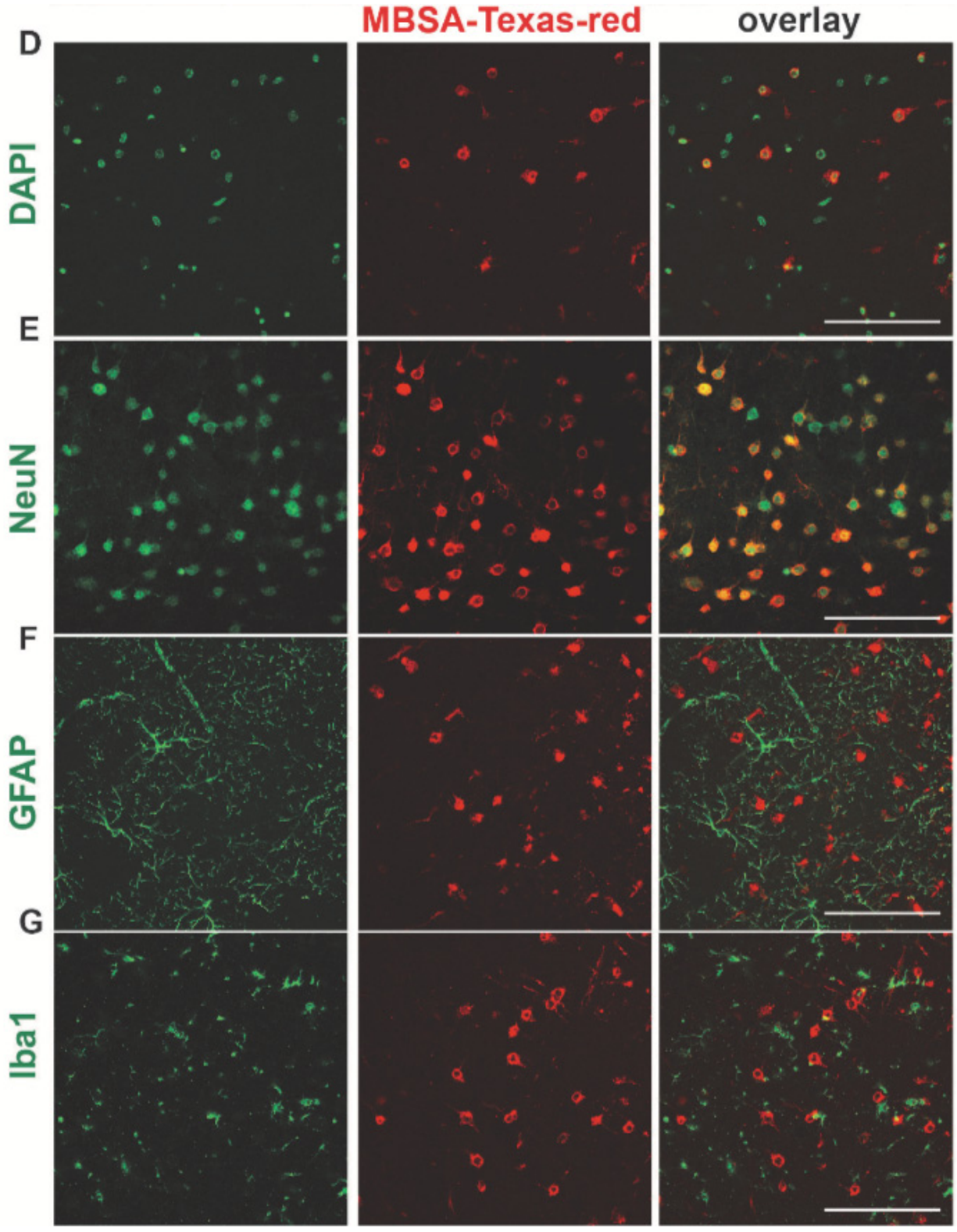
MBSA-Texas-red
overlay
D
DAPI
E
NeuN
F
GFAP
G
Iba1

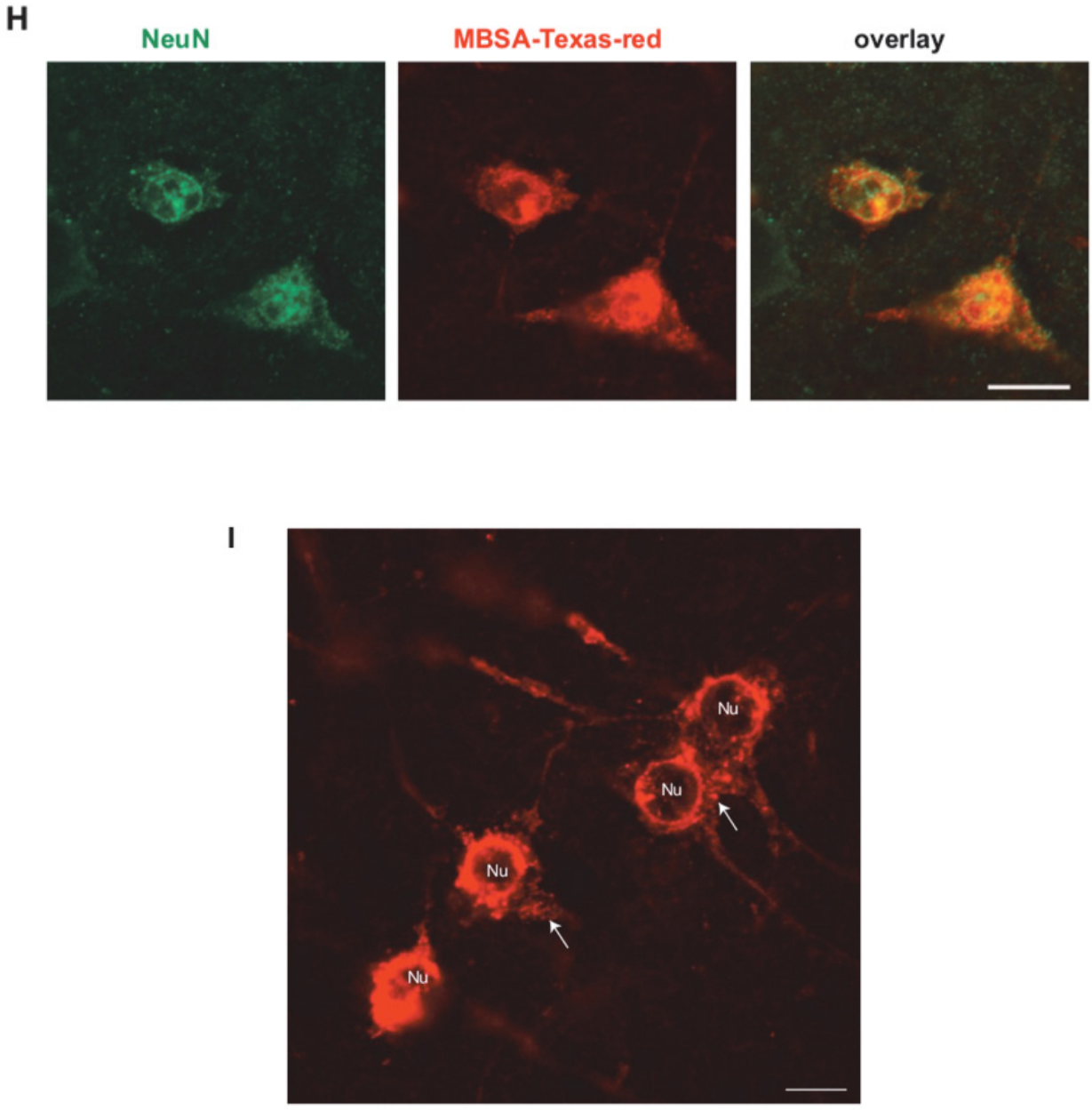

Figure 22: Cortical neurons internalize MBSA.

A) Internalization of MBSA-Texas red by Raw264.7 cells. B) BSA-Texas red is not internalized by Raw264.7 cells; scale bar is 5 μm. C) MBSA-Texas red colocalizes with lysotracker within 90 minutes. D) Internalization of MBSA-Texas red by cells in mouse cortex (red), counterstained with DAPI (green). E) Internalization of MBSA-Texas red by cells in mouse cortex (red),

counterstained with NeuN (green). F) Internalization of MBSA-Texas red by cells in mouse cortex (red), counterstained with GFAP (green). G) Internalization of MBSA-Texas red by cells in mouse cortex (red), counterstained with Iba1 (green). Scale bar for D to G is 100 μm. H) High magnification image of MBSA-Texas red (red) in cortical neurons counterstained with NeuN (green), scale bar is 15μm. I) High magnification image of MBSA-Texas red in cortical neurons showing discrete punctate in somatodendritic region indicative of vesicles (endocytic), Nu represents nucleus, scale bar for B is 10 μm.

In order to corroborate these observations, we repeated our experiments with another well characterized SR ligand polyG. We examined the uptake of polyG labeled with FAM on acute cortical slices. Our data show that NeuN positive cells rapidly internalize polyG but not polyadenylic acid (polyA) indicating that cortical neurons express a large number of functional SRs on the surface (Figure 23A, B).

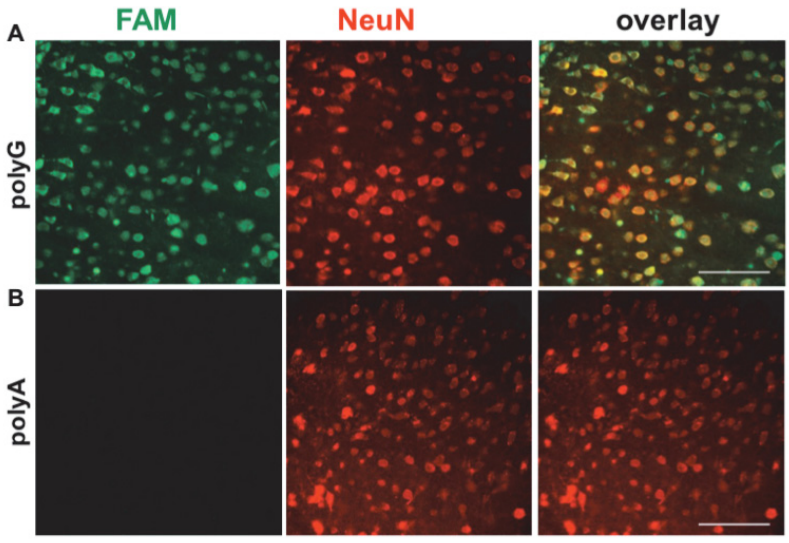

Figure 23: PolyG but not polyA can be internalized by cortical neurons.

A) Internalization of polyG-FAM by NeuN positive cells in mouse cortex. B) PolyA-FAM is not

internalized by cortical cells; scale bar for C and D is 100 μm.

Appx. 1.4 Discussion

Here, we have started to investigate if neurons could be targeted in vivo for potential therapeutic interventions. Our imaging results indicate most cells in the cortex that internalized detectable quantities of SR ligands are NeuN positive. Thus, contrary to expectations, neurons rather than microglia or astrocytes endocytose SR ligands in the cortex. Till date neuronal endocytosis has been mostly examined in context of synapses. Our data highlights the presence of highly active receptor-mediated endocytosis in the somatodendritic region. SRs type A, B, D, F, G can bind to MBSA and SRs type A, B, G, H, I can bind to polyG (Platt and Gordon 1998). Therefore, the type of SRs in neuron should belong to one of these classes. Our study does not verify if the same neurons are capable of internalizing both ligands simultaneously. Future investigations on how many different kinds of SRs are expressed by the same neuron will shed more light on the function of SRs on neurons. This approach next needs to be tried in retina to see if retinal neurons can be targeted. If so, it may prove beneficial to target small molecules in the model of ONH in an attempt to rescue the described phenotypes.

Summary

We first characterized the subcortical visual pathway in a *CASK* heterozygous knockout mouse model. Results showed that the mutant mice displayed thinning optic nerves, loss of RGC, reactive astrogliosis and an increased volume of retinal terminals. However, no signs of myelination defects were observed. We then studied the timing of onset of the ophthalmic pathologies using the same mouse model. Quantifications of optic nerve cross-sectional area revealed that the thinning of optic nerves started at postnatal day 6, but no loss of RGC was

observed at this time. RGC loss was however observed by P22. Moreover, we found that deletion of CASK after maturation did not produce obvious ONA. We also provide some evidence indicating that cerebellar hypoplasia and ONH can be separated genetically. By deleting CASK specifically from all neurons, we demonstrate CASK has a far more important role in neuronal maturation than observed in the hypomorphic mouse models. Finally, our data indicate that, like in macrophages, SR ligands may be useful for targeting drugs and bioactive molecules to neurons. In conclusion, *CASK*-linked ONH is a complex developmental neuropathology with some degenerative pathological components and is independent of *CASK*-linked microcephaly.

References

- Alarcon, R., C. Fuenzalida, M. Santibanez and R. von Bernhardi (2005). "Expression of scavenger receptors in glial cells. Comparing the adhesion of astrocytes and microglia from neonatal rats to surface-bound beta-amyloid." J Biol Chem **280**(34): 30406-30415.
- Anitei, M., M. Ifrim, M. A. Ewart, A. E. Cowan, J. H. Carson, R. Bansal and S. E. Pfeiffer (2006). "A role for Sec8 in oligodendrocyte morphological differentiation." J Cell Sci **119**(Pt 5): 807-818.
- Anjum, R., H. Ayoubian and F. Schmitz (2014). "Differential synaptic distribution of the scaffold proteins Cask and Caskin1 in the bovine retina." Mol Cell Neurosci **62**: 19-29.
- Atasoy, D., S. Schoch, A. Ho, K. A. Nadasy, X. Liu, W. Zhang, K. Mukherjee, E. D. Nosyreva, R. Fernandez-Chacon, M. Missler, E. T. Kavalali and T. C. Sudhof (2007). "Deletion of CASK in mice is lethal and impairs synaptic function." Proc Natl Acad Sci U S A **104**(7): 2525-2530.
- Balasubramanian, R. and L. Gan (2014). "Development of retinal amacrine cells and their dendritic stratification." Current ophthalmology reports **2**(3): 100-106.

- Bassett, E. A. and V. A. Wallace (2012). "Cell fate determination in the vertebrate retina." Trends in neurosciences **35**(9): 565-573.
- Biederer, T., Y. Sara, M. Mozhayeva, D. Atasoy, X. Liu, E. T. Kavalali and T. C. Sudhof (2002). "SynCAM, a synaptic adhesion molecule that drives synapse assembly." Science **297**(5586): 1525-1531.
- Biederer, T. and T. C. Sudhof (2001). "CASK and protein 4.1 support F-actin nucleation on neurexins." J Biol Chem **276**(51): 47869-47876.
- Birkebaek, N. H., L. Patel, N. B. Wright, J. R. Grigg, S. Sinha, C. M. Hall, D. A. Price, I. C. Lloyd and P. E. Clayton (2003). "Endocrine status in patients with optic nerve hypoplasia: relationship to midline central nervous system abnormalities and appearance of the hypothalamic-pituitary axis on magnetic resonance imaging." J Clin Endocrinol Metab **88**(11): 5281-5286.
- Blair, H. J., V. Reed, E. Gormally, J. B. Wilson, J. Novak, R. R. McInnes, S. J. Phillips, B. A. Taylor and Y. Boyd (2000). "Positioning of five genes (CASK, ARX, SAT, IMAGE cDNAs 248928 and 253949) from the human X chromosome short arm with respect to evolutionary breakpoints on the mouse X chromosome." Mammalian Genome **11**(8): 710-712.
- Bowmaker, J. K. and H. Dartnall (1980). "Visual pigments of rods and cones in a human retina." The Journal of physiology **298**(1): 501-511.
- Brown, M. S., S. K. Basu, J. Falck, Y. Ho and J. L. Goldstein (1980). "The scavenger cell pathway for lipoprotein degradation: Specificity of the binding site that mediates the uptake of negatively-charged LDL by macrophages." Journal of supramolecular structure **13**(1): 67-81.

- Burglen, L., S. Chantot-Bastaraud, C. Garel, M. Milh, R. Touraine, G. Zanni, F. Petit, A. Afenjar, C. Goizet, S. Barresi, A. Coussement, C. Ioos, L. Lazaro, S. Joriot, I. Desguerre, D. Lacombe, V. des Portes, E. Bertini, J. P. Siffroi, T. B. de Villemeur and D. Rodriguez (2012). "Spectrum of pontocerebellar hypoplasia in 13 girls and boys with CASK mutations: confirmation of a recognizable phenotype and first description of a male mosaic patient." Orphanet J Rare Dis **7**: 18.
- Butz, S., M. Okamoto and T. C. Sudhof (1998). "A tripartite protein complex with the potential to couple synaptic vesicle exocytosis to cell adhesion in brain." Cell **94**(6): 773-782.
- Cao, X. and K. Tabuchi (2017). "Functions of synapse adhesion molecules neurexin/neuroligins and neurodevelopmental disorders." Neurosci Res **116**: 3-9.
- Carelli, V., F. N. Ross-Cisneros and A. A. Sadun (2004). "Mitochondrial dysfunction as a cause of optic neuropathies." Progress in Retinal and Eye Research **23**(1): 53-89.
- Caruana, G. (2002). "Genetic studies define MAGUK proteins as regulators of epithelial cell polarity." International Journal of Developmental Biology **46**(4): 511-518.
- Chen, C. A., J. Yin, R. A. Lewis and C. P. Schaaf (2017). "Genetic causes of optic nerve hypoplasia." J Med Genet **54**(7): 441-449.
- Cohen, A. R., D. F. Woods, S. M. Marfatia, Z. Walther, A. H. Chishti and J. M. Anderson (1998). "Human CASK/LIN-2 binds syndecan-2 and protein 4.1 and localizes to the basolateral membrane of epithelial cells." J Cell Biol **142**(1): 129-138.
- Dangata, Y. Y. and M. H. Kaufman (1997). "Myelinogenesis in the optic nerve of (C57BL x CBA) F1 hybrid mice: A morphometric analysis." European Journal of Morphology **35**(1): 3-17.

- De Morsier, G. (1956). "Etudes sur les dystrophies cranioen-cephaliques 3. Agenesie du septum lucidum avec malformation du tractus optique." Schweiz Arch Neurol Psychiatr **77**: 267-292.
- Dimitratos, S. D., D. G. Stathakis, C. A. Nelson, D. F. Woods and P. J. Bryant (1998). "The location of human CASK at Xp11.4 identifies this gene as a candidate for X-linked optic atrophy." Genomics **51**(2): 308-309.
- Do, M. T. H. and K.-W. Yau (2010). "Intrinsically photosensitive retinal ganglion cells." Physiological reviews **90**(4): 1547-1581.
- Dobbing, J. and J. Sands (1979). "Comparative Aspects of the Brain Growth Spurt." Early Human Development **3**(1): 79-83.
- Edvardson, S., A. Shaag, O. Kolesnikova, J. M. Gomori, I. Tarassov, T. Einbinder, A. Saada and O. Elpeleg (2007). "Deleterious mutation in the mitochondrial arginyl-transfer RNA synthetase gene is associated with pontocerebellar hypoplasia." Am J Hum Genet **81**(4): 857-862.
- Ek, U., E. Fernell and L. Jacobson (2005). "Cognitive and behavioural characteristics in blind children with bilateral optic nerve hypoplasia." Acta Paediatr **94**(10): 1421-1426.
- Erskine, L. and E. Herrera (2014). "Connecting the retina to the brain." ASN neuro **6**(6): 1759091414562107.
- Fallon, L., F. Moreau, B. G. Croft, N. Labib, W. J. Gu and E. A. Fon (2002). "Parkin and CASK/LIN-2 associate via a PDZ-mediated interaction and are co-localized in lipid rafts and postsynaptic densities in brain." J Biol Chem **277**(1): 486-491.
- Fox, M. A., J. R. Sanes, D. B. Borza, V. P. Eswarakumar, R. Fassler, B. G. Hudson, S. W. John, Y. Ninomiya, V. Pedchenko, S. L. Pfaff, M. N. Rheault, Y. Sado, Y. Segal, M.

J. Werle and H. Umemori (2007). "Distinct target-derived signals organize formation, maturation, and maintenance of motor nerve terminals." Cell **129**(1): 179-193.

- Garcia-Filion, P. and M. Borchert (2013). "Optic nerve hypoplasia syndrome: a review of the epidemiology and clinical associations." Curr Treat Options Neurol **15**(1): 78-89.
- Goldowitz, D., R. C. Cushing, E. Laywell, G. D'Arcangelo, M. Sheldon, H. O. Sweet, M. Davisson, D. Steindler and T. Curran (1997). "Cerebellar disorganization characteristic of reeler in scrambler mutant mice despite presence of reelin." J Neurosci **17**(22): 8767-8777.
- Goldstein, J. L., Y. Ho, S. K. Basu and M. S. Brown (1979). "Binding site on macrophages that mediates uptake and degradation of acetylated low density lipoprotein, producing massive cholesterol deposition." Proceedings of the National Academy of Sciences **76**(1): 333-337.
- Graf, E. R., X. Z. Zhang, S. X. Jin, M. W. Linhoff and A. M. Craig (2004). "Neurexins induce differentiation of GABA and glutamate postsynaptic specializations via neuroligins." Cell **119**(7): 1013-1026.
- Graw, J. (2010). Eye development. Current topics in developmental biology, Elsevier. **90:** 343-386.
- Gray, H. (1878). Anatomy of the human body, Lea & Febiger.
- Guillery, R., E. Polley and F. Torrealba (1982). "The arrangement of axons according to fiber diameter in the optic tract of the cat." The Journal of Neuroscience **2**(6): 714-721.
- Guy, J., E. A. Ellis, K. Kelley and G. M. Hope (1989). "Spectra of G ratio, myelin sheath thickness, and axon and fiber diameter in the guinea pig optic nerve." J Comp Neurol **287**(4): 446-454.

- Guyton, A. C. and J. E. Hall (1992). "Human physiology and mechanisms of disease."
- Hackett, A., P. S. Tarpey, A. Licata, J. Cox, A. Whibley, J. Boyle, C. Rogers, J. Grigg, M. Partington, R. E. Stevenson, J. Tolmie, J. R. Yates, G. Turner, M. Wilson, A. P. Futreal, M. Corbett, M. Shaw, J. Gecz, F. L. Raymond, M. R. Stratton, C. E. Schwartz and F. E. Abidi (2010). "CASK mutations are frequent in males and cause X-linked nystagmus and variable XLMR phenotypes." Eur J Hum Genet **18**(5): 544-552.
- Hammer, S., A. Monavarfeshani, T. Lemon, J. Su and M. A. Fox (2015). "Multiple Retinal Axons Converge onto Relay Cells in the Adult Mouse Thalamus." Cell Rep **12**(10): 1575-1583.
- Hata, Y., S. Butz and T. C. Sudhof (1996). "CASK: a novel dlg/PSD95 homolog with an N-terminal calmodulin-dependent protein kinase domain identified by interaction with neurexins." J Neurosci **16**(8): 2488-2494.
- Hayashi, S. and A. P. McMahon (2002). "Efficient recombination in diverse tissues by a tamoxifen-inducible form of Cre: a tool for temporally regulated gene activation/inactivation in the mouse." Developmental biology **244**(2): 305-318.
- Hofmeyer, K., C. Maurel-Zaffran, H. Sink and J. E. Treisman (2006). "Liprin-alpha has LAR-independent functions in R7 photoreceptor axon targeting." Proc Natl Acad Sci U S A **103**(31): 11595-11600.
- Hong, S. T. and W. Mah (2015). "A Critical Role of GIT1 in Vertebrate and Invertebrate Brain Development." Exp Neurobiol **24**(1): 8-16.
- Hoskins, R., A. F. Hajnal, S. A. Harp and S. K. Kim (1996). "The C. elegans vulval induction gene lin-2 encodes a member of the MAGUK family of cell junction proteins." Development **122**(1): 97-111.

- Hoyt, C. S. and W. V. Good (1992). "Do we really understand the difference between optic nerve hypoplasia and atrophy?" Eye (Lond) **6 (Pt 2)**: 201-204.
- Hoyt, W., S. Kaplan, M. Grumbach and J. Glaser (1970). "Septo-optic dysplasia and pituitary dwarfism." The Lancet **295**(7652): 893-894.
- Hsueh, Y. P. (2006). "The role of the MAGUK protein CASK in neural development and synaptic function." Curr Med Chem **13**(16): 1915-1927.
- Hsueh, Y. P., T. F. Wang, F. C. Yang and M. Sheng (2000). "Nuclear translocation and transcription regulation by the membrane-associated guanylate kinase CASK/LIN-2." Nature **404**(6775): 298-302.
- Hsueh, Y. P., F. C. Yang, V. Kharazia, S. Naisbitt, A. R. Cohen, R. J. Weinberg and M. Sheng (1998). "Direct interaction of CASK/LIN-2 and syndecan heparan sulfate proteoglycan and their overlapping distribution in neuronal synapses." J Cell Biol **142**(1): 139-151.
- Hu, H. T., H. Umemori and Y. P. Hsueh (2016). "Postsynaptic SDC2 induces transsynaptic signaling via FGF22 for bidirectional synaptic formation." Scientific Reports **6**.
- Huang, T. N. and Y. P. Hsueh (2017). "Calcium/calmodulin-dependent serine protein kinase (CASK), a protein implicated in mental retardation and autism-spectrum disorders, interacts with T-Brain-1 (TBR1) to control extinction of associative memory in male mice." Journal of Psychiatry & Neuroscience **42**(1): 37-47.
- Kaur, S., S. Jain, H. B. Sodhi, A. Rastogi and Kamlesh (2013). "Optic nerve hypoplasia." Oman J Ophthalmol **6**(2): 77-82.
- Kolb, H. (1995). "Simple anatomy of the retina."

- LaConte, L. E., V. Chavan, C. Liang, J. Willis, E. M. Schonhense, S. Schoch and K. Mukherjee (2016). "CASK stabilizes neurexin and links it to liprin-alpha in a neuronal activity-dependent manner." Cellular and molecular life sciences : CMLS **73**(18): 3599-3621.
- LaConte, L. E. W., V. Chavan, C. Liang, J. Willis, E. M. Schonhense, S. Schoch and K. Mukherjee (2016). "CASK stabilizes neurexin and links it to liprin-alpha in a neuronal activity-dependent manner." Cellular and Molecular Life Sciences **73**(18): 3599-3621.
- Leonoudakis, D., L. R. Conti, C. M. Radeke, L. M. M. McGuire and C. A. Vandenberg (2004). "A multiprotein trafficking complex composed of SAP97, CASK, Veli, and Mint1 is associated with inward rectifier Kir2 potassium channels." Journal of Biological Chemistry **279**(18): 19051-19063.
- Lewandoski, M., K. M. Wassarman and G. R. Martin (1997). "Zp3-cre, a transgenic mouse line for the activation or inactivation of loxP-flanked target genes specifically in the female germ line." Curr Biol **7**(2): 148-151.
- Li, Y. J., Z. Y. Wei, Y. Yan, Q. W. Wan, Q. S. Du and M. J. Zhang (2014). "Structure of Crumbs tail in complex with the PALS1 PDZ-SH3-GK tandem reveals a highly specific assembly mechanism for the apical Crumbs complex." Proceedings of the National Academy of Sciences of the United States of America **111**(49): 17444-17449.
- Luo, L. (2015). Principles of neurobiology, Garland Science.
- Magnus, H. (1884). "Zur Karuistik der angelborenen Schnerven-milbildungen." Klin Monatsbl Augenheilkd **2**: 85-87.
- Marieb, E. N. and K. Hoehn (2007). Human anatomy & physiology, Pearson Education.

- Marquez-Rosado, L., D. Singh, H. Rincon-Arano, J. L. Solan and P. D. Lampe (2012). "CASK (LIN2) interacts with Cx43 in wounded skin and their coexpression affects cell migration." J Cell Sci **125**(Pt 3): 695-702.
- Marquez-Rosado, L., D. Singh, H. Rincon-Arano, J. L. Solan and P. D. Lampe (2012). "CASK (LIN2) interacts with Cx43 in wounded skin and their coexpression affects cell migration." Journal of Cell Science **125**(3): 695-702.
- Maximov, A., T. C. Sudhof and I. Bezprozvanny (1999). "Association of neuronal calcium channels with modular adaptor proteins." J Biol Chem **274**(35): 24453-24456.
- Michieletto, P., P. Bonanni and S. Pensiero (2011). "Ophthalmic findings in Angelman syndrome." Journal of Aapos **15**(2): 158-161.
- Mok, K. H. and V. W.-h. Lee (2002). "Disc-to-macula distance to disc-diameter ratio for optic disc size estimation." Journal of glaucoma **11**(5): 392-395.
- Moog, U., T. Bierhals, K. Brand, J. Bautsch, S. Biskup, T. Brune, J. Denecke, C. E. de Die-Smulders, C. Evers, M. Hempel, M. Henneke, H. Yntema, B. Menten, J. Pietz, R. Pfundt, J. Schmidtke, D. Steinemann, C. T. Stumpel, L. Van Maldergem and K. Kutsche (2015). "Phenotypic and molecular insights into CASK-related disorders in males." Orphanet Journal of Rare Diseases **10**.
- Moog, U., K. Kutsche, F. Kortum, B. Chilian, T. Bierhals, N. Apeshiotis, S. Balg, N. Chassaing, C. Coubes, S. Das, H. Engels, H. Van Esch, U. Grasshoff, M. Heise, B. Isidor, J. Jarvis, U. Koehler, T. Martin, B. Oehl-Jaschkowitz, E. Ortibus, D. T. Pilz, P. Prabhakar, G. Rappold, I. Rau, G. Rettenberger, G. Schluter, R. H. Scott, M. Shoukier, E. Wohlleber, B. Zirn, W. B. Dobyns and G. Uyanik (2011). "Phenotypic spectrum associated with CASK loss-of-function mutations." J Med Genet **48**(11): 741-751.

- Mosier, M. A., M. F. Lieberman, W. R. Green and D. L. Knox (1978). "Hypoplasia of the optic nerve." Arch Ophthalmol **96**(8): 1437-1442.
- Mukherjee, K., H. R. Clark, V. Chavan, E. K. Benson, G. J. Kidd and S. Srivastava (2016). "Analysis of Brain Mitochondria Using Serial Block-Face Scanning Electron Microscopy." J Vis Exp(113).
- Mukherjee, K., S. Parashuraman, G. Krishnamurthy, J. Majumdar, A. Yadav, R. Kumar, S. K. Basu and A. Mukhopadhyay (2002). "Diverting intracellular trafficking of Salmonella to the lysosome through activation of the late endocytic Rab7 by intracellular delivery of muramyl dipeptide." Journal of cell science **115**(18): 3693-3701.
- Mukherjee, K., M. Sharma, R. Jahn, M. C. Wahl and T. C. Sudhof (2010). "Evolution of CASK into a Mg2+-sensitive kinase." Sci Signal **3**(119): ra33.
- Mukherjee, K., M. Sharma, H. Urlaub, G. P. Bourenkov, R. Jahn, T. C. Sudhof and M. C. Wahl (2008). "CASK Functions as a Mg2+-independent neurexin kinase." Cell **133**(2): 328-339.
- Mukherjee, K., J. B. Slawson, B. L. Christmann and L. C. Griffith (2014). "Neuron-specific protein interactions of Drosophila CASK-beta are revealed by mass spectrometry." Frontiers in molecular neuroscience **7**: 58.
- Mukhopadhyay, A., G. Chaudhuri, S. K. Arora, S. Sehgal and S. K. Basu (1989). "Receptor-mediated drug delivery to macrophages in chemotherapy of leishmaniasis." Science **244**(4905): 705-707.
- Najm, J., D. Horn, I. Wimplinger, J. A. Golden, V. V. Chizhikov, J. Sudi, S. L. Christian, R. Ullmann, A. Kuechler, C. A. Haas, A. Flubacher, L. R. Charnas, G. Uyanik, U. Frank, E. Klopocki, W. B. Dobyns and K. Kutsche (2008). "Mutations of CASK cause an X-

linked brain malformation phenotype with microcephaly and hypoplasia of the brainstem and cerebellum." Nat Genet **40**(9): 1065-1067.

- Nakajiri, T., K. Kobayashi, N. Okamoto, M. Oka, F. Miya, K. Kosaki and H. Yoshinaga (2015). "Late-onset epileptic spasms in a female patient with a CASK mutation." Brain Dev **37**(9): 919-923.
- Newman, E. and A. Reichenbach (1996). "The Müller cell: a functional element of the retina." Trends in neurosciences **19**(8): 307-312.
- Olsen, O., H. Liu, J. B. Wade, J. Merot and P. A. Welling (2002). "Basolateral membrane expression of the Kir 2.3 channel is coordinated by PDZ interaction with Lin-7/CASK complex." Am J Physiol Cell Physiol **282**(1): C183-195.
- Omri, S., B. Omri, M. Savoldelli, L. Jonet, B. Thillaye-Goldenberg, G. Thuret, P. Gain, J.-C. Jeanny, P. Crisanti and F. Behar-Cohen (2010). "The outer limiting membrane (OLM) revisited: clinical implications." Clinical ophthalmology (Auckland, NZ) **4**: 183.
- Parr, J. R., N. J. Dale, L. M. Shaffer and A. T. Salt (2010). "Social communication difficulties and autism spectrum disorder in young children with optic nerve hypoplasia and/or septo-optic dysplasia." Dev Med Child Neurol **52**(10): 917-921.
- Parson, S. H., B. Dhillon, G. S. Findlater and M. H. Kaufman (1995). "Optic-Nerve Hypoplasia in the Fetal Alcohol Syndrome - a Mouse Model." Journal of Anatomy **186**: 313-320.
- Platt, N. and S. Gordon (1998). "Scavenger receptors: diverse activities and promiscuous binding of polyanionic ligands." Chemistry & biology **5**(8): R193-R203.

- Plüddemann, A., S. Mukhopadhyay and S. Gordon (2011). "Innate immunity to intracellular pathogens: macrophage receptors and responses to microbial entry." Immunological reviews **240**(1): 11-24.
- Qi, J., Y. Su, R. Sun, F. Zhang, X. Luo and Z. Yang (2005). "CASK inhibits ECV304 cell growth and interacts with Id1." Biochem Biophys Res Commun **328**(2): 517-521.
- Qi, J., Y. Y. Su, R. J. Sun, F. Zhang, X. F. Luo, Z. C. Yang and X. D. Luo (2005). "CASK inhibits ECV304 cell growth and interacts with Id1." Biochemical and Biophysical Research Communications **328**(2): 517-521.
- R Sparrrow, J., D. Hicks and C. P Hamel (2010). "The retinal pigment epithelium in health and disease." Current molecular medicine **10**(9): 802-823.
- Saadati, H. G., H. Y. Hsu, K. B. Heller and A. A. Sadun (1998). "A histopathologic and morphometric differentiation of nerves in optic nerve hypoplasia and leber hereditary optic neuropathy." Archives of Ophthalmology **116**(7): 911-916.
- Saitsu, H., M. Kato, H. Osaka, N. Moriyama, H. Horita, K. Nishiyama, Y. Yoneda, Y. Kondo, Y. Tsurusaki, H. Doi, N. Miyake, K. Hayasaka and N. Matsumoto (2012). "CASK aberrations in male patients with Ohtahara syndrome and cerebellar hypoplasia." Epilepsia **53**(8): 1441-1449.
- Samuels, B. A., Y. P. Hsueh, T. Shu, H. Liang, H. C. Tseng, C. J. Hong, S. C. Su, J. Volker, R. L. Neve, D. T. Yue and L. H. Tsai (2007). "Cdk5 promotes synaptogenesis by regulating the subcellular distribution of the MAGUK family member CASK." Neuron **56**(5): 823-837.

- Sato, K.-i. (2017). "Reference interval for the disc-macula distance to disc diameter ratio in a large population of healthy Japanese adults: a prospective, observational study." Medicine **96**(15).
- Saunders, K. J., D. L. Mcculloch and A. M. Kerr (1995). "Visual Function in Rett-Syndrome." Developmental Medicine and Child Neurology **37**(6): 496-504.
- Scheiffele, P., J. H. Fan, J. Choih, R. Fetter and T. Serafini (2000). "Neuroligin expressed in nonneuronal cells triggers presynaptic development in contacting axons." Cell **101**(6): 657-669.
- Schoch, S., G. Cibelli and G. Thiel (1996). "Neuron-specific gene expression of synapsin I. Major role of a negative regulatory mechanism." J Biol Chem **271**(6): 3317-3323.
- Schwarz, O. (1915). "Ein fall von mangelhafter bildung beider sehnerven." Albrecth von Graefes Arch Klin Ophthalmol.
- Sharp, A., D. Robinson and P. Jacobs (2000). "Age- and tissue-specific variation of X chromosome inactivation ratios in normal women." Hum Genet **107**(4): 343-349.
- Slawson, J. B., E. A. Kuklin, A. Ejima, K. Mukherjee, L. Ostrovsky and L. C. Griffith (2011). "Central regulation of locomotor behavior of Drosophila melanogaster depends on a CASK isoform containing CaMK-like and L27 domains." Genetics **187**(1): 171-184.
- Srivastava, S., R. McMillan, J. Willis, H. Clark, V. Chavan, C. Liang, H. Zhang, M. Hulver and K. Mukherjee (2016). "X-linked intellectual disability gene CASK regulates postnatal brain growth in a non-cell autonomous manner." Acta Neuropathol Commun **4**: 30.
- Srivastava, S., R. McMillan, J. Willis, H. Clark, V. Chavan, C. Liang, H. Y. Zhang, M. Hulver and K. Mukherjee (2016). "X-linked intellectual disability gene CASK regulates

postnatal brain growth in a non-cell autonomous manner." Acta Neuropathologica Communications **4**.

- Sterman, A. B. and N. Sposito (1984). "Motoneuron axosomatic synapses are altered in axonopathy." Journal of Neuropathology & Experimental Neurology **43**(2): 201-209.
- Strauss, O. (2005). "The retinal pigment epithelium in visual function." Physiological reviews **85**(3): 845-881.
- Su, J., C. V. Haner, T. E. Imbery, J. M. Brooks, D. R. Morhardt, K. Gorse, W. Guido and M. A. Fox (2011). "Reelin is required for class-specific retinogeniculate targeting." J Neurosci **31**(2): 575-586.
- Su, J., R. S. Stenbjorn, K. Gorse, K. Su, K. F. Hauser, S. Ricard-Blum, T. Pihlajaniemi and M. A. Fox (2012). "Target-derived matricryptins organize cerebellar synapse formation through α3β1 Integrins." Cell reports **2**(2): 223-230.
- Sümbül, U., S. Song, K. McCulloch, M. Becker, B. Lin, J. R. Sanes, R. H. Masland and H. S. Seung (2014). "A genetic and computational approach to structurally classify neuronal types." Nature communications **5**: 3512.
- Taban, M., B. H. Cohen, A. David Rothner and E. I. Traboulsi (2006). "Association of optic nerve hypoplasia with mitochondrial cytopathies." J Child Neurol **21**(11): 956-960.
- Tavares, G. A., E. H. Panepucci and A. T. Brunger (2001). "Structural characterization of the intramolecular interaction between the SH3 and guanylate kinase domains of PSD-95." Molecular Cell **8**(6): 1313-1325.
- Vilensky, J. A., W. Robertson and C. A. Suarez-Quian (2015). The Clinical Anatomy of the Cranial Nerves: The Nerves of" On Old Olympus Towering Top", John Wiley & Sons.

- Wagner, N., K. D. Wagner, H. Scholz, K. M. Kirschner and A. Schedl (2006). "Intermediate filament protein nestin is expressed in developing kidney and heart and might be regulated by the Wilms' tumor suppressor Wt1." Am J Physiol Regul Integr Comp Physiol **291**(3): R779-787.
- Walker, A. S., G. E. Goings, Y. Kim, R. J. Miller, A. Chenn and F. G. Szele (2010). "Nestin reporter transgene labels multiple central nervous system precursor cells." Neural Plast **2010**: 894374.
- Wei, Z., S. Zheng, S. A. Spangler, C. Yu, C. C. Hoogenraad and M. Zhang (2011). "Liprin-mediated large signaling complex organization revealed by the liprin-alpha/CASK and liprin-alpha/liprin-beta complex structures." Mol Cell **43**(4): 586-598.
- Williams, R. and L. Chalupa (1983). "An analysis of axon caliber within the optic nerve of the cat: evidence of size groupings and regional organization." The Journal of Neuroscience **3**(8): 1554-1564.
- Wu, J. and J. J. Hablitz (2005). "Cooperative activation of D1 and D2 dopamine receptors enhances a hyperpolarization-activated inward current in layer I interneurons." Journal of Neuroscience **25**(27): 6322-6328.
- Zani, I. A., S. L. Stephen, N. A. Mughal, D. Russell, S. Homer-Vanniasinkam, S. B. Wheatcroft and S. Ponnambalam (2015). "Scavenger receptor structure and function in health and disease." Cells **4**(2): 178-201.
- Zeki, S. M., J. Dudgeon and G. Dutton (1991). "Reappraisal of the ratio of disc to macula/disc diameter in optic nerve hypoplasia." British journal of ophthalmology **75**(9): 538-541.

- Zhang, H., Y. J. Su, W. W. Zhou, S. W. Wang, P. X. Xu, X. L. Yu and R. T. Liu (2014). "Activated scavenger receptor A promotes glial internalization of abeta." PLoS One **9**(4): e94197.
- Zhang, X., J. M. Serb and M. H. W. Greenlee (2011). "Mouse retinal development: a dark horse model for systems biology research." Bioinformatics and biology insights **5**: BBI. S6930.
- Zhen, M. and Y. S. Jin (1999). "The liprin protein SYD-2 regulates the differentiation of presynaptic termini in C-elegans." Nature **401**(6751): 371-375.
- Zhu, Y., M. I. Romero, P. Ghosh, Z. Ye, P. Charnay, E. J. Rushing, J. D. Marth and L. F. Parada (2001). "Ablation of NF1 function in neurons induces abnormal development of cerebral cortex and reactive gliosis in the brain." Genes Dev **15**(7): 859-876.